VIBRATION OF NEARBY STRUCTURES INDUCED BY HIGH-SPEED RAIL TRANSIT

by

Pei-wen Chen

A Dissertation Presented to the
FACULTY OF THE GRADUATE SCHOOL
UNIVERSITY OF SOUTHERN CALIFORNIA
In Partial Fulfillment of the
Requirements for the Degree
DOCTOR OF PHILOSOPHY
(CIVIL ENGINEERING)

December 2008

Acknowledgements

I am so happy to have the research done to this point. I really want to thank my super advisor, Professor H.L. Wong, also known as Doc, who lead me to this field and gave me plenty of help. His favor to me might affect my whole life, and I really appreciate it. I want to thank my family members, especially my gracious parents and my dearest aunt, who always gave me lots of support and encouragement, which made me continued until the end. I thank those friends who gave me supports and helped me find valuable data. Last, but not least, I wish to thank my examination committee members, Professor Vincent W. Lee, Professor James E. Moore, III, Professor Najmedin Meshkati and Professor Jiin-Jen Lee for guiding me in research. I wish to thank METRANS for the research support which provided me with the tools for the analyses.

Table of Contents

List of Figures

List of Tables

Abstract

This dissertation is centered around a case study of the Taiwan High Speed Rail (THSR) concerning the issues of ground borne vibration and its environmental effects on the metropolitan areas which it serves. As the speed and weight of high speed trains increase, the vibrations caused by the transportation system can seriously affect the nearby locales's ability to attract high technology manufacturers and many existing factories have relocated. The THSR was selected for its readily available geotechnical and structural data from a long history of earthquake studies and it is ideal for a detailed analysis. The THSR route traverses through densely populated areas of Western Taiwan where 97% of its population resides. The work herein includes a study of the vibration generated by deeply embedded pile groups of elevated tracks, used in 70% of THSR. Many previous analyses concentrated mostly on ground surface induced vibrations. It is shown that the soil-structure interaction effect of a resonant bridge could amplify the vibration at ground level as the mass of the bridge contributes as a dynamic factor.

Chapter One
Introduction

The research devoted to high-speed rail transportation and its impact on the surrounding environment is extensive; especially in Europe and Japan, where this mode of transportation is critical to everyday life. Detailed studies have been made on nearly every aspect which concern rail transit: from the design of mechanical components, to rail infrastructures and to environmental impact caused by noise and vibration. The analyses and experiments conducted required sophisticated modern methods and many challenging theoretical problems remain.

As followed by economic expansion, the response of fast development of the high speed passenger transportation market is in high demand all over the world. High speed railroad is one of the advanced public transportations which match the conditions of high speed and high-passenger-load. As we can see, some of the developed countries already built high speed rail systems, and some of the developing countries are contemplating construction. The first built high speed rail was Shinkansen in Japan (1964), and then there were TGV in France (1981), ICE in Germany (1991), AVE in Spain (1992), KTX in Korea (2004) and THSR in Taiwan (2007). When Shinkansen began, the highest velocity of the rail was 210 km/h. Afterwards, the velocities of all the high speed rails and even Shinkansen nowadays are operating at more than 250 km/h. Taiwan high speed rail (THSR) has also been completed and started to operate in early 2007. The highest speed of Taiwan high speed rail is estimated to be 300 km/h.

Dowding (2000) described how transit or construction vibration can generate ground waves which interact with a nearby structure in a manner similar to that of seismic waves, although with a much smaller amplitude. A response spectrum approach, an earthquake engineering tool, was actually used to determine whether the vibration could resonate with certain modes of a floor, or a wall. Direct acoustic waves can penetrate a wall if the frequency of the sound wave coincides with a natural frequency of the wall and the interior of the wall can serve as a giant loud speaker, generating acoustic waves at an intensity far above the incident wave. Train noise has a lower frequency content than other modes of transportation, which is from about 8 to 100 Hz. The frequency below 20 Hz is known as Infrasound and it will not affect the human ear but the resulting vibration for sensitive equipment housed in nearby buildings could be undesirable. The higher frequency ground waves generally attenuate quickly through distance in the highly damped top soil layers. The lower frequency waves, however, can be measured many meters away.

One exciting area of research in recent years of ground borne vibration aspect is the special case when the train speed exceeds the compressional wave and shear wave velocity of the soil medium. The rapid loading condition from the track causes an elastic shock wave because the train arrives at a specific location before it can be notified by a propagated P-wave or S-wave. The shock wave, although its amplitude may not be large, behaves as a plane wave and it can travel a greater distance.

Madshus and Kaynia (2000) noted the general consensus of the research community that rail infrastructures deteriorate quickly if the speed of the train is increased. Although no specific reference was made regarding the soil properties underneath the rail track, it is safe to assume that high stresses exerted on the soil medium and on the rail supporting structure play a major role in their rapid deterioration. Kim and Drabkin (1994) recorded soil settlement in an experiment even with low-level vibrations.

DeGrande and Schillemans (2001) used as an example a soil condition on a European HST track between Paris and Brussels, having a shear wave velocity of 80 m/sec for the top

1.4m, 133 m/sec for the next 1.9m and 226 m/sec for the assumed half space below. The 80 m/sec value is below some of the HST's operating velocities which range from 220 to 315 km/hr, the latter can be converted to 88 m/sec. Dowding (2000) reported that the Swedish site is composed of a 2 m stiff crust that overlays 5 m of soft marine clay, which in turn overlays a half space of stiff clay. The soft layer at Ledsgard has a shear wave velocity of only 40 m/sec.

In Los Angeles and in most areas in California, the soil condition is firm and the top-layer shear wave velocity is mostly 150 m/sec or far above. According to the ROSRINE geological website, there are only 3 sites with top-layer shear wave velocity less than 150 m/sec and 4 other sites that was measured at 150 m/sec. There are areas, However, that the soil profile is extremely soft. For example, a section of the Alameda Corridor near the city of Long Beach in California has soil types SM (Silty Sand), ML (Inorganic Silt and very fine Sand), and CL (Inorganic Clays of low to medium plasticity). These soil types have Young's Moduli of 4000, 12000 and 18000 kg/m^2, respectively, and a specific weight of 17.2 kN/m^3. Using theory of elasticity, one can approximate the compressional wave velocity to be approximately 65, 83 and 101 m/sec, respectively. Since the Poisson's ratio was estimated as 0.2 by the geological report, the shear wave velocities are respectively, 40, 51 and 62 m/sec. Therefore, over long distances that a train route may cover, there would be spots in every project that require special attention.

In this thesis proposal, several methods developed mostly in earthquake engineering research will be applied to transit vibration. Although the loading level is lower, the dynamic response of the structures are similar regardless it is the railway bridges or the nearby structures. The ground waves, earthquake induced or mechanically induced, also have similarities when it is propagated through a layered soil medium. The research in the area of soil-structure interaction is also applicable here because the incident waves excite the structure in the same way that seismic waves do. One advantage of the current application in transit structure is that the linear theory is a better approximation since the amplitude of the excitation is well within the range of linear analyses.

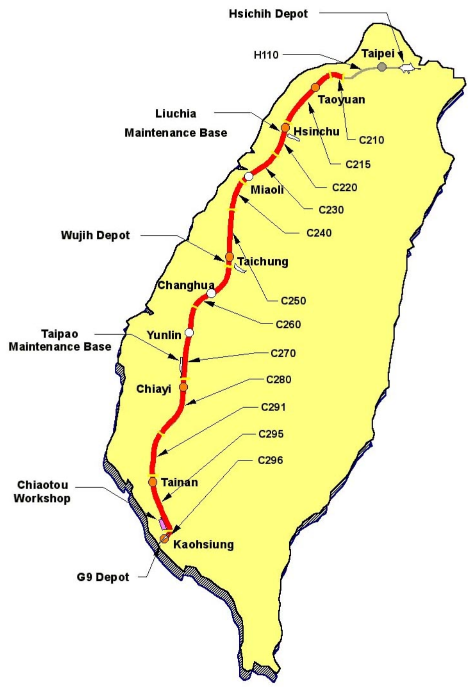

Figure 1.1 – THSR route through densely populated Western Taiwan.

The controversial THSR, the Taiwan High Speed Railway project, will be used as a case study for the proposed methods. It will provide a basis to demonstrate the validity and flexibility of these methods. The THSR has a planned route through Western Taiwan (see Fig 1.1) which goes within 200 to 300 meters of a large cluster of High Technology buildings in Southern Taiwan. It was unprecedented that a government would authorize the construction of a high speed rail through a soft soil layer area so near a well established industrial district such as the Tainan Science Park in the southern City of Tainan. Besides the political and contractual problems of that project, it is a major concern that the small vibration, undetectable by human, could affect the sensitive instruments of the

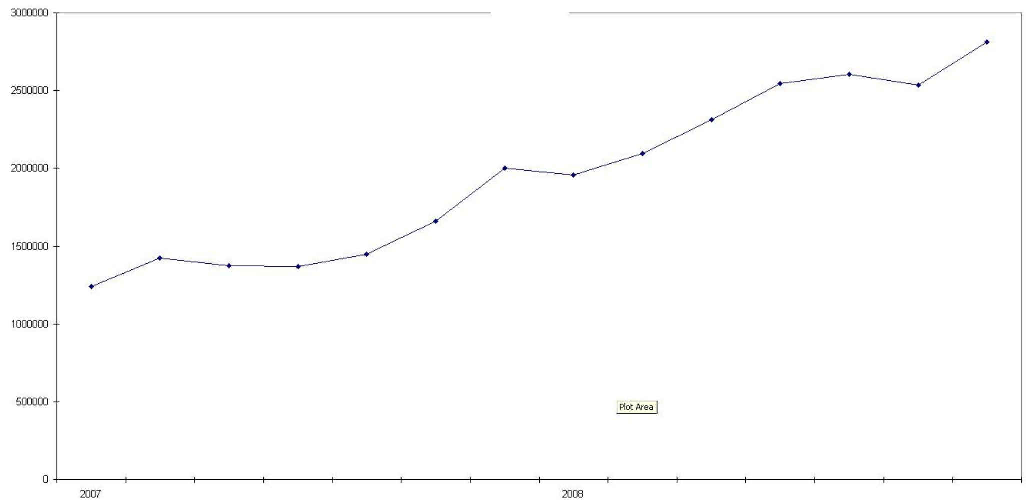

Figure 1.2 – THSR ridership trend.

semiconductor industry. Since the ideal vibration level of the industrial area which locate around 200m from rail track should be 48 dB or lower, the vibration level of the operating THSR in northern Taiwan did not meet that standard. As a result, some of those factories in southern Taiwan have relocated ahead of the completion of the transit project before THSR reached Tainan. The list below provides a sample of some companies affected by THSR.

- Winbond Electronics Corp., a semiconductor company which manufactures memory chips and integrate circuits, moved its 12-inch wafer plant to Taichung Science Park.
- Silicon Integrated Systems Co., a semiconductor firm, moved its 12-inch wafer plant from Tainan Science Park.
- Chi Mei Electronics Corp., a company which produces TFT-LCD products, postponed decision to build a Fab. 5 plant until the vibration level by THSR is fully investigated.

- Mosel Vitelic Inc., a semiconductor company, moved its 12-inch wafer plant from Tainan Science Park.

- United Microelectronics Corp., a semiconductor manufacturer, changed its plan from building 5 plants to only 1 plant in Tainan Science Park. It now considers building plants in another country, Singapore and others. It also slowed the plant building plan in Tainan Science Park.

Although there was a great uproar concerning the THSR, the reasons for the rail system may be justified. It will reduce the highly congested transportation problem of Western Taiwan. The high speed rail will provided the benefits of safe mass transit plus the advantage of energy conservation and lower air pollution. After the transport service started, it effectively solved the crowded traffic problem and balanced the develop of Western Taiwan. THSR also increased the efficiency and integrated buses, traditional railroad, and metro transportation system to become one high speed public transportation network. Fig 1.2 shows that ridership of THSR has increased steadily, from an estimated 1.25-million passengers per year in early 2007 to nearly 3-million at the end of 2008. Although the system is still in debt from construction, it is beginning to justify its goals and becomes less of a burden to Taiwan's financial outlay.

The THSR has changed the mode of transportation for many travelers, Fig. 1.3 shows that domestic air travel has decreased significantly. In two years, the number of daily domestic flights has gone down from 3400 in early 2007 to less than 100 in late 2008. The number of domestic air travelers has gone, for the same period, from 285,000 to less than 10,000. The main reason is that it is more convenient to go to the numerous and attractive train stations rather than a few highly congested airports. The travel time is rough the same

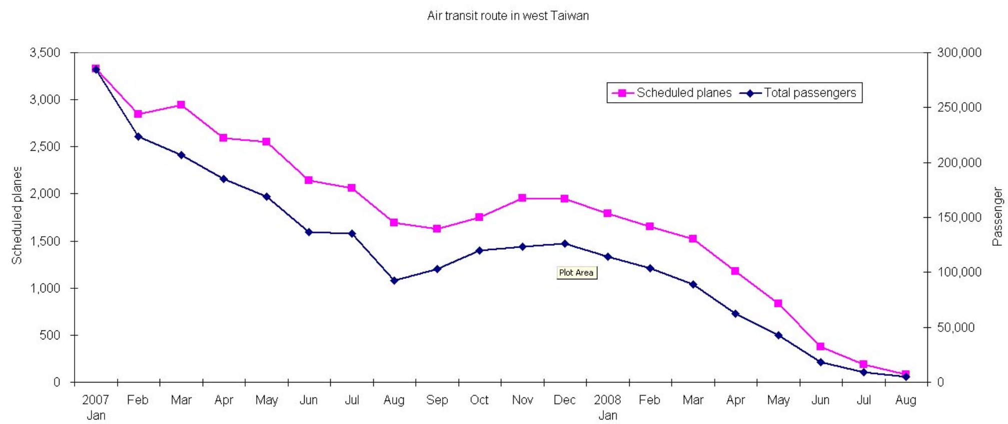

Figure 1.3 – Decrease in domestic air travel in Taiwan.

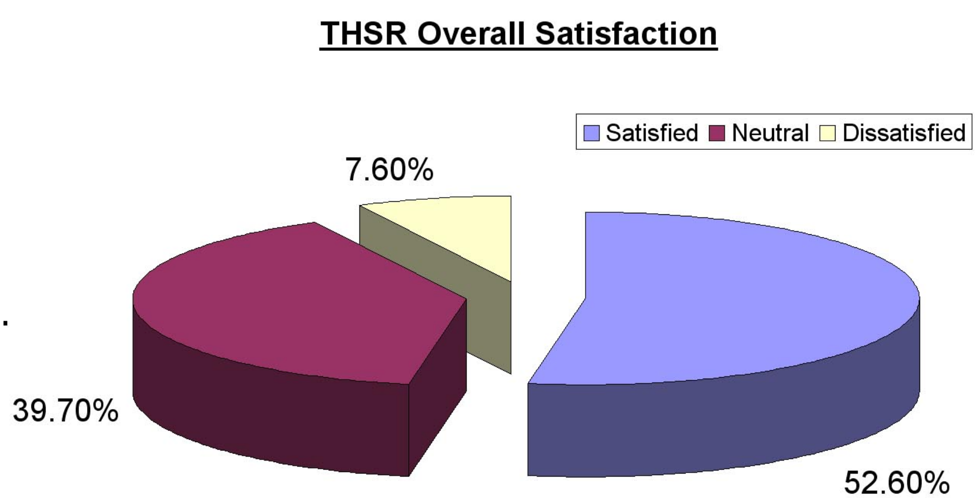

Figure 1.4 – THSR passenger satisfaction rating.

even though airplanes travel at a higher speed. The cost of a train ride is also significantly less than that of an airplane ticket.

Being the longest bridge-like structure in the world, having most of its tracks elevated, THSR gives pride to citizens of Taiwan. The train route connects the major cities Taipei in the north, Taichung in central Taiwan and Tainan and Kaosiung in the south. Many other smaller cities in between those major urban centers will also see significant economic development. As shown in Fig. 1.4, over half of the passengers are satisfied with the THSR service, with nearly 40

Issues to be resolved are the safety of the trains and the significant environmental impact that may be amplified further as the speed of the trains increase. There are already signs of plaster falling off walls for some older residents and Fig. 1.5 shows an embankment of a water channel failed due to excessive vibration from a bridge column. Due to high vibration levels, the concrete wall developed cracks and over time, the water seepage increased the damage and finally the failure of the entire embankment. This type of problems would occur more often near wet and soft soil areas in the center of the agricultural region.

According to the administrator of the Taiwan high speed rail, the major problem of the vibration is caused by the resonance of the bridges when the train travels at a certain critical speed. This problem not only affects the local residents, but also affects the safety of the trains. This type of dynamic moving load problems will be a subject in Chapters 4 and 6. In Chapter 4, a detailed analysis of a bridge structure will be made to determine it resonance frequencies. Simple soil springs will be added to the base of the columns to investigate possible changes of the resonance frequencies due to various types of soil conditions. A more sophisticated analysis will be performed in Chapter 6 using a soil-structure interaction approach derived in the field of earthquake engineering after the frequency dependent foundation impedance functions are obtained in Chapter 5. In Chapter 2, the soil conditions throughout Taiwan will be compiled using the extensive earthquake engineering database and 4 representative soil profiles will be proposed to represent a majority of soil conditions in the country. Chapter 3 will investigate whether the depth of the vibration sources from deep piles would affect the wave propagation characteristics of outgoing waves from the

Figure 1.5 – Crumbling of embankment due to excessive vibration.

train tracks. Since most of the rails of THSR are elevated, the vibration of nearby areas is different from the vibrations created by ground surface-borne train tracks. This issue is important environmental impact studies of transit system in other parts of the country or elsewhere in the world. Perhaps a simple soil test by a dropped weight is not sufficient to analyze the wave propagation characteristic of a site. All the related issues of THSR provides an interesting and challenging topic for this particular dissertation.

Chapter Two
Site Geology

Since the case study in this dissertation is related to the propagation of waves away from the THSR rail, it is important to study the geological conditions near the rail structure and the wave propagating media. The THSR is located in Western Taiwan where most of the areas are alluvial soil, important for the cultivation of vegetation. Although Taiwan is well known for its electronics industry, it is still considered an agricultural country because they export more agricultural products than import. The agricultural areas are located in the southwestern part of Taiwan and near Taipei City, mainly in Yunlin, Chiayi, and Tainan Counties. The central and eastern parts of Taiwan have mostly metamorphic rock, schist and slate, which explains why those locations are sparsely populated, having less than 3% of the total population.

With most of its population on the western side of Taiwan, the factories are also located amidst the overcrowded cities. Most of the high technology industries are concentrated in Hsinchu and Tainan Science Parks, with the new locations in Taichung science park making a push for more opportunities in the near future. Taichung, aided by the vibration problems caused by THSR in Tainan, has recently captured many of the semiconductor factories originally planned for Tainan.

After some fierce political battles, the THSR project was approved for the reason that a high-speed train system is badly needed to serve its population and to reduce traffic and pollution. The highly populated areas are all located along the route and that includes Taipei, the largest population, Kaoshiung, the second largest population, and locations in Taipei, Taichung and Tainan counties. The THSR serves basically 97% of the population of Taiwan.

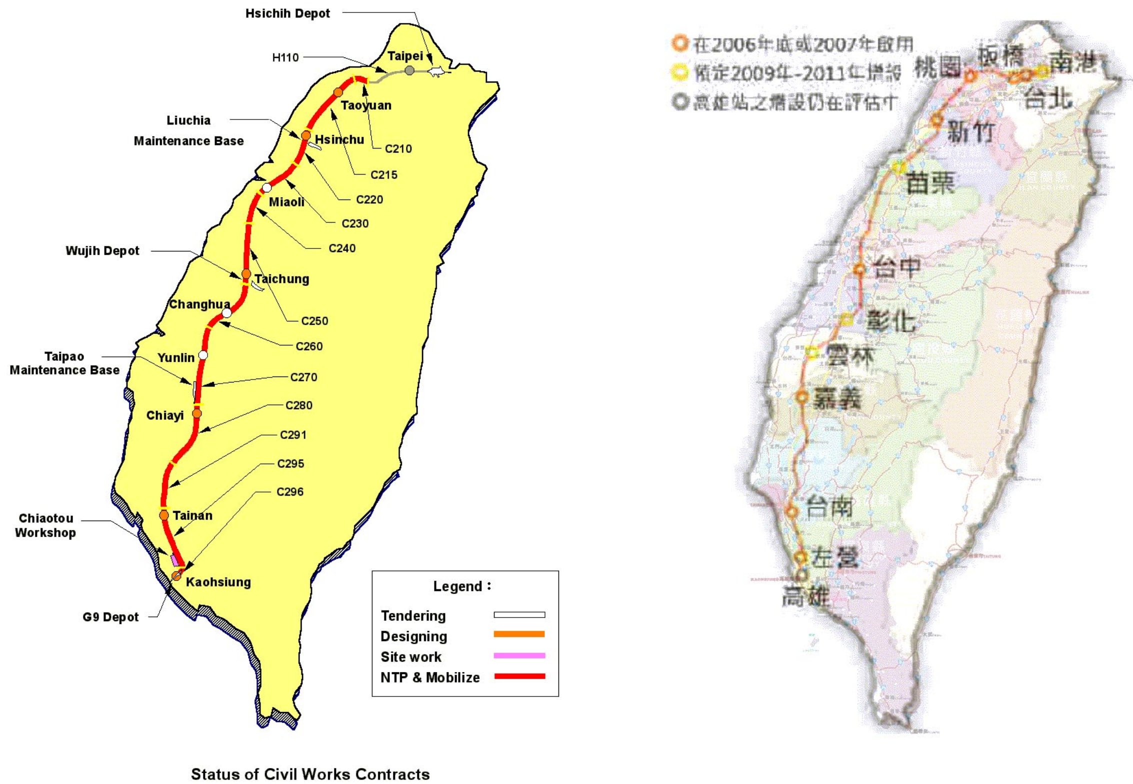

Figure 2.1 – Operating Territory of THSR in Taiwan.

One fortunate coincidence which aids the wave propagation research is the fact that Taiwan has high seismic activities and it is prone to some major earthquakes. For that reason, major geophysical and geological research activities have been ongoing for many years. As a byproduct, many borehole experiments were made all throughout the country by the National Center for Research on Earthquake Engineering (NCREE). Some records used within this chapter are obtained by public sources. For the purpose of the present study, using the Green's Function computer program developed by Luco and Apsel (1983a, 1983b), the soil medium can be approximated as a viscoelastic layered soil medium. The input data is minimal, the shear wave (S-wave) velocity and the compressional wave or primary wave (P-wave) velocity will suffice. The geological data can be approximated by layers, there is no theoretical restriction on the number of layers allowed.

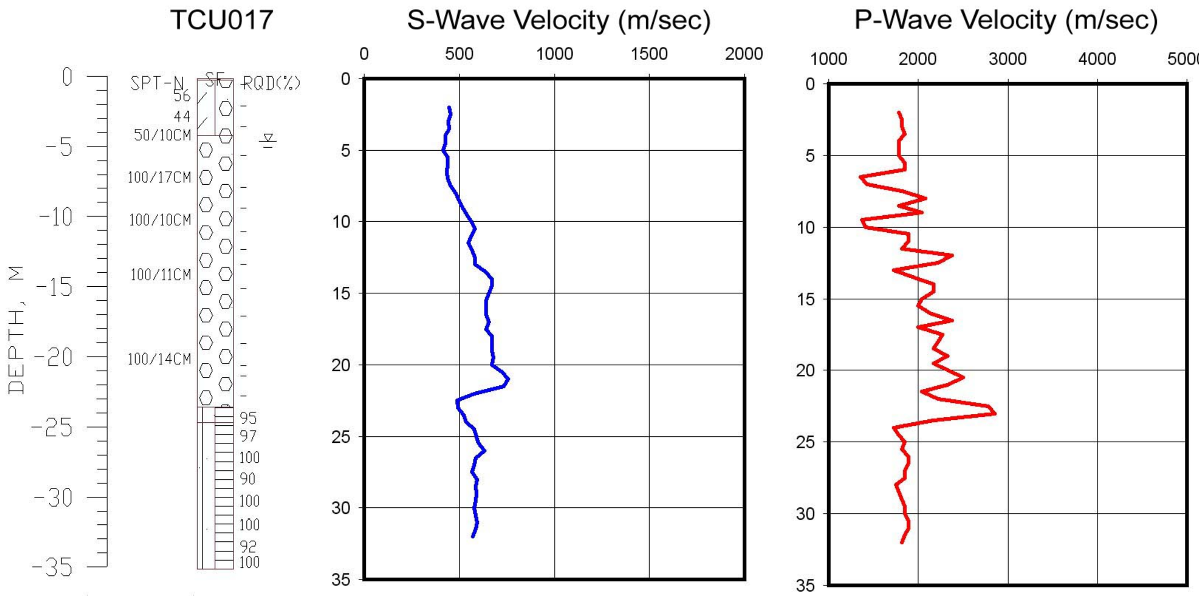

Figure 2.2 – Hsinchu County Soil Profile TCU017.
Hsinchu Science Park Senior High School.

Listed in Table 2.1 are the sites considered for the present research. Widely varied conditions exist throughout the areas investigated. Consider first the soil profile characterized by the plots in Fig. 2.2, it is located at the Hsinchu Science Park Senior High School campus in Hsinchu County; it is labeled with site index TCU017.

The TCU017 is on a relatively hard soil, having S-wave velocity of approximately 500 m/sec and a P-wave velocity of 1900 m/sec near the surface and somewhat higher in depth. From the shapes of the wave velocity profiles, this site is quite near the idealized concept of a semi-infinite space. This site and several other sites with similar properties will be classified as a typical Soil Profile 1 in later studies.

Consider next the soil profile characterized by the plots in Fig. 2.3, it is located at the Hsin-Shih Elementary School in Tainan County; it is labeled with site index CHY021. The CHY021 is on a relatively soft soil, having S-wave velocity of less than 200 m/sec and a P-wave velocity of 1500 m/sec near the surface and significantly higher in depth for S-wave

Borehole	Location
TAP 019	Taipei
TAP 054	Banciao
TCU 083	Taoyuan
TCU 017	Hsinchu
TCU 035	Miaoli
TCU 063	Taichung
TCU 116	Changhua
CHY 002	Yunlin
CHY 095	Chiayi
CHY 021	Tainan
KAU 060	Kaohsiung

Table 2.1 – Borehole records near THSR stations.

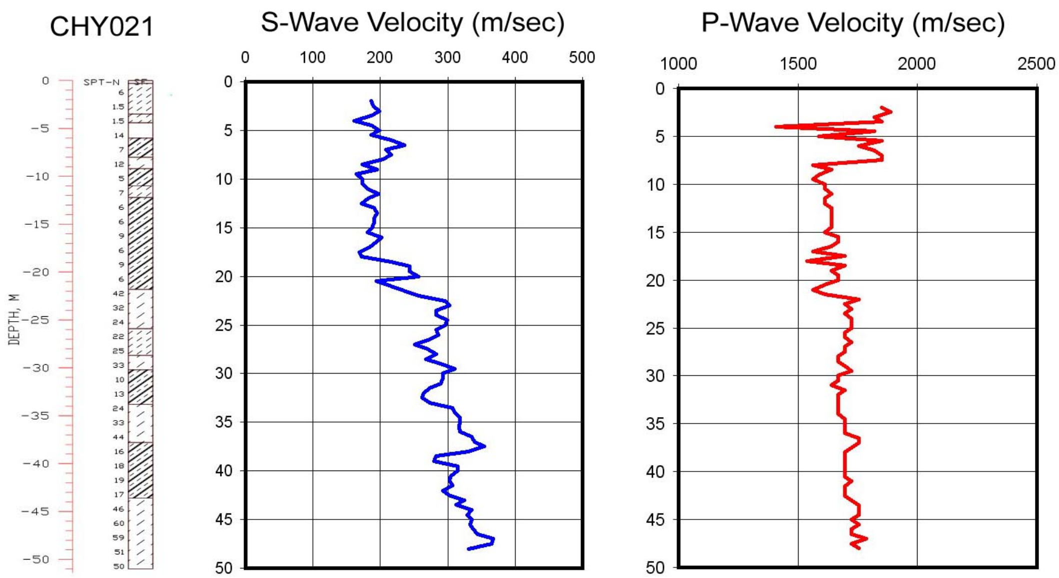

Figure 2.3 – Tainan County Soil Profile CHY021.
Hsin-Shih Elementary School.

velocity. The P-wave velocity, however, is somewhat uniform, suggesting that the Poisson Ratio changes with depth. The reason for the change of Poisson's Ratio is probably caused by the moisture content of soil, perhaps caused by a high water table. This site can be represented by a viscoelastic layered medium; it can be roughly classified as a relatively soft medium as typical Soil Profile 3 in later studies.

The next soil profile to be analyzed is that shown in Fig. 2.4, it is located at the Lien-Shih Elementary School in Yunlin County, labeled with site index CHY002. This particular site is considered one of the softest sites in the country, having S-wave velocity dipping below 150 m/sec and a P-wave velocity as low as 1200 m/sec near the surface and not much higher in depth. This site can be represented by a viscoelastic layered medium, it can be roughly classified, as many other rice field type of sites, as typical Soil Profile 4 in later studies.

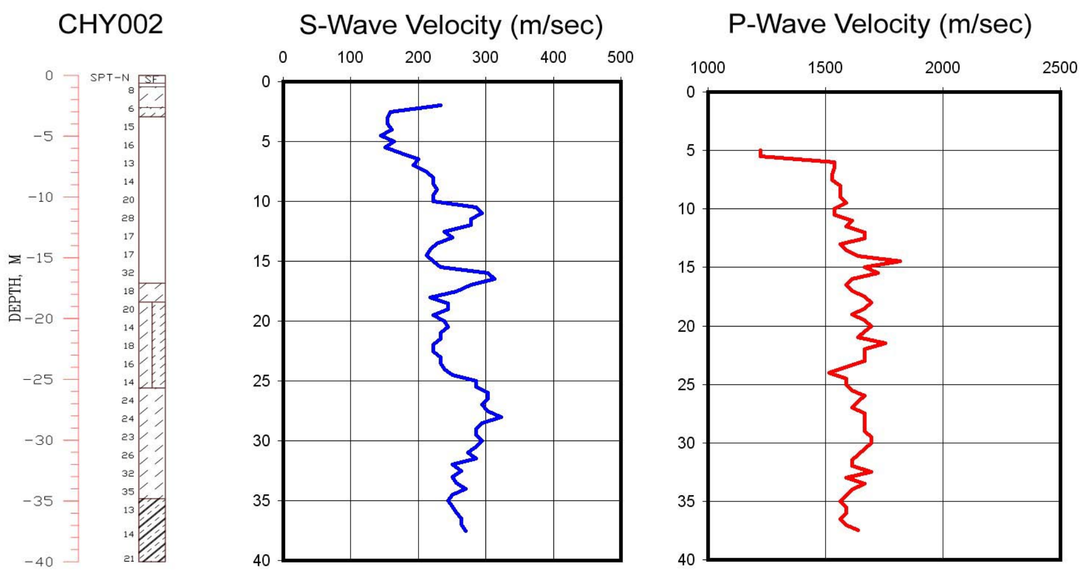

Figure 2.4 – Yunlin County Soil Profile CHY002.
Lien-Shih Elementary School.

One more soil profile to consider is located at the Wu-Jih Elementary School in Taichung County, labeled with site index TCU063. This particular site is considered to be a medium site in terms of hardness of soil. It has a distinct one layer over rock. The S-wave velocity in the top layer is approximately 350 m/sec and a P-wave velocity is about 1250 m/sec near the surface. Beneath this top layer, the half space below is that of the hardest site. This will be classified as Soil Profile 2 in later studies.

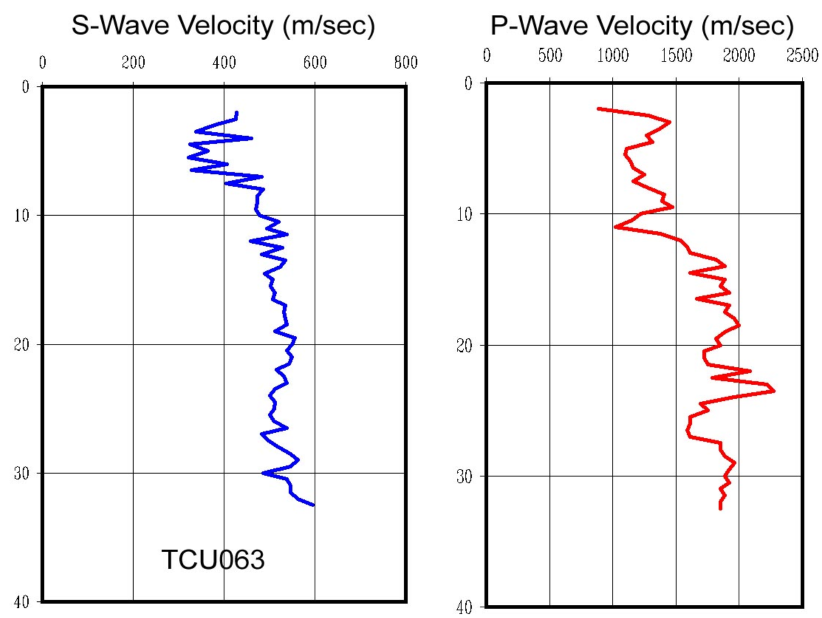

Figure 2.5 –Taichung County Soil Profile TCU063.
Wu-Jih Elementary School.

The four soil profiles chosen for the wave studies are shown in Fig. 2.6, where they are represented by one uniform layer in Soil Profile 1 and three uniform layers in Soil Profiles 2, 3 and 4. The support system for structures found on Soil Profiles 1 and 2 can be shallow pile groups. But for Soil Profiles 3 and 4, pile lengths of over 45 meters might be required to safely support the railway structures. The properties to be provided to operate the Green's Function program are β, the shear wave velocity; α, the compressional wave velocity; D, the depth of a particular layer; and ρ, the specific gravity of the soil layer. Most of the

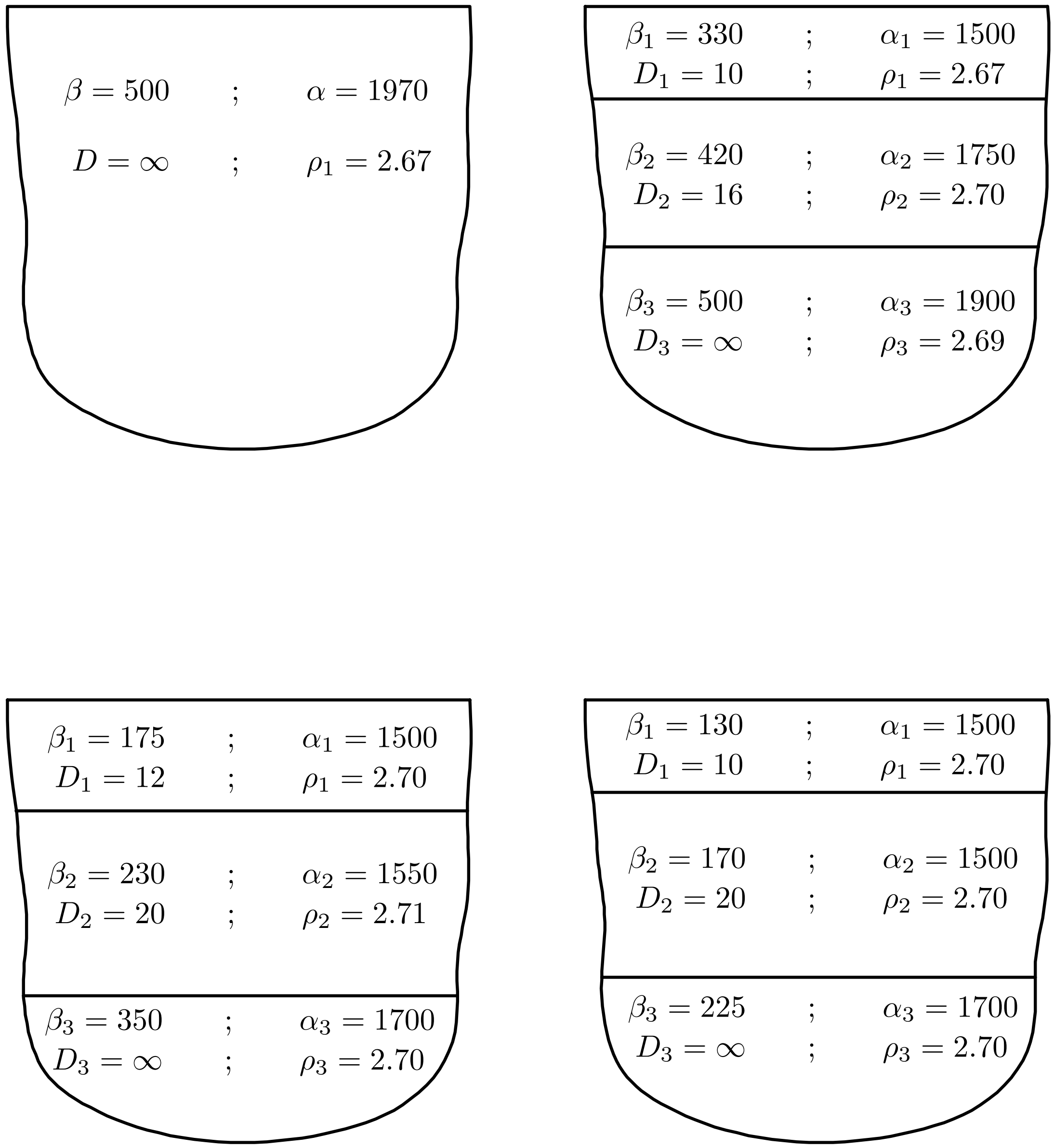

Figure 2.6 – Idealized Soil Profiles Representative of THSR Conditions.

values of ρ are approximately 2.7, a dimensionless number, the actual mass density can be obtained by multiplying the mass density of water, $1000\,\mathrm{kg/m^3}$.

Chapter Three

Wave Propagation Characteristics of Sites

Wave propagation has always been one of the main research topics in seismology and earthquake engineering. Long period waves are of interest in exploration seismology while medium to short period (high frequency) waves are important to earthquake engineering. There are basically two major types of numerical methods available for the study of waves: the finite element method and the continuum mechanics method. The finite element method has the flexibility for analyzing models with difficult geometrical shapes and nonlinear material properties; but its formulation requires a volume integral over the model and that limits the method's effectiveness for the studies with large dimensions. The continuum mechanics method, at best, can model the earth as a layered semi-infinite space and its solution can be written as a superposition of the fundamental solution, known as Green's functions. The radiating boundary condition, for the far field, is automatically satisfied. Both methods have limitations, but the continuum method suits the present wave propagation problem better.

The Green's functions for a load traveling at a constant velocity along a straight line were developed by deBarros and Luco (1992) and have been applied to a class of diffraction problems for canyons and tunnels (Luco et al 1990). These functions are complex valued and a significant programming effort was required to implement them. They can be adapted and applied to the transportation problem at hand because it can readily model the properties of geological layers, for example, the properties of wave velocities, mass densities, layer thicknesses and damping factors, etc. The Green's functions for a stationary load, developed by Luco and Apsel (1983a, 1983b), can be applied for a moving load across the surface of the earth medium, similar to that of a surface-borne railroad track, the response at locations away from the track can be calculated using phase shifts for loads at different track locations. The phase factors are determined by the train velocity

Working with Green's Functions in the frequency domain, transient solutions can be obtained using Digital Fourier Transform for the motion in a soil medium subjected to time-dependent loads caused by a passing train. Once the frequency dependent transfer function is determined for an observation station, solution for different time dependent loading histories could be evaluated without additional effort. The THSR has 30% surface-borne tracks and 70% elevated track on bridges. The surface loads yield a mathematical formulation which requires integration over the length of the track. But buried loads to the soil medium through the pile group foundations at 30-meter intervals reduces the mathematical formulation from an infinite integral to a discrete sum. The loads for the latter case are applied only through the columns and the pile groups.

3.1 – Application of Stationary Green's Functions

Dr. Apsel's program can analyze a stack of viscoelastic layers over a half space with the freedom of choice for a wide range of soil properties, the only important requirement is that the materials are linear. The Green's functions were derived in the cylindrical coordinates for displacements, in the form of

$$U(R, \psi, z_s, z_o, \vec{\rho}, \vec{\beta}, \vec{\nu}, \vec{\xi}_\beta, \vec{\xi}_\alpha, \vec{D})e^{i\omega t}/r \qquad , \tag{3.1}$$

and for stresses or tractions in the form of

$$T(R, \psi, z_s, z_o, \vec{\rho}, \vec{\beta}, \vec{\nu}, \vec{\xi}_\beta, \vec{\xi}_\alpha, \vec{D})e^{i\omega t}/r^2 \qquad , \tag{3.2}$$

in which r is the radial distance from the point source, ψ is the azimuthal angle, z_s is the depth of the source point, z_o is the depth of the observation point, $\vec{\beta}$ is the array of S-wave velocities, $\vec{\rho}$ is the array of mass densities, $\vec{\nu}$ is the array of Poisson ratios, $\vec{\xi}_\beta$ is the array of S-wave damping ratios, $\vec{\xi}_\alpha$ is the array of P-wave damping ratios, and $\vec{D}$ is the array of layer depths. For the application on surface supported tracks, $z_s = z_o = 0$, because the load and the observer are both on the ground surface. For elevated railways with columns supported by pile foundations, z_s, the source point, would be distributed over depth.

Consider now the coordinate systems illustrated in Fig. 3.1. Noticeably, the polar coordinate system is defined with the z-axis pointing downward, which is a typical coordinate system used in most classical geophysical problems. The origin of the polar coordinate system is defined at the source point, $\vec{r}_s$, therefore, the observation point, $\vec{r}_o$, is located at the coordinates, (r, ψ, z), in which

$$r = |\vec{r}_o - \vec{r}_s| = \sqrt{(x_o - x_s)^2 + (y_o - y_s)^2} \tag{3.3}$$

and

$$\psi = \arg(\vec{r}_o - \vec{r}_s) = \tan^{-1}\left(\frac{y_o - y_s}{x_o - x_s}\right) \qquad . \tag{3.4}$$

The z-dependency of the Green's Functions is included in the functions, U and T. In this thesis' formulation, only the displacement Green's Functions, U, are needed. More specifically, the displacement Green's Functions in cylindrical coordinates, require f_{rz} and f_{zz} for a vertical load and f_{rr}, $f_{\psi r}$ and f_{zr} for a horizontal load.

In the polar coordinate system, all horizontal point forces can be represented by $P_r(\psi_0)$ because the reference angle can be varied to match any orientation. Therefore, the general displacement-force relationship can be written in a form of a 3×2 matrix as

$$\left\{\begin{array}{c} u_r(r,\psi) \\ u_\psi(r,\psi) \\ u_z(r,\psi) \end{array}\right\} = \frac{1}{\mu r}\begin{bmatrix} f_{rr}\cos(\psi-\psi_0) & f_{rz} \\ f_{\psi r}\sin(\psi-\psi_0) & 0 \\ f_{zr}\cos(\psi-\psi_0) & f_{zz} \end{bmatrix}\left\{\begin{array}{c} P_r(\psi_0) \\ P_z \end{array}\right\} \qquad . \tag{3.5}$$

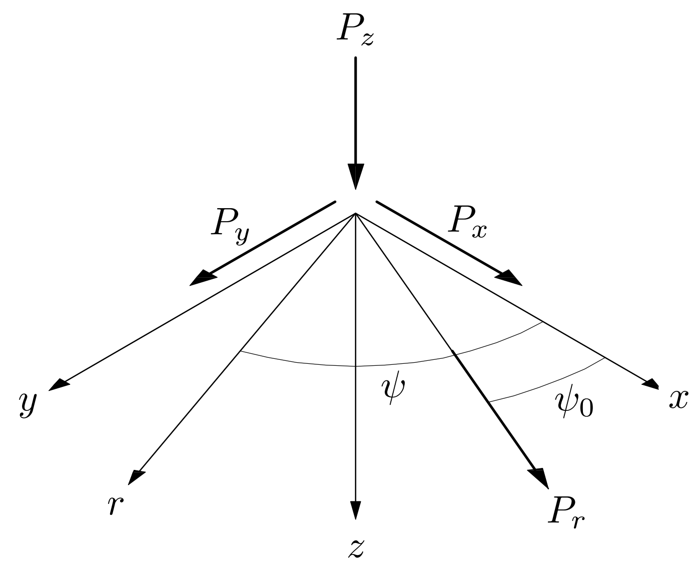

Figure 3.1 – The Definition of the Cylindrical Coordinate System.

To obtain a displacement-force relationship in the Cartesian coordinate system, the following mapping for the forces and the displacements may be used:

$$\left\{\begin{array}{c} P_x(\vec{r}_s) \\ P_y(\vec{r}_s) \\ P_z(\vec{r}_s) \end{array}\right\} = \left\{\begin{array}{c} P_r(0) \\ P_r(\pi/2) \\ P_z \end{array}\right\} \quad , \tag{3.6}$$

and

$$\left\{\begin{array}{c} u_x(\vec{r}) \\ u_y(\vec{r}) \\ u_z(\vec{r}) \end{array}\right\} = \begin{bmatrix} \cos\psi & -\sin\psi & 0 \\ \sin\psi & \cos\psi & 0 \\ 0 & 0 & 1 \end{bmatrix} \left\{\begin{array}{c} u_r(r,\psi) \\ u_\psi(r,\psi) \\ u_z(r,\psi) \end{array}\right\} \quad . \tag{3.7}$$

For the first step, Eq. (3.6), can be used with Eq. (3.5) to relate the displacements in polar coordinates to the forces in Cartesian Coordiante as

$$\left\{\begin{array}{c} u_r(r,\psi) \\ u_\psi(r,\psi) \\ u_z(r,\psi) \end{array}\right\} = \frac{1}{\mu r} \begin{bmatrix} f_{rr}\cos\psi & f_{rr}\sin\psi & f_{rz} \\ f_{\psi r}\sin\psi & -f_{\psi r}\cos\psi & 0 \\ f_{zr}\cos\psi & f_{zr}\sin\psi & f_{zz} \end{bmatrix} \left\{\begin{array}{c} P_x(\vec{r}_s) \\ P_y(\vec{r}_s) \\ P_z(\vec{r}_s) \end{array}\right\} \quad , \tag{3.8}$$

Apply now the transformation in Eq. (3.7) to both sides of Eq. (3.8), the result is a displacement-force relationship in Cartesian Coordinates written as

$$\left\{ \begin{array}{c} u_x(\vec{r}) \\ u_y(\vec{r}) \\ u_z(\vec{r}) \end{array} \right\} = \frac{1}{\mu r} [G] \left\{ \begin{array}{c} P_x(\vec{r}_s) \\ P_y(\vec{r}_s) \\ P_z(\vec{r}_s) \end{array} \right\} \qquad , \tag{3.9}$$

in which

$$[G] = \begin{bmatrix} f_{rr}\cos^2\psi - f_{\psi r}\sin^2\psi & (f_{rr} + f_{\psi r})\sin\psi\cos\psi & f_{rz}\cos\psi \\ (f_{rr} + f_{\psi r})\sin\psi\cos\psi & f_{rr}\sin^2\psi - f_{\psi r}\cos^2\psi & f_{rz}\sin\psi \\ f_{zr}\cos\psi & -f_{zr}\sin\psi & f_{zz} \\ \end{bmatrix} \qquad . \tag{3.10}$$

In Cartesian Coordinates, the factors, $\sin\psi$ and $\cos\psi$, can be evaulated simply as

$$\sin\psi = \frac{y - y_s}{r} \qquad , \tag{3.11}$$

and

$$\cos\psi = \frac{x - x_s}{r} \qquad . \tag{3.12}$$

3.2 – Moving Load Formulation for Surface Sources

Using the stationary harmonic point load in the previous section, a moving point load can be simulated by changing the location of the source point as a function of time, t. A time shrift factor, $\exp(i\omega(t - x/c))$, represents a load moving in the postive x direction while the factor, $\exp(i\omega(t + x/c))$, represents a load moving in the negative x direction. The parameter, c, is is the speed of the load and the quotient, x/c, has a unit of time.

In the schematic depicted in Fig. 3.2, a moving vertical point load, P_z, is at location $(x, 0)$ and the observation point is defined at $(0, h)$. The vertical displacement at that instant shown can be expressed as

$$u_z(0, h, x, \omega) = \frac{f_{zz}(\omega\sqrt{x^2 + h^2})}{\sqrt{x^2 + h^2}} e^{i\omega t} e^{-i\omega x/c} \qquad . \tag{3.13}$$

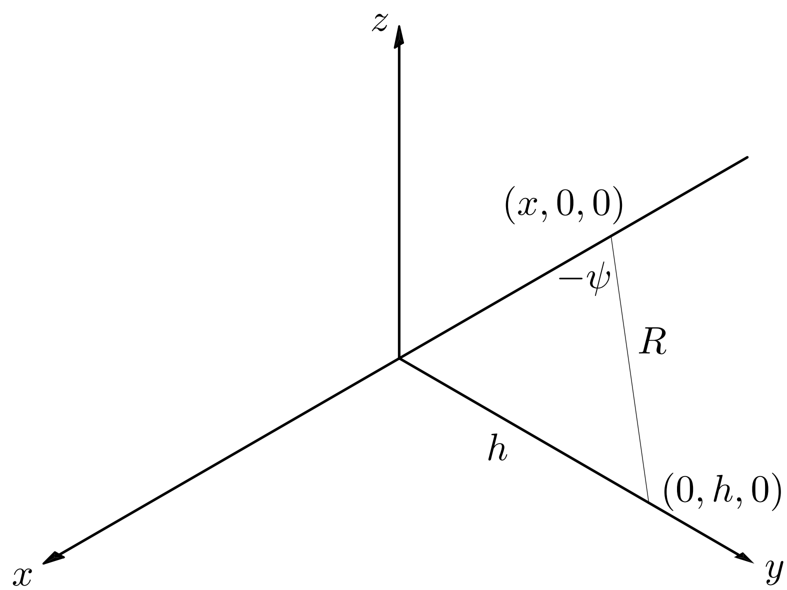

Figure 3.2 – Schematic of a moving load at $(x, 0)$ and an observer at $(0, h)$.

Accumulating the effects of the moving load over the entire x-axis, integrate Eq. (3.13) over x to yield

$$u_z(0, h, \omega) = \left[\int_{-\infty}^{\infty} \frac{f_{zz}(\omega\sqrt{x^2 + h^2})}{\sqrt{x^2 + h^2}} \, e^{-i\omega x/c} \, dx \right] e^{i\omega t} \qquad . \tag{3.14}$$

In the above equation, the phase factor, $\exp(-i\omega x/c)$, accounts for the position of the load as a function of time.

Using the third column of the matrix $[G]$ as defined in Eq. (3.10) and substituting $\sin\psi = -h/R$ and $\cos\psi = -x/R$, the x and y components of the displacement can also be obtained as

$$u_x(0, h, \omega) = \left[\int_{-\infty}^{\infty} \frac{x \, f_{rz}(\omega\sqrt{x^2 + h^2})}{x^2 + h^2} \, e^{-i\omega x/c} \, dx \right] e^{i\omega t} \qquad , \tag{3.15}$$

and

$$u_y(0,h,\omega) = \left[-h \int_{-\infty}^{\infty} \frac{f_{rz}(\omega\sqrt{x^2+h^2})}{x^2+h^2}\, e^{-i\omega x/c}\, dx\right] e^{i\omega t} \qquad . \tag{3.16}$$

The complex functions, u_x, u_y and u_z, of Eqs. (3.14), (3.15), and (3.16) represents the fundamental solutions that can be used to form solution for more specific geometries. The train loads are distributed dynamically from the axles of the train onto a pair of deformable tracks; and then through the sleepers onto the ballast overlying the soil medium. The loads of the train can be approximated by a uniform distribution over the ballast in the direction perpendicular to the track while the load parallel to the track is a function of time and is dependent of the train speed, c.

In the frequency domain, the displacements as frequency dependent functions can be expressed as linear combination of the load function, $L(\omega)$, as

$$u_x(0,h,\omega) = U_x(0,h,\omega)L(\omega) \qquad , \tag{3.17}$$

$$u_y(0,h,\omega) = U_y(0,h,\omega)L(\omega) \qquad , \tag{3.18}$$

$$u_z(0,h,\omega) = U_z(0,h,\omega)L(\omega) \qquad , \tag{3.19}$$

in which U_x, U_y, and U_z are the transfer functions between the load function $L(\omega)$ and the horizontal displacements, u_x, u_y and the vertical displacement, u_z, respectively. The transfer functions, U, are the integrals, over the length of the track, of the fundamental solutions or the Green's Functions.

The process for calculating transient displacement response is to first find the Fourier Transform of the load function, $L(t)$, as

$$L(\omega) = \int_{-\infty}^{\infty} L(t)e^{-i\omega t}\, dt \qquad , \tag{3.20}$$

and then obtain the displacements using the Inverse Fourier Transformation as

$$u_x(0,h,t) = \frac{1}{2\pi}\int_{-\infty}^{\infty} U_x(0,h,\omega)L(\omega)e^{i\omega t}\,d\omega \qquad , \tag{3.21}$$

$$u_y(0,h,t) = \frac{1}{2\pi}\int_{-\infty}^{\infty} U_y(0,h,\omega)L(\omega)e^{i\omega t}\,d\omega \qquad , \tag{3.22}$$

$$u_z(0,h,t) = \frac{1}{2\pi}\int_{-\infty}^{\infty} U_z(0,h,\omega)L(\omega)e^{i\omega t}\,d\omega \qquad . \tag{3.23}$$

In the frequency domain, it is easy to find the transfer functions for velocity as $\dot{U} = i\omega U$, and that for acceleration as $\ddot{U} = -\omega^2 U$.

3.3 – The Loading Time Function

Since the problem at hand is a linear approximation, the superposition of solutions is permitted. A finite element model was made for the track over the sleepers and ballast for one single train axle and the load distribution for the one axle is obtained a function of $L(|x - x_s|)$, in which x_s is the location of the axle load. Since the observation point was defined at $x = 0$ and $y = h$, the function as a function of time is $L(c|t - t_s|)$, in which t_s is the time of arrival of that particular axle at $x = 0$.

The maximum axle load for the THSR is 14 tonnes. The total length of a 12-car train is about 305 meters and the time for it to pass a reference point is about 3.7, 4.9, and 7.3 seconds for train speeds of 300 km/hr (83,33 m/sec), 225 km.hr (62.5 m/sec) and 150 km/hr (41.67 m/sec), respectively. With each axle load represented approximately by pulses, the faster train speed will cause the loads to be spaced closer in time and the effective load per unit length would be higher, but for a shorter time. The total weight of the train is 503 metric tonnes.

Four soil profiles were selected based on the work in Chapter 2 and they will be used here for some preliminary results.

3.4 – Analysis of Ground-Borne Vibration

A finite element model of a track-sleeper-ballist system was created to estimate how a point load from a wheel is spread to the soil medium below. Assume the weight of a train car is equally distributed to 4 axles and there are generally 12 cars used for a train. Nine of Twelve cars are powered and each of these weighs 42.5 tonnes and three other are nonpowered cars and each of the latter weighs 41.5 tonnes. A total of 48 axles carry the train load of 503 tonnes and the arrival time of the axles loads at a particular location is determined by the speed of the train.

The shear wave velocity of the top layers of the soil models introduced in Fig. 2.6 are 500 m/sec, 330 m/sec, 175 m/sec, 130 m/sec, for soil profiles #1, #2, #3 and #4, respectively. Each of the soil profiles has its lowest shear wave velocity well above the maximum THSR operating speed of approximately 80 m/sec, therefore, the possibility of a train generating ground shock waves in Taiwan is unlikely. This is an important result because ground-level shock waves behave as a plane wave and it can travel greater distances with high ampitudes.

As mentioned in Chapter One, many semi-conductor factories have relocated to avoid the excessive vibration level caused by THSR. For sensitive instrumentation, the standard vibration level of 48dB is to be the total vibration intensity, which includes the vibration intensity of ambient and the vibration caused by the train. The defintion of a decibel is shown in the following equation:

$$\text{dB} = 20 \log_{10} \left(\frac{v_m}{v_{\text{ref}}} \right) \quad . \tag{3.24}$$

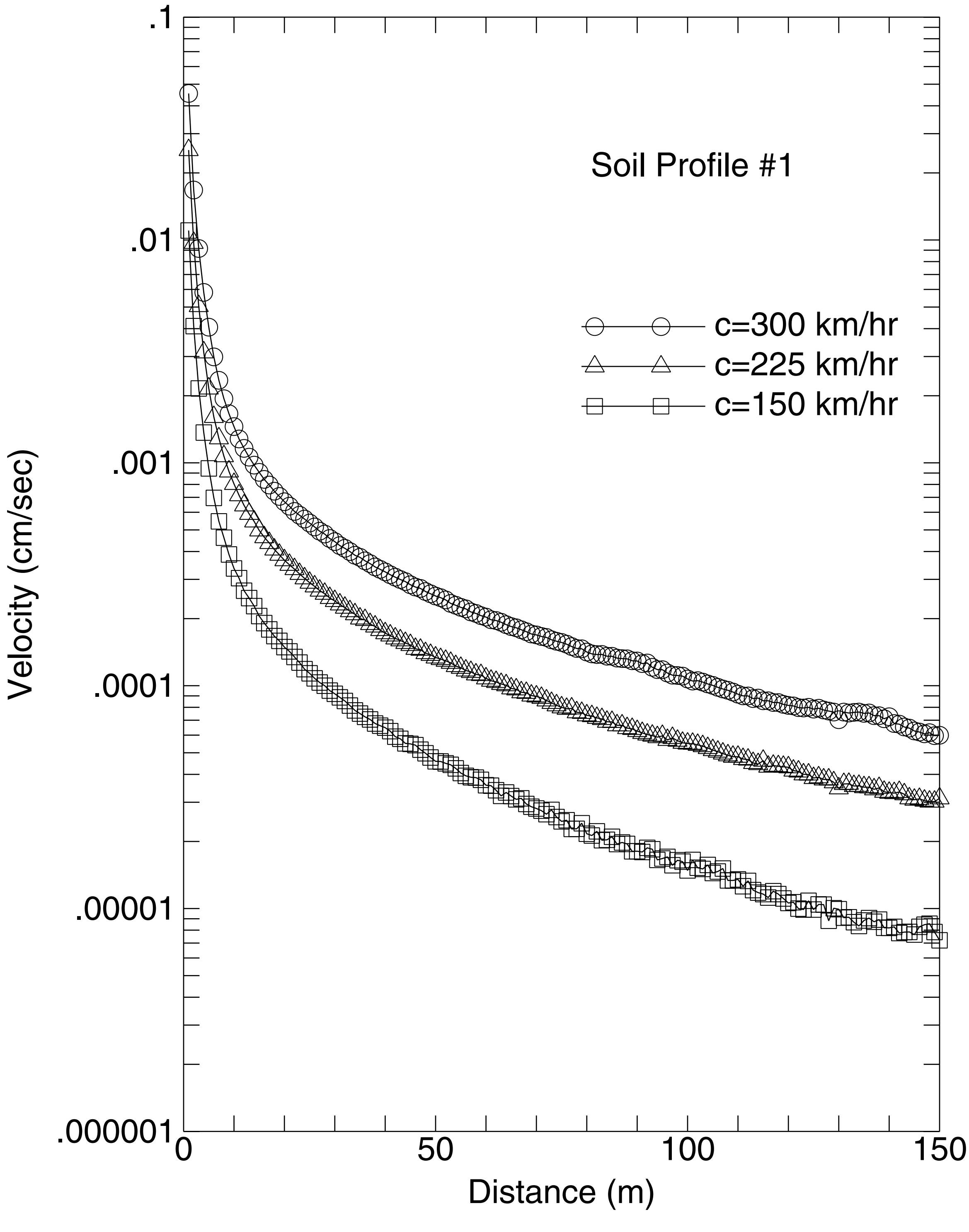

Figure 3.3 – Vertical velocities (cm/sec) induced by a
High-Speed Train on Soil Profile #1.

Using a reference level of 10^{-6} in/sec, 48 dB translate to 6.38×10^{-4} cm/sec. For less sensitive factories, an acceptable level is 90 dB and that translates to a velocity of 8.03×10^{-2} cm/sec. These are the values to watch for in the graphs which follow.

Shown in Figures 3.3 through 3.6 are four plots which illstrate the decay of velocity amplitudes as a function of perpendicular distance from the track, they represent computed results for soil profiles #1 through #4, respectively. In each plot, there are 3 lines defined by a symbol: a circle to identify responses to a fast train operating at 300 km/hr, higher than the normal speed of THSR. The line with triangular symbols is used for response to a medium speed train at 225 km/hr, closer to the actual operating speed. Finally, the line with square symbols show the response to a slower moving train at 150 km/hr, a speed that a train would operate near a crowded city center.

In Fig. 3.3, the response of a firm soil medium represented by soil profile #1 is shown. The vertical velocity in cm/sec was plotted using a logarithmic scale and the figure clearly indicates that a faster train would cause more vibration than a slower one. As indicated earlier, the higher speed tends to compress the total load of the train in a shorter period of time at a source point and thus, a high load per unit length of the track. The response curves are also quite smooth because a uniform soil medium has no reflection nor refraction from a layered structure beneath the ground surface. At high train speed, the vibration level drops to 48 dB approximately 30 meters from the track. If the train is slow, the 48 dB level can be reached within 10 meters of the track. This result is valid only for surface train tracks.

Fig. 3.4 shows the response of a medium soil medium represented by soil profile #2. With it's top layer shear wave velocity at 330 m/sec, compared to 500 m/sec for soil profile #1, it has roughly $(330/500)^2$, or 44% the stiffness of soil profile #1. This is still considered to be a good foundation to build a train track on, as the 48 dB vibration is reached as near

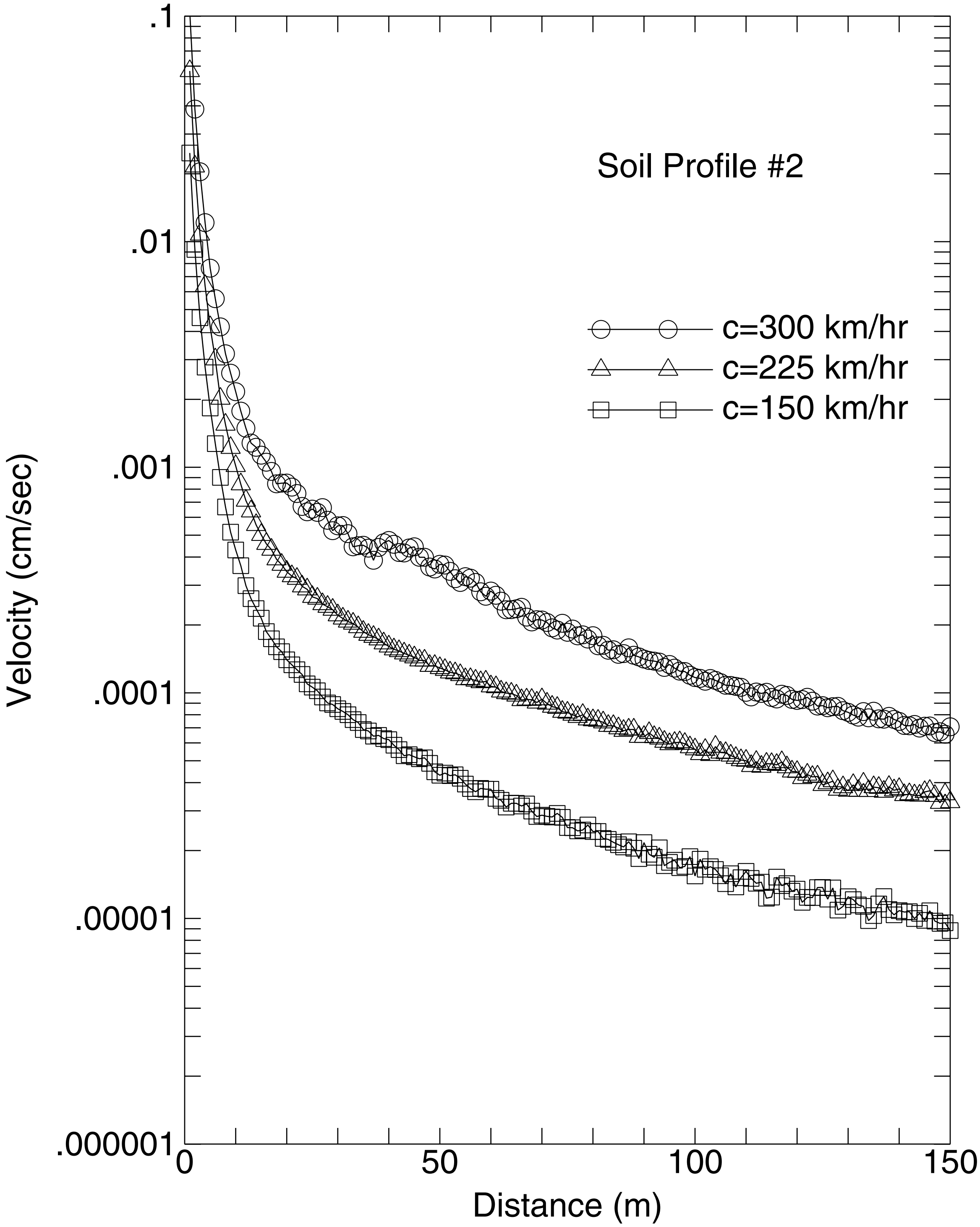

Figure 3.4 – Vertical velocities (cm/sec) induced by a High-Speed Train on Soil Profile #2.

as 30 meters from the track for a fast train and 15 meters from the track for a slower train. Without a large contrast of layer stiffness between the top layer and those below it, there is a minimal effect of soil layering on the response.

Figures 3.5 and 3.6 show the response of two softer layered soil medium, soil profiles #3 and #4. The top layer of soil profile #3 has a shear wave velocity of 175 m/sec while the top layer of soil profile #4 has a shear velocity of 130 m/sec. Based on those numbers, it appears that soil profile #3 is stiffer than soil profile #4, but the layers of the two profiles are quite different and caused some surprising results in the analyses to follow. Overall, soil profile #3 appears to be less stable, the results show considerable resonance behavior of the top layers over a stiffer half space below.

For a fast train, the 48 dB level can be achieved for soil profile #3 when it is over 60 meters away from the train track. For a slow train, the same can be accomplished with a distance of 25 meters. The results indicated that significant vibration should die down roughly one street away from the train track. At greater distances away from the track, perhaps over 100 meters away, the responses become less predictable and random, many different incident waves now exist because of reflected waves from the layers below. Later plots in the time domain will illustrate more clearly the resonance effects caused by vibration energy being trapped in the top layers.

Fig. 3.6 illustrates that the vibration level is significantly higher for very soft soil profiles near the agricultural areas. Although the stiffness of the top layer is too small to carry large loads, the vibration generated is significant because of resonance. Most likely, for soil media with this type of soft top layers, pile foundations are required. Therefore, the plots shown in Fig. 3.6 is an academic exercise rather than results of practical importance. But it is kept in this section to illustrate the difference between the stiff and soft soil layer.

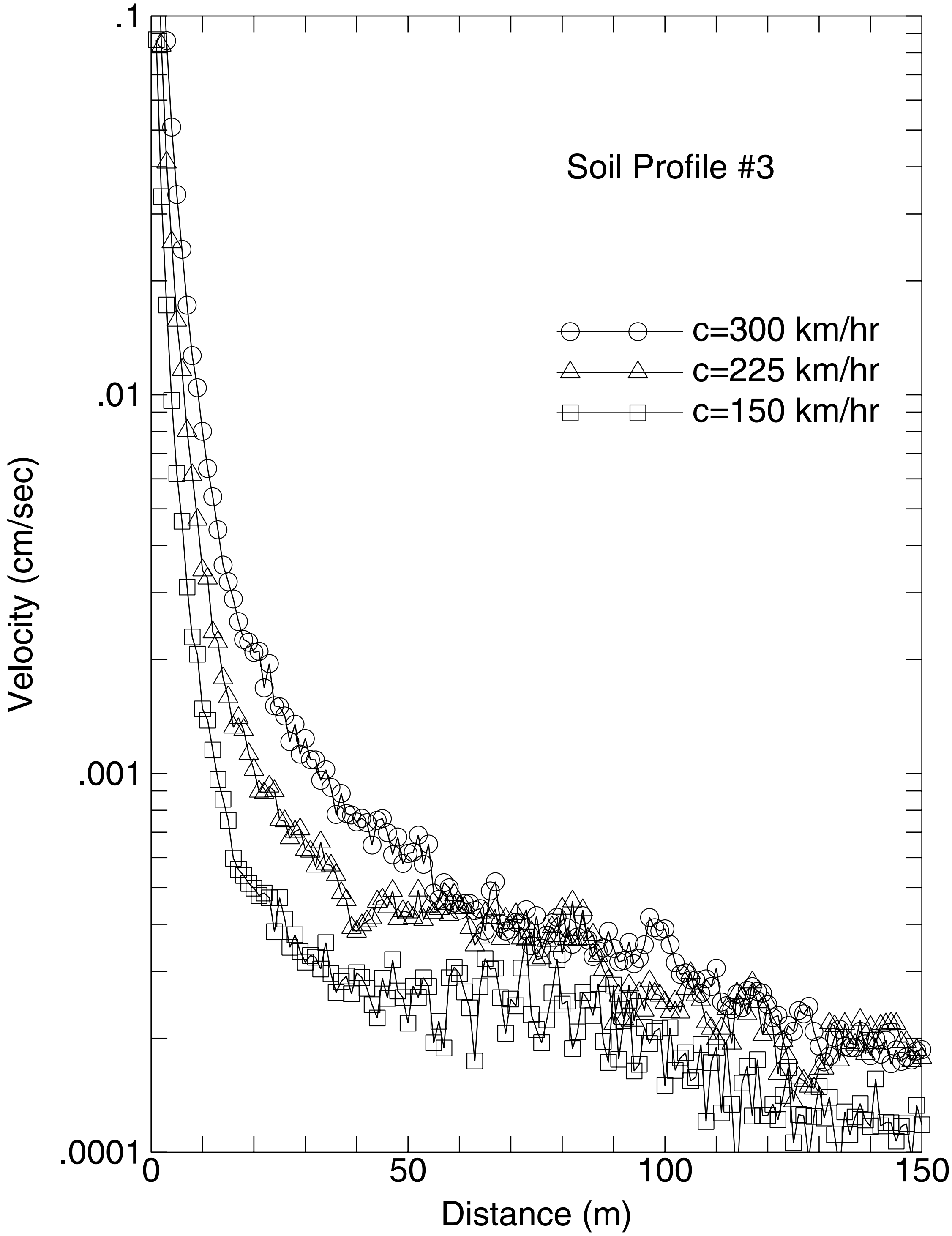

Figure 3.5 – Vertical velocities (cm/sec) induced by a High-Speed Train on Soil Profile #3.

For this particular soil profile, the 48 dB level is reach at a much larger distance of 130 meters away from the track and a shorter distance of 100 meters if the train is slower.

3.5 – Time Histories of Train Generated Vibration

The results in Figures 3.3 through 3.6 are the maximum velocity values for the time histories calculated at various perpendicular distances from the train track. But a great deal can be learn by studying the time histories themselves. Shown in Fig. 3.7 is the response of the uniform firm soil medium to the fast train at 300 km/hr. The top plot is the loading function $L(t)$ normalized by a factor of 10 kilo-Newtons to fit the scale. The spiking appearence of the loading function is caused by the fact that there are separation between the wheels and the track is loaded and unloaded quickly, depending on the speed of the train.

The next five plots beneath the loading function in Fig. 3.7 are the response of at distances of 1, 2, 3, 4 and 5 meters away from the track. They are plotted on a common scale so it is clear that the attenuation is very quick. That is the reason why the earlier plots were made with a logarithmic scale. Beneath the in-close responses are 4 plots made for larger distances of 20 meters, 50 meters, 75 meters and 100 meters from the track. Significantly different scales are used for the distance responses to see how the shape of the vibration has changed over distance. It is clear that the response near the track has a similar shape to the loading function, i.e., large loading and unloading type of cyclic response. The distance results, though much smaller, have different shapes. The low frequency vibration has started about 2 seconds before the train arrives at the same x-coordinate as the observer. For subsonic loading, as all these cases are, the vibration can reach the observer before the train arrives. Clearly, for a uniform soil medium such as soil profile #1, the distant response has a very low frequency content because the higher frequency components have been damped out.

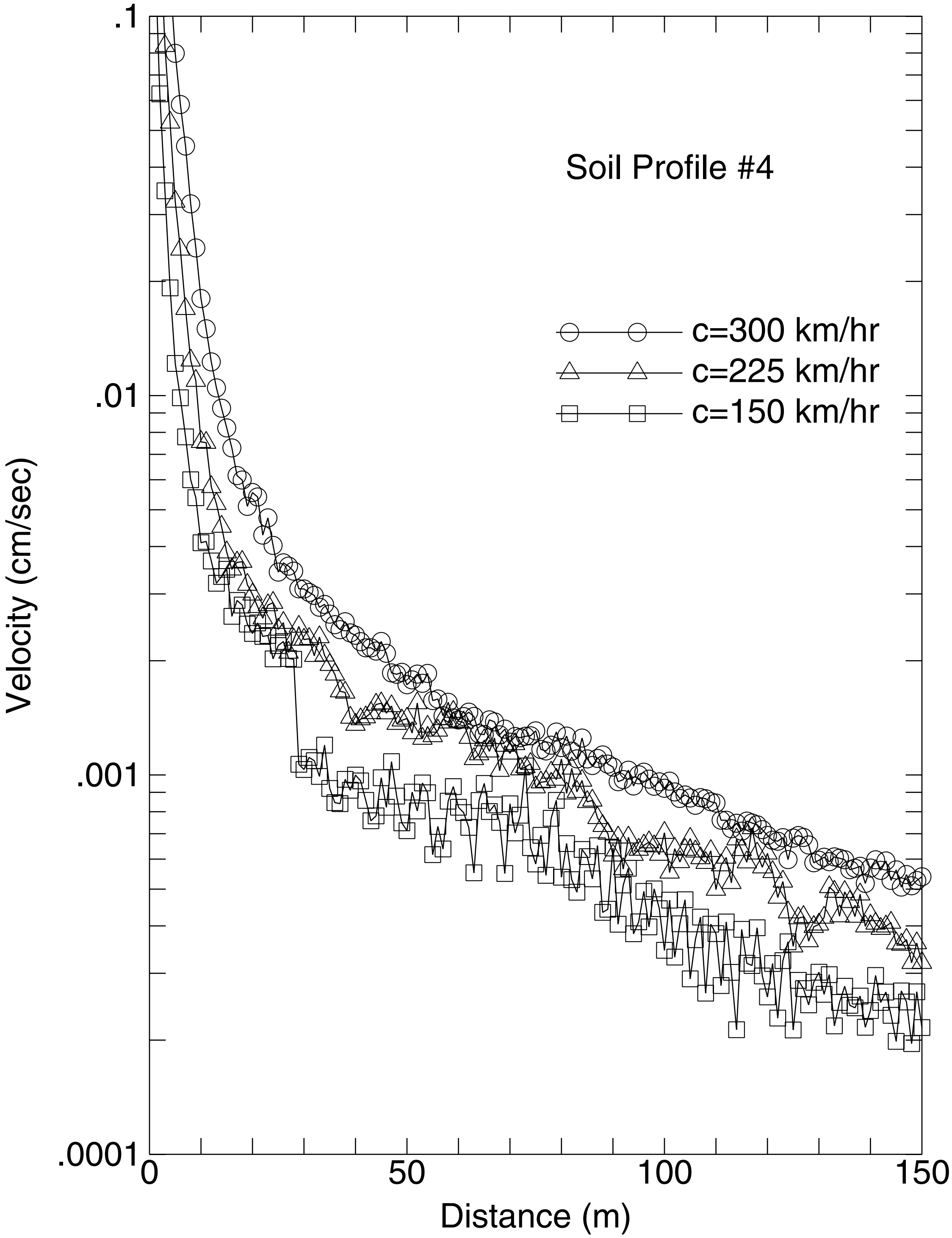

Figure 3.6 – Vertical velocities (cm/sec) induced by a High-Speed Train on Soil Profile #4.

Shown in Fig. 3.8 is the response to the same loading on soil profile #2. The near-track locations have similar response, although slightly larger. But the response at 20 meters appears entirely different because of the interference of waves caused by the underlying stiffer layer. For the farther locations, the same higher frequency content exists and it is quite clear that it is a characteristic that the soil medium processes.

Figures 3.9 and 3.10 show more resonance of the soil layers in responses far away from the source. Although the level of vibration has signifcantly been reduced at the far distances, but the resonance frequency of the soil layer could be near the resonance frequency of a structure and that could amplify the amplitude of the vibration. With different types of buildings near the THSR route in densely populated Taiwan, it is not unlikely that some structure would have a similar resonance frequency. It is also possible that some sensitive equipment inside a factory could have a mounting unit which has a vulnerability at some of these same frequencies.

Fig. 3.10 is the response of soil profile #4 to the slower train speed of 150 km/hr. In a densely populated city center, such as Tainan Science Park, the trains normally operate at a lower speed. For such the case, the vibration level is entirely affected by the resonance behavior of the soil layer. At greater distances, the fundamental modes of the soil layer is clearly depicted in the vibration singals.

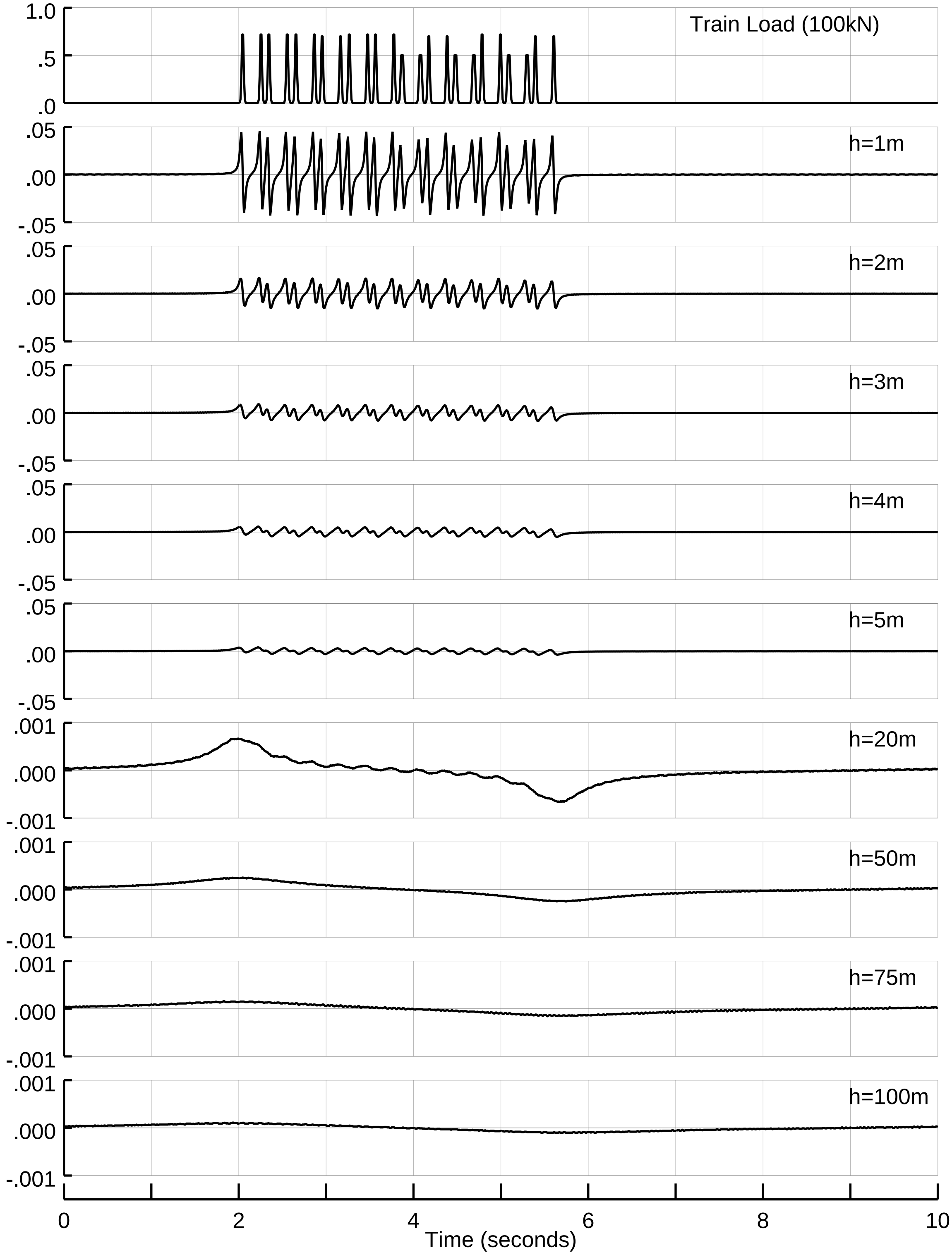

Figure 3.7 – Vertical velocities (cm/sec) induced by a High-Speed Train on Soil Profile #1.

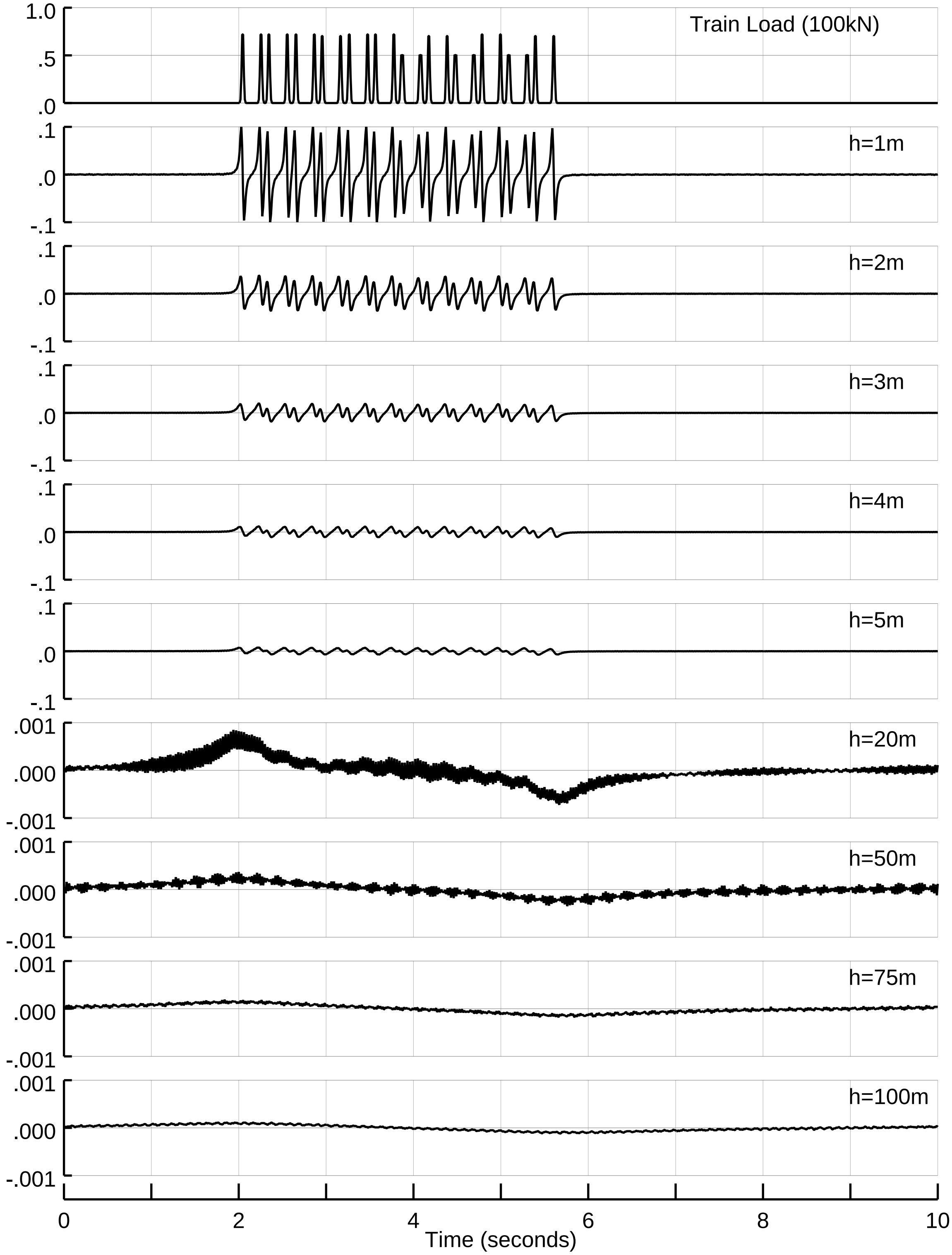

Figure 3.8 – Vertical velocities (cm/sec) induced by a High-Speed Train on Soil Profile #2.

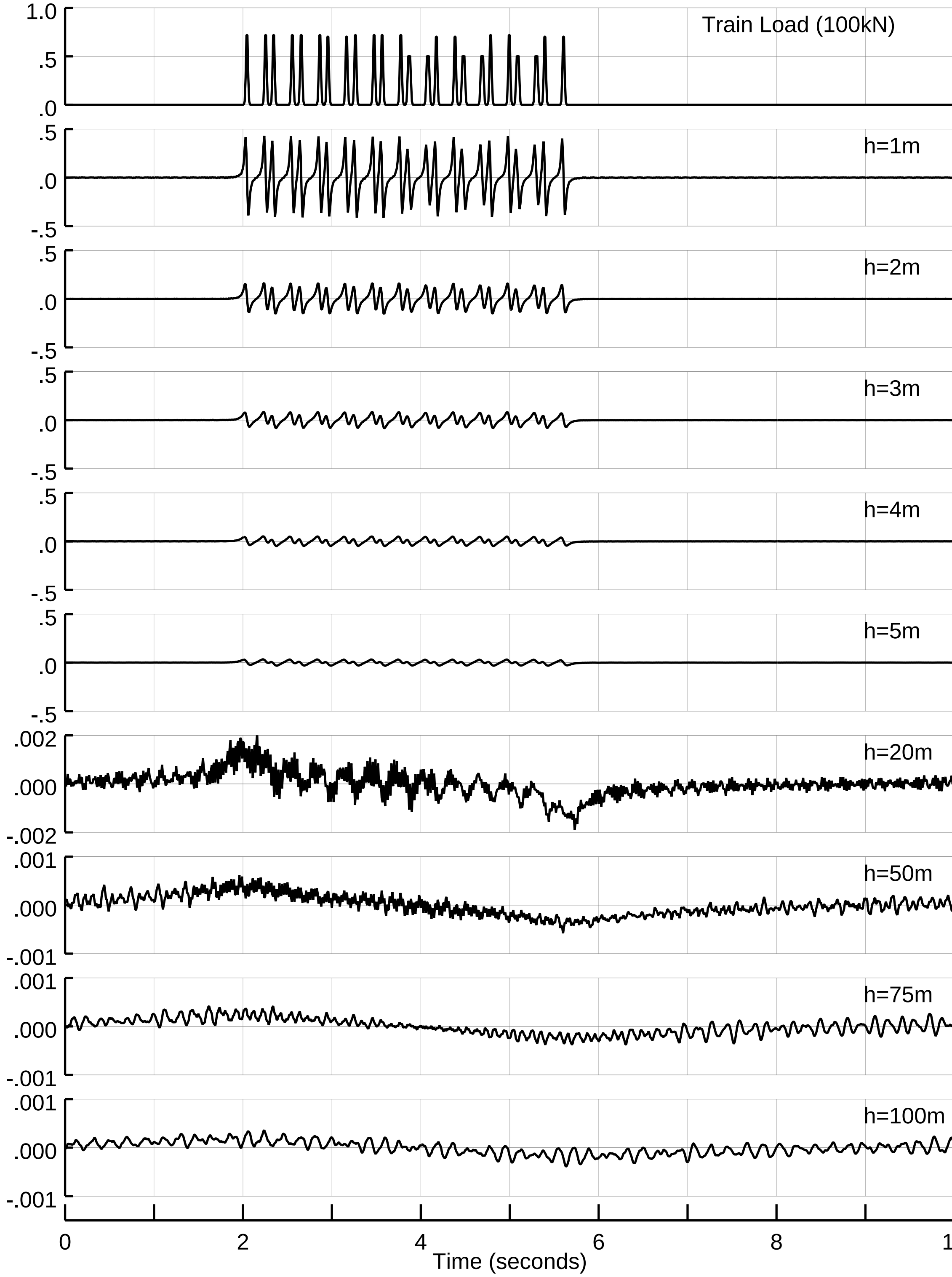

Figure 3.9 – Vertical velocities (cm/sec) induced by a High-Speed Train on Soil Profile #3.

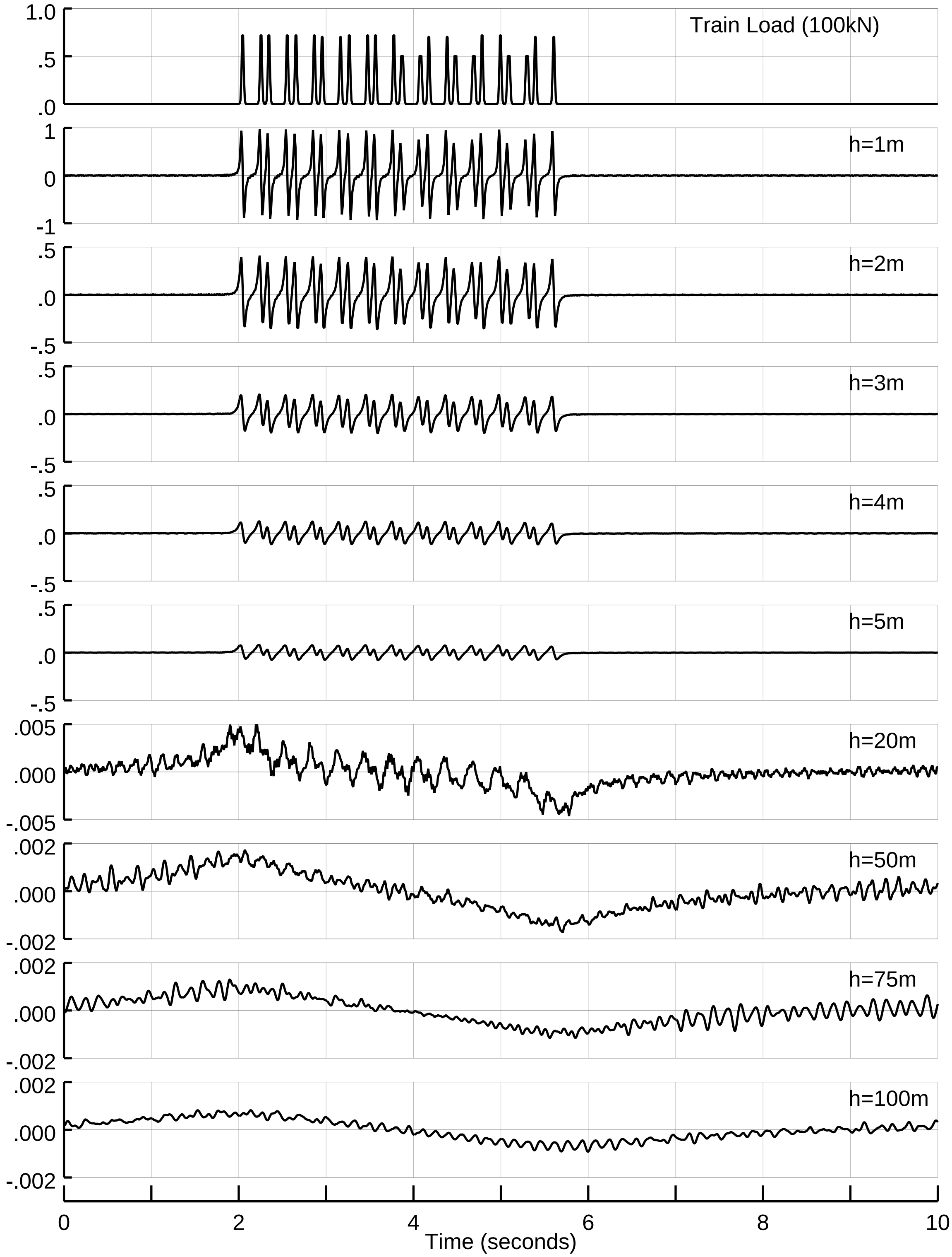

Figure 3.10 – Vertical velocities (cm/sec) induced by a High-Speed Train on Soil Profile #4.

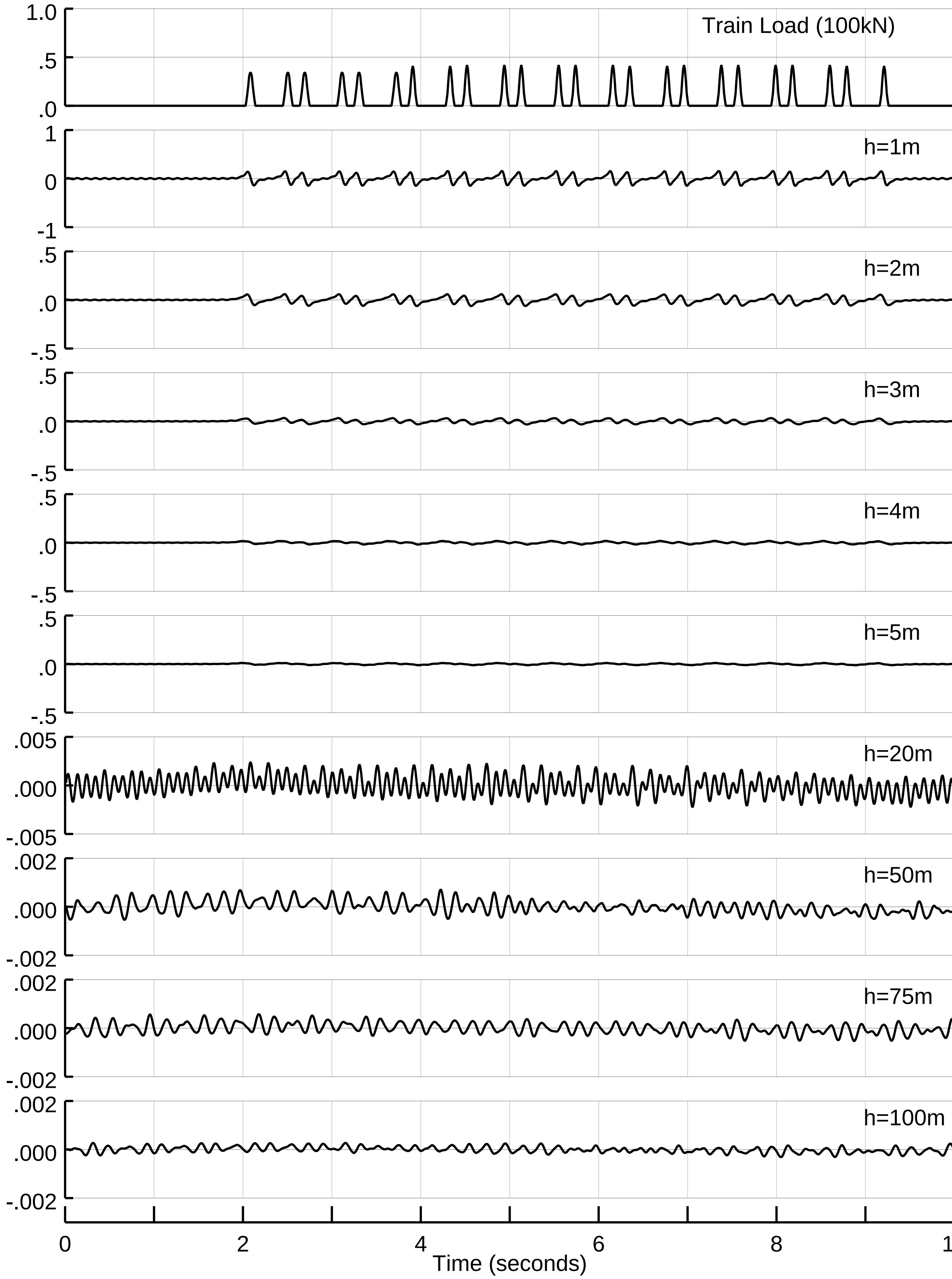

Figure 3.11 – Vertical velocities (cm/sec) induced by a
Slower Train on Soil Profile #4.

3.6 – Effect of Source Depth on Vibration Level

The previous sections concentrated on ground response to a load applied on the top of the surface. Since 70% of THSR rails are elevated with the bridge supported by columns roughly 30 meters apart. The sources are therefore not on the surface but rather, the load carrying members are buried deeply into the soil medium as long piles in pile groups. In this section, an anaysis of the effect of the depth of the load will be analyzed by a simple model in which a maximum axle load of 14 tonnes load is (1) applied on the surface, (2) distributed over a depth of 20 meters and (3) distributed over a depth of 40 meters.

Shown in Fig. 3.12 are the velocity response to a harmonic load applied in soil profiles 1 and 2 as defined in Fig. 2.6. These two soil profiles are the stiffer of the four profiles, therefore, the amplitude of the velocity is lower. The left column of graphs represents the response for soil profile 1 at distances of 5m, 25m and 100m from the source. The right column of figuresrepresents the same for results for soil profile 2. It is consistent that the deeply distributed source model has a significantly lower response than that of the surface loads. This brings to light the validity of experiments conducted by dropping a heavy weight at the surface of a medium and then measure the response of the surrounding area; the recorded data would overestimate the response if the load is to be distributed beneath the surface by a pile foundation.

Shown in Fig 3.13 are the velocity response reported in the same manner except for soil profiles 3 and 4, the softer soil profiles encountered in the THSR project. It is still clear that the deeply distributed loads reduces the response as compared to a surface load. There are some overlapping of amplitudes at larger distances from the source, but the deep sources help excite the softer top layers and some resonance may occur. The time domain response is expected to yield a similar reduction of amplitudes because the transfer functions in the frequency domain are consistently lower for the deeply embedded sources.

3.7 – Ground Motion Generated by Elevated Bridges with Pile Foundations

One factor remains to be investigated is that the load on one particular column could be much larger than the surface loading at a given location. With the length of the train at 305 meters long and the span of the columns at approximately 30 meters, one tenth of the weight of the train could be applied to a column at any given time. The load on one pile group can be 50 tonnes, whereas the highest value for surface track is a combination of two axles, side by side, giving rise to a load of 22 tonnes. The load of 50 tonnes is basically a simple application of equilibrium concepts of Newton's First Law; the dynamic effects of the bridge will be considered later in Chapter Four. Once the resonance of the bridge enters into the analysis, the load from a column could be significantly larger than the 50 tonnes estimated.

Assume the elevated concrete bridge is rigid and that the load is distributed uniformly by a free body diagram as shown in the schematic in Fig. 3.14. The elevated bridge is supported by columns with spacing of 30 meters. A traveling axle load, P_0, is applied at a location q from the center column and it would generate a loading function of time as

$$P(t) = \left(1 - \frac{\mid q(t) \mid}{30}\right) P_0 \qquad , \tag{3.25}$$

in which P_0 is the value of the axle load. With the location of the i-th axle load defined by

$$x_i(t) = ct + d_i \qquad , \tag{3.26}$$

in which c is the velocity of the train and d_i is the distance of the i-th axle measured from the head of the train.

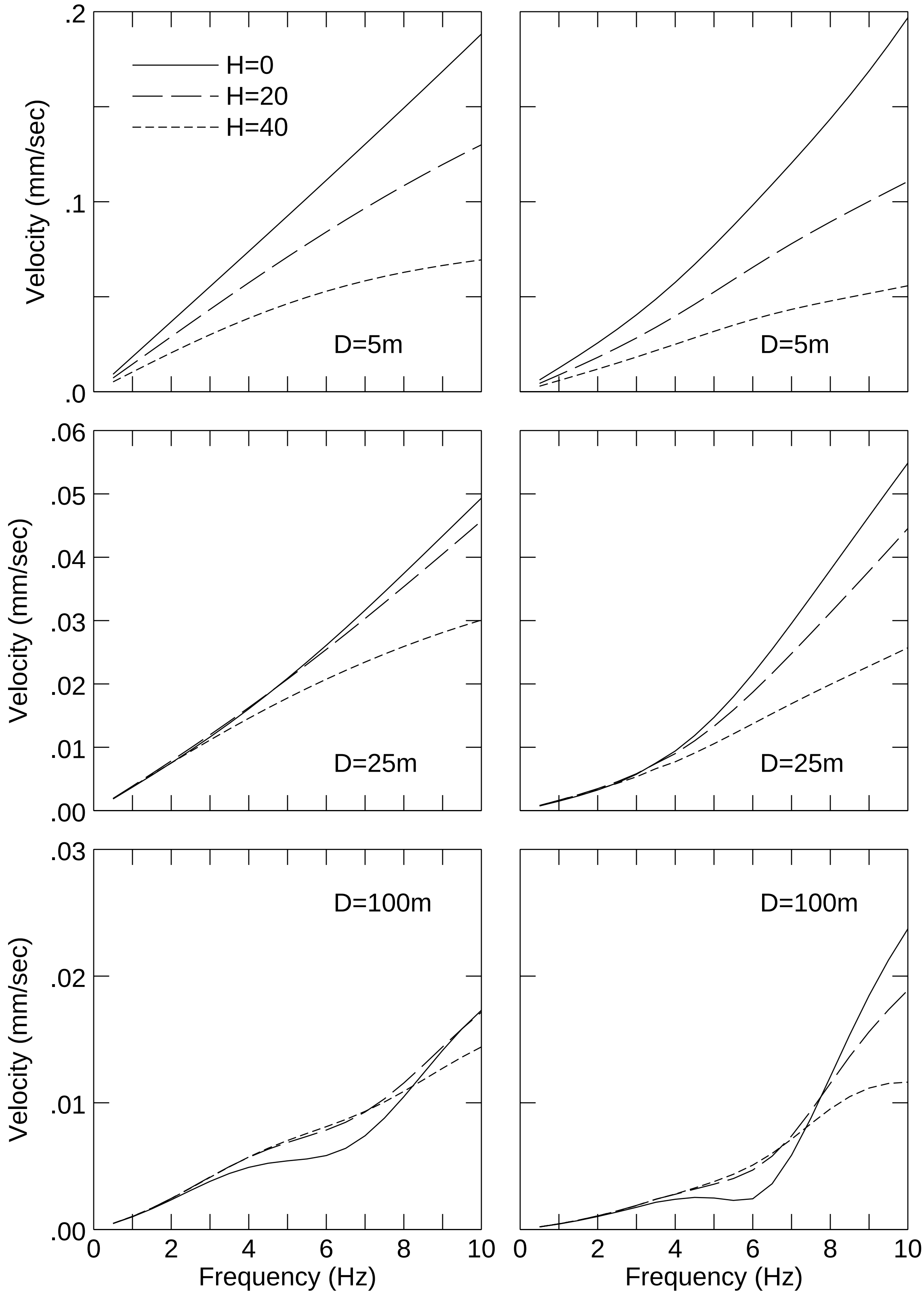

Figure 3.12 – Harmonic velocities (mm/sec) induced by point loads of various depths. Soil Profiles 1 and 2.

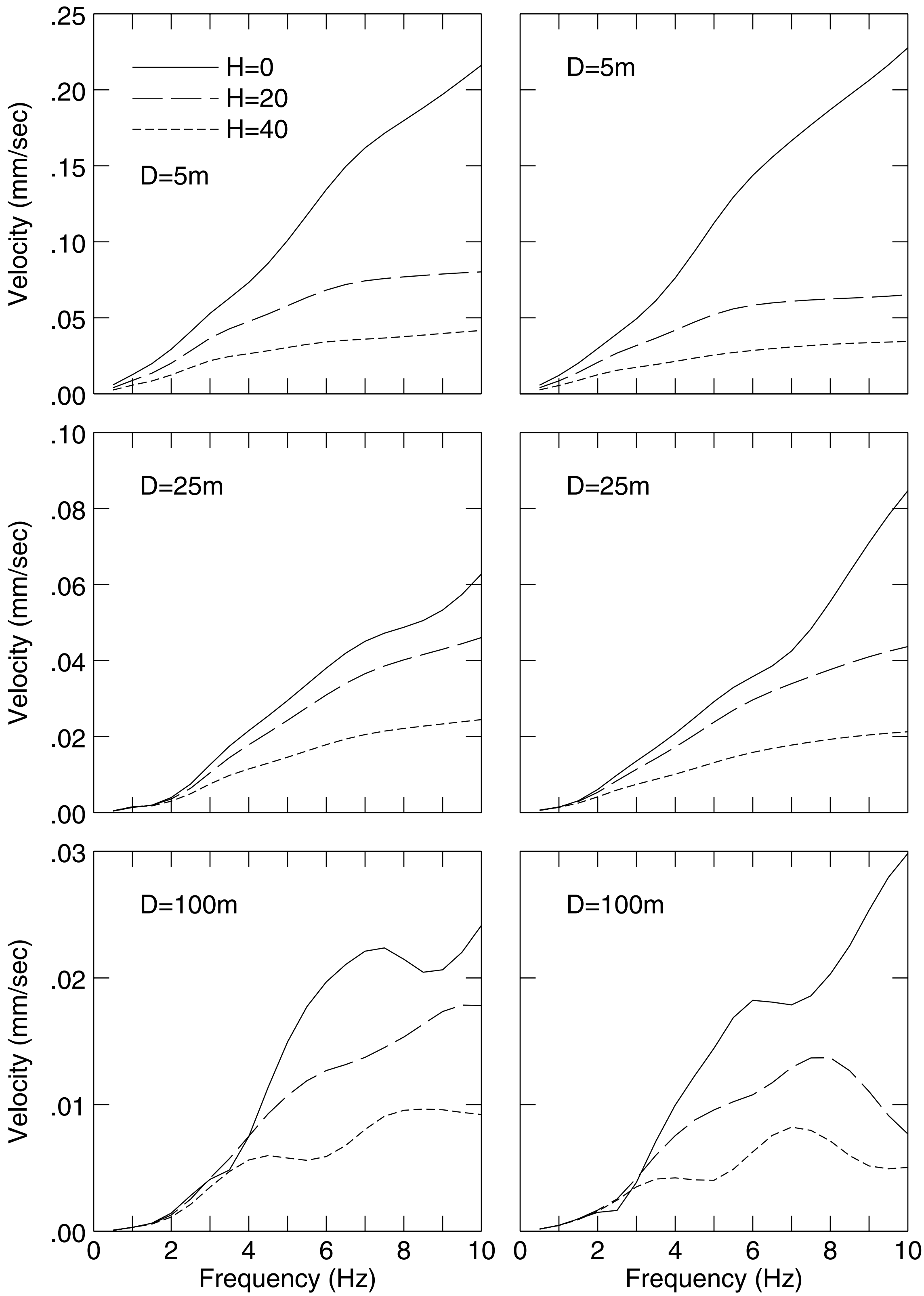

Figure 3.13 – Harmonic velocities (mm/sec) induced by point loads of various depths. Soil Profiles 3 and 4.

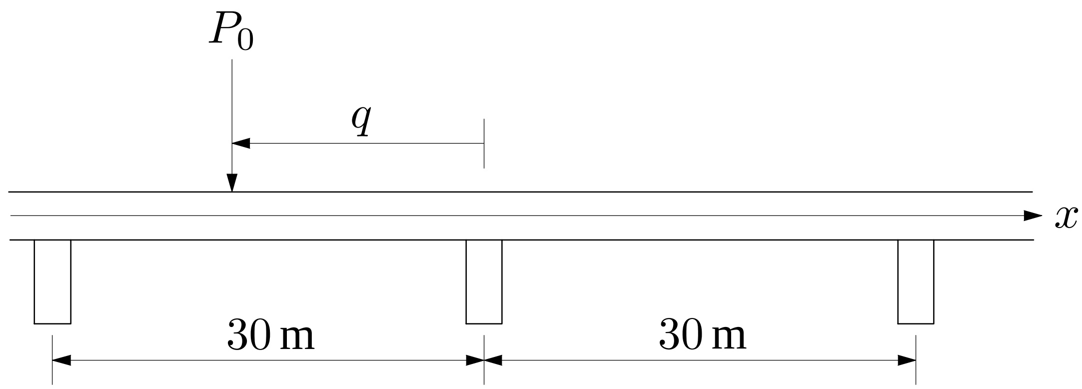

Figure 3.14 – Moving load on a rigid elevated bridge.

Using the configuration as shown in Fig. 3.14, $q_i(t)$ for the i-th axle can be defined as

$$q_i(t) = x_i(t) - 30 \qquad ; \qquad -30 < q_i(t) < 30 \qquad . \tag{3.27}$$

The restrictive range of ± 30 is placed on $q_i(t)$ because the axle loads outside that range would be supported by a different column. For a train with N_a axles, the load function $L(t)$ at a particular column is

$$L(t) = \sum_{i=1}^{N_a} \left(1 - \frac{|\, q(t) \,|}{30} \right) P_i \qquad , \tag{3.28}$$

in which P_i is the load of the i-th axle.

Shown in Fig. 3.15 is the column load function for a 503 tonnes train traveling at speeds of 300 km/hr, 225 km/hr and 150 km/hr. The maximum value of the load is the same; it is the weight of the train within the span of 30 meters. From first glance, the load for the slowest train speed should cause more ground vibration because it is a high load applied over a longer period of time. But the results to be shown later do not follow that logic because the shorter duration load at c=300 km/hr has a higher frequency content than the

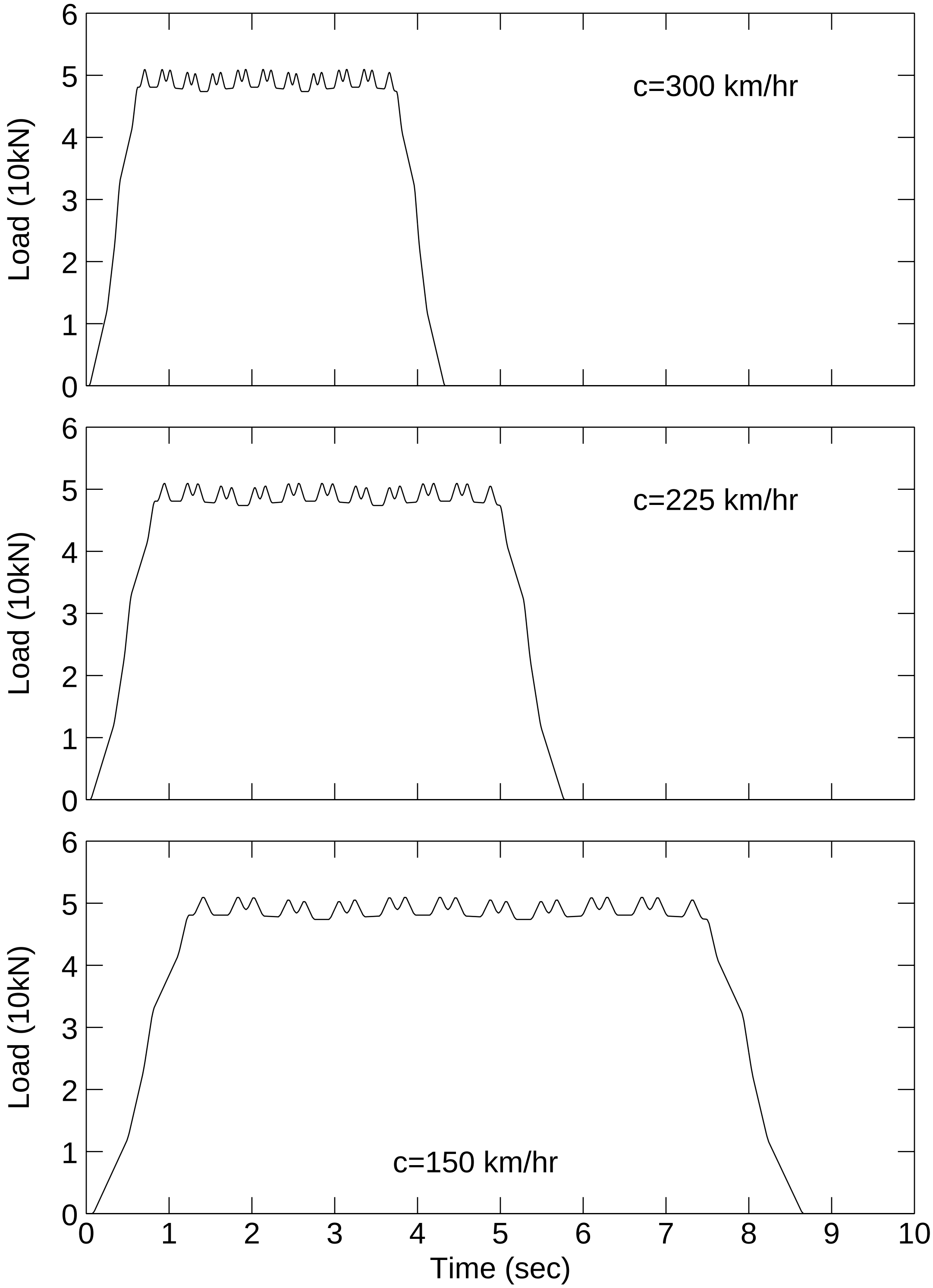

Figure 3.15 – Loading time functions on a column.

longer duration load profiles and the high frequency components cause higher velocities and accelerations.

Since the train is assumed to operate at a constant speed, the load applied at one particular column would be the same at another column, except, delayed by a time factor τ. Consider the difference between $L(t)$ and $L(t-\tau)$ by first taking the Fourier Transform of $L(t)$ as

$$L(\omega) = \int_{-\infty}^{\infty} L(t)\, e^{-i\omega t}\, dt \qquad . \tag{3.29}$$

The loading function, $L(t-\tau)$, has a similar Fourier Transform defined as

$$L_\tau(\omega) = \int_{-\infty}^{\infty} L(t-\tau)\, e^{-i\omega t}\, dt \qquad . \tag{3.30}$$

Using a variable substitution, $q = t - \tau$ and $t = q + \tau$,

$$\begin{aligned} L_\tau(\omega) &= \int_{-\infty}^{\infty} L(q)\, e^{-i\omega(q+\tau)}\, dq \\ &= e^{-i\omega\tau} \int_{-\infty}^{\infty} L(q)\, e^{-i\omega q}\, dq = e^{-i\omega\tau} L(\omega) \end{aligned} \tag{3.31}$$

The expression in Eq. 3.31 is useful for determining the loading function in the frequency domain. Let $L_0(\omega)$ be defined as the Fourier Transform of the loading function $L_0(t)$ specified at a reference column at location x_0. Then the Fourier Transform of the loading function $L_i(t)$ at the i-th column can be expressed as

$$L_i(\omega) = e^{-i\omega(x_i - x_0)/c} L_0(\omega) \qquad , \tag{3.32}$$

in which the time factor $(x_i - x_0)/c$ has replaced the time delay symbol τ in Eq. (3.31).

Shown in Fig. 3.16 is a schematic of the configuration of the elevated bridge structure. At an observation point at a perpendicular distance h from the bridge, its harmonic motion can be calculated using the Green's Function, f_{zz}, as

$$U_z(\omega) = \sum_{j=-N}^{N} \frac{f_z z(\omega, R)}{\mu R} L_j(\omega) \qquad , \tag{3.33}$$

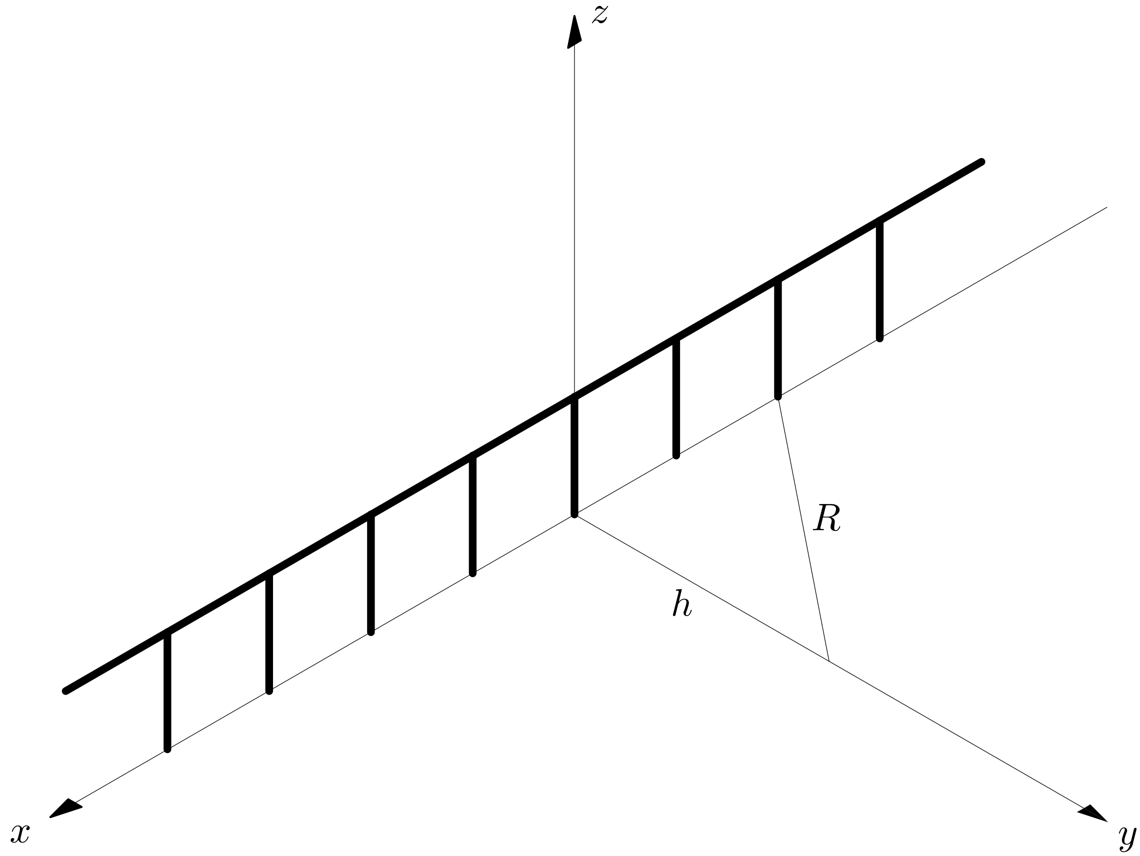

Figure 3.16 – Elevated bridge stucture with equally spaced columns.

in which $R = \sqrt{(x_j - x_0)^2 + h^2}$, μ is the reference shear modulus of the soil medium, and N is a sufficiently large number to include the vibration from a distance column. Using the expression in Eq. (3.32), Eq. (3.33) can be simplified as

$$U_z(\omega) = L_0(\omega) \sum_{j=-N}^{N} e^{-i\omega(x_j - x_0)/c} \frac{f_{zz}(\omega, R)}{\mu R} \qquad , \tag{3.34}$$

The velocity time histories can be obtained from the displacement transfer function as

$$v_z(t) = \frac{1}{2\pi} \int_{-\infty}^{\infty} i\omega U_z(\omega) \, e^{i\omega t} \, d\omega \qquad . \tag{3.35}$$

Shown in Figures 3.17 through 3.21 are the logarithm of velocities generate for soil profiles 2, 3 and 4, respectively. Soil profile #1 was not analyzed in this section because the soil property is firm enough that pile foundations are not required. In each graph, there are three lines for the three different train speed. The lines are identified by 3 symbols, circles for 300 km/hr, triangles for 225 km/hr and squares for 150 km/hr. Figures 3.17, 3.18 and 3.20 show the responses in soil profiles #2, #3 and #4, respectively, for a pile depth of 20 meters. Figures 3.19 and 3.21 show results for a pile depth of 40 meters for soil profiles #3 and #4. Soil profile #2 is sufficiently firm to have only shallow piles.

The curves for this section, with embedded loads, are significantly different from those in the section with surface loads. For small distances such as $h < 5$, the embedded results are an order of magnitude smaller. For large distances such as $h > 100$, however, the surface results are an order of magnitude lower, having the reverse effect. The trend of the surface loaded results have much steeper slopes while the embedded results are more flat over distance. The results indicates that while the piles distribute a large percentage of the load beneath the surface to cause a smaller disturbance on the surface near the columns, the buried loads transmit a great deal of the energy to the far field through the resonance of the layers. The wave medium becomes a wave guide and some Love waves are generated and the surface waves can propagate a longer distance.

Some time histories at various distances are shown in Figures 3.22 through 3.24 for a high speed train (300 km/hr) on soil profiles #2, #3 and #4, respectively. The pile depth for soil profile #2 is 20 meters while for the other two profiles the pile depth is 40 meters. It is clear that the velocity time histories diminish at a much slower rate. These figures are plotted on the same scale for $h = 1$ and for $h = 100$, whereas the figures for the surface loads required different scales for the long-distance results.

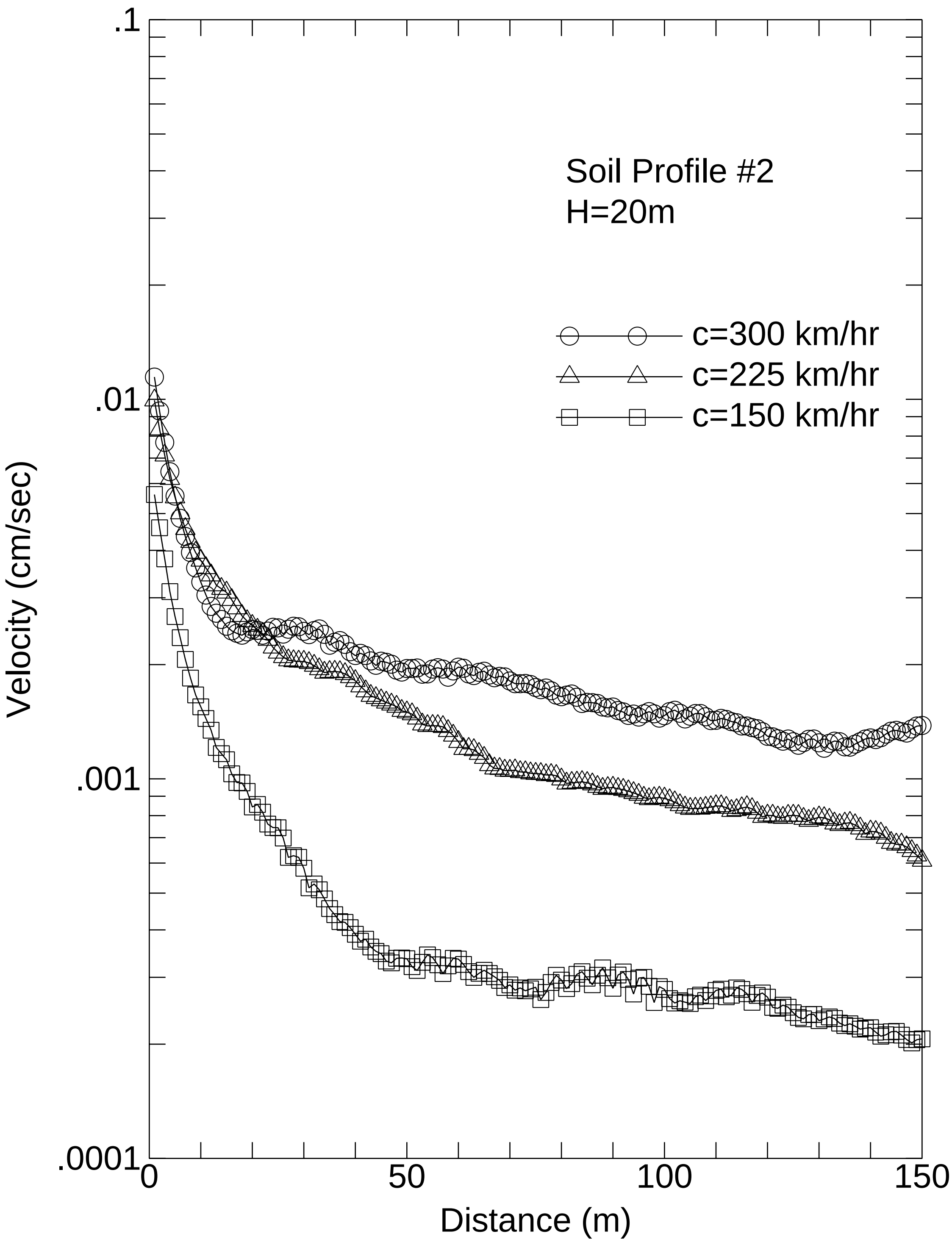

Figure 3.17 – Vertical velocities (cm/sec) induced by a High-Speed Train on Soil Profile #2. Pile depth: 20m.

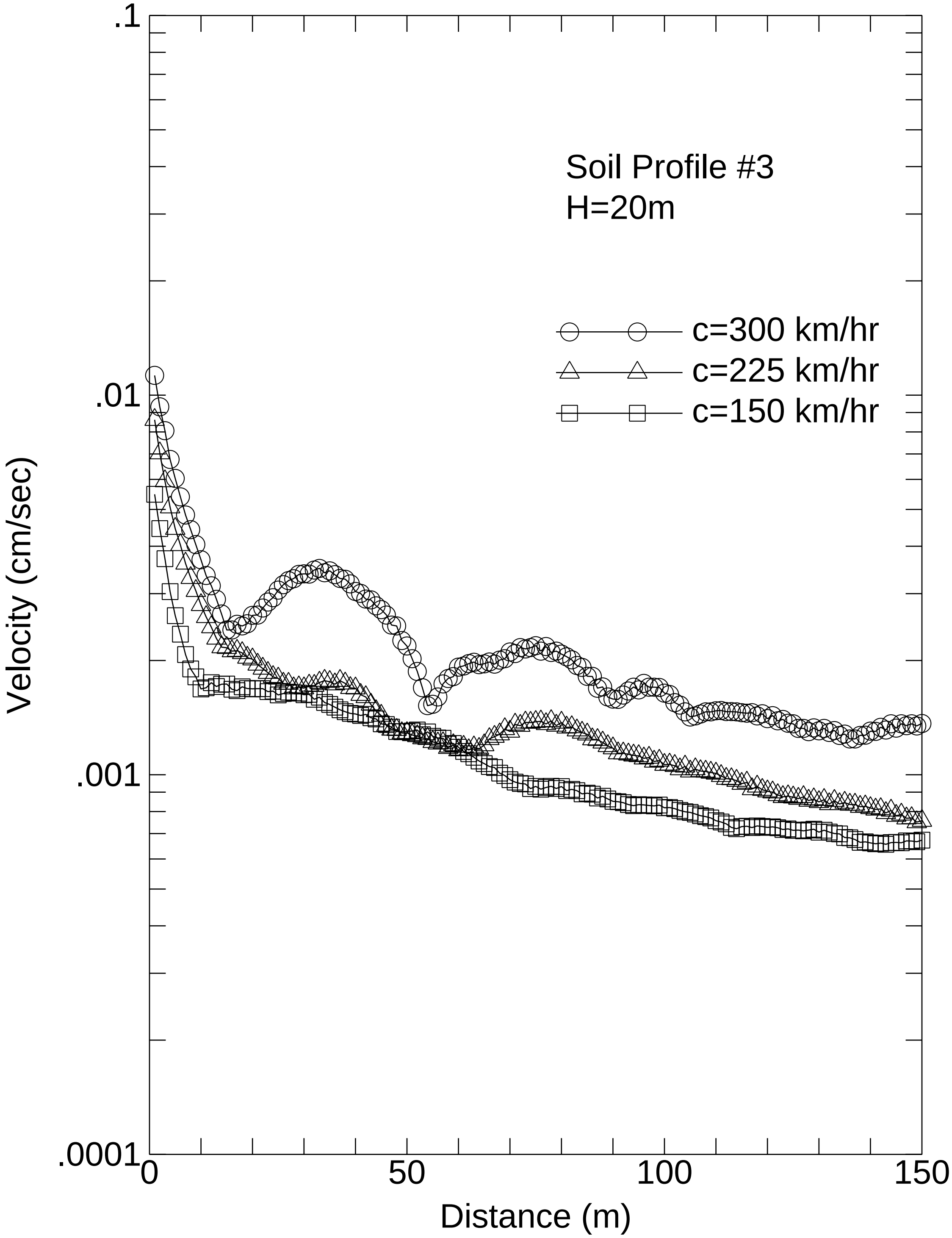

Figure 3.18 – Vertical velocities (cm/sec) induced by a High-Speed Train on Soil Profile #3. Pile depth: 20m.

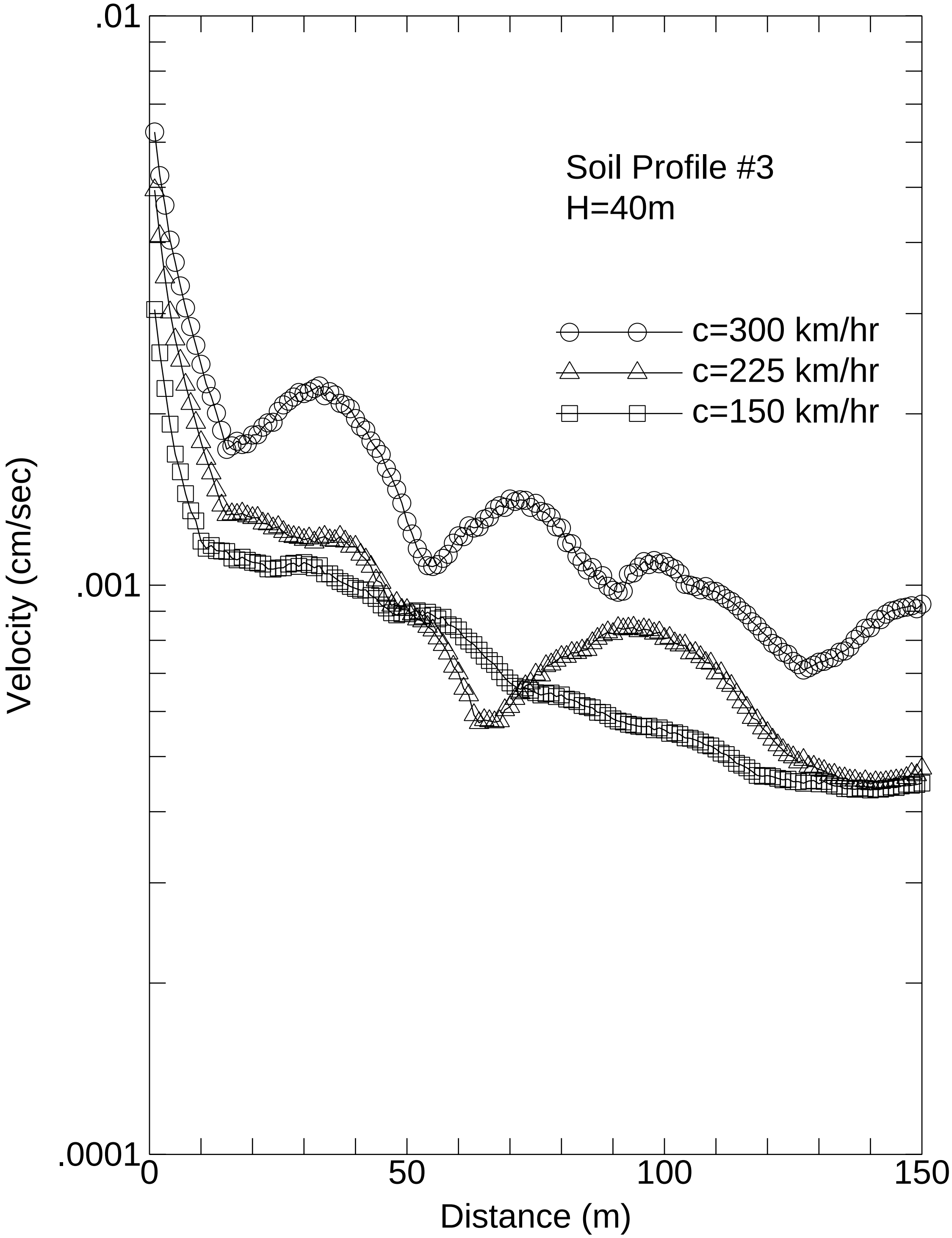

Figure 3.19 – Vertical velocities (cm/sec) induced by a High-Speed Train on Soil Profile #3. Pile depth: 40m.

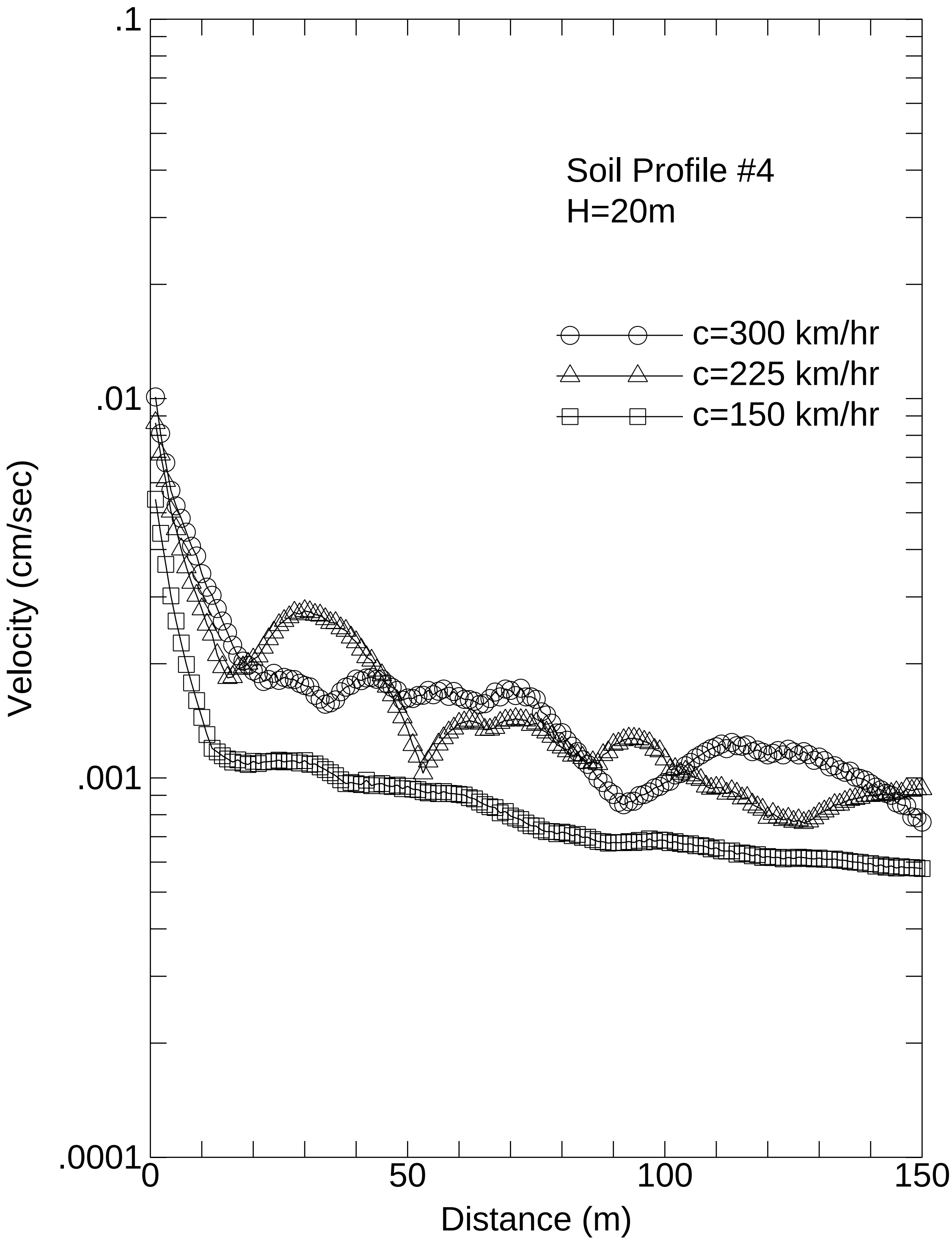

Figure 3.20 – Vertical velocities (cm/sec) induced by a High-Speed Train on Soil Profile #4. Pile depth: 20m.

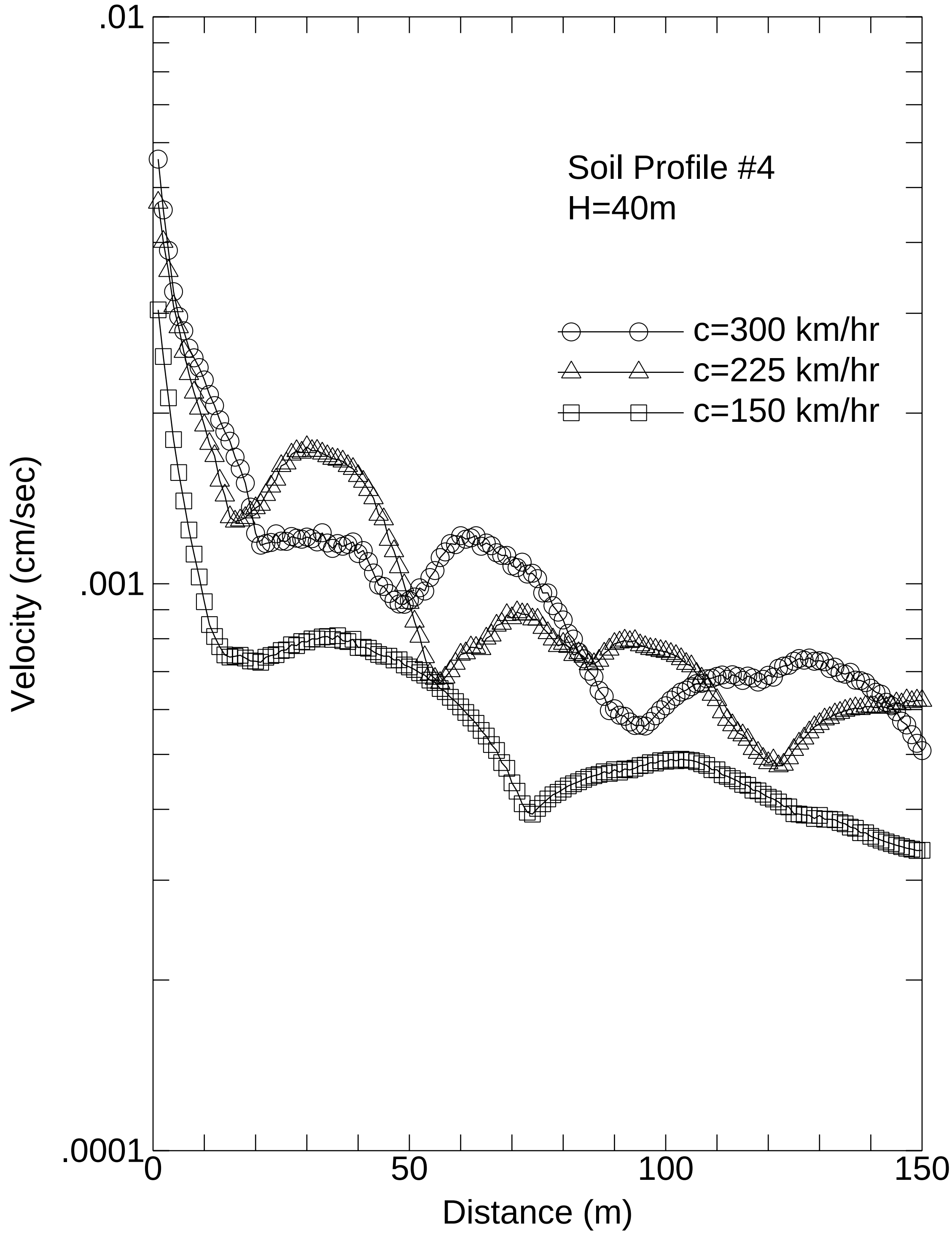

Figure 3.21 – Vertical velocities (cm/sec) induced by a High-Speed Train on Soil Profile #4. Pile depth: 40m.

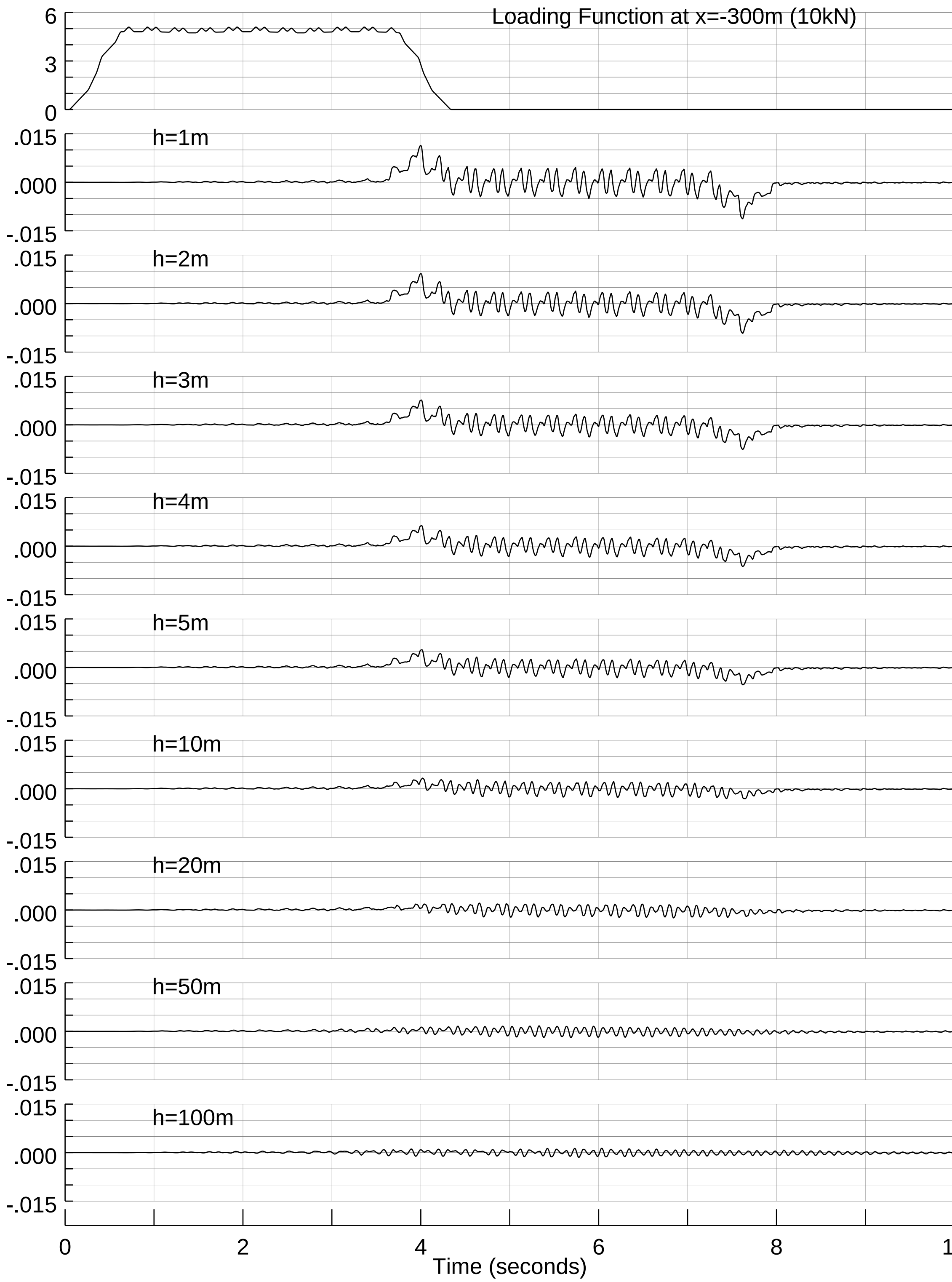

Figure 3.22 – Vertical velocities (cm/sec) induced by a fast train on Soil Profile #2. Pile depth: 20m.

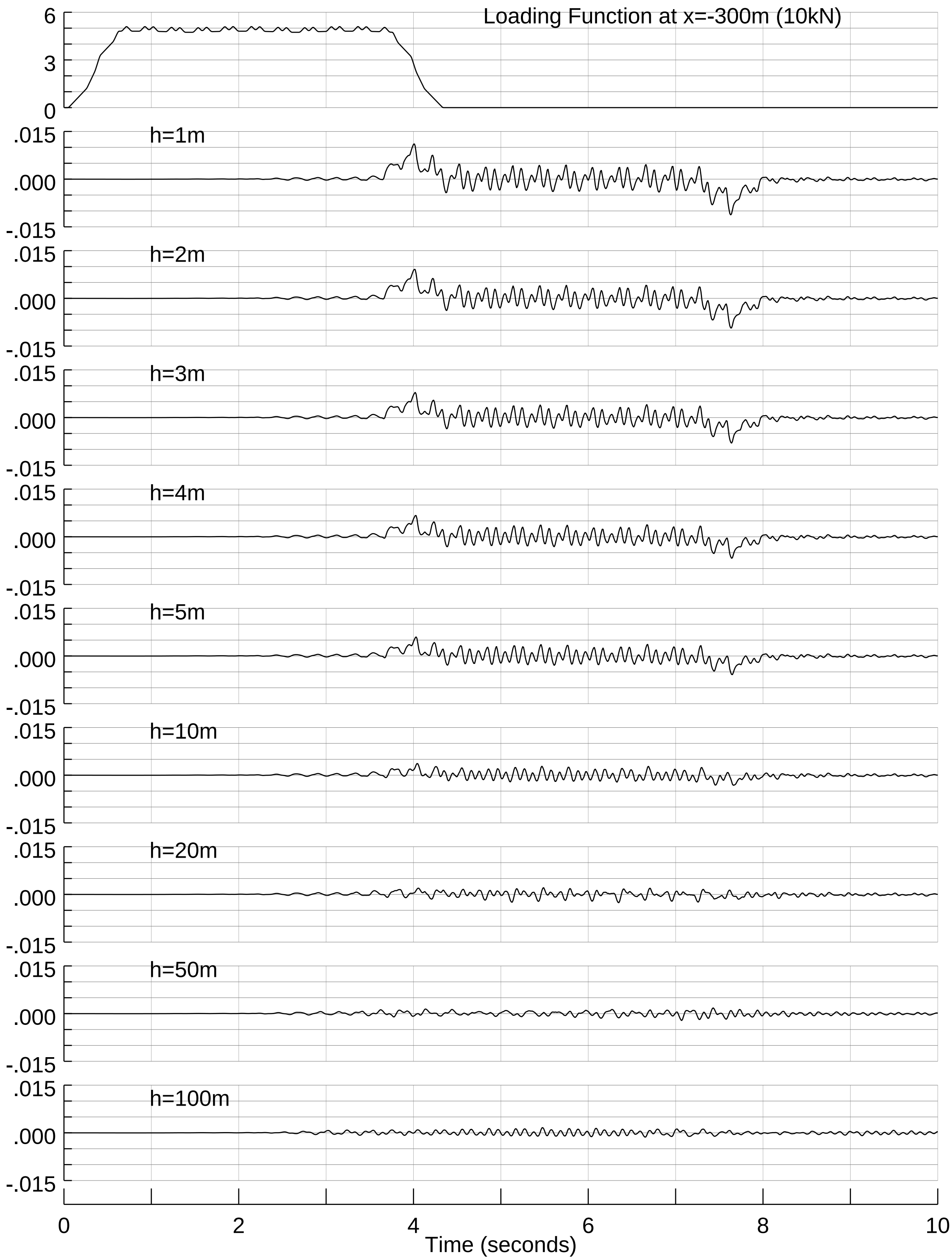

Figure 3.23 – Vertical velocities (cm/sec) induced by a fast train on Soil Profile #3. Pile depth: 40m.

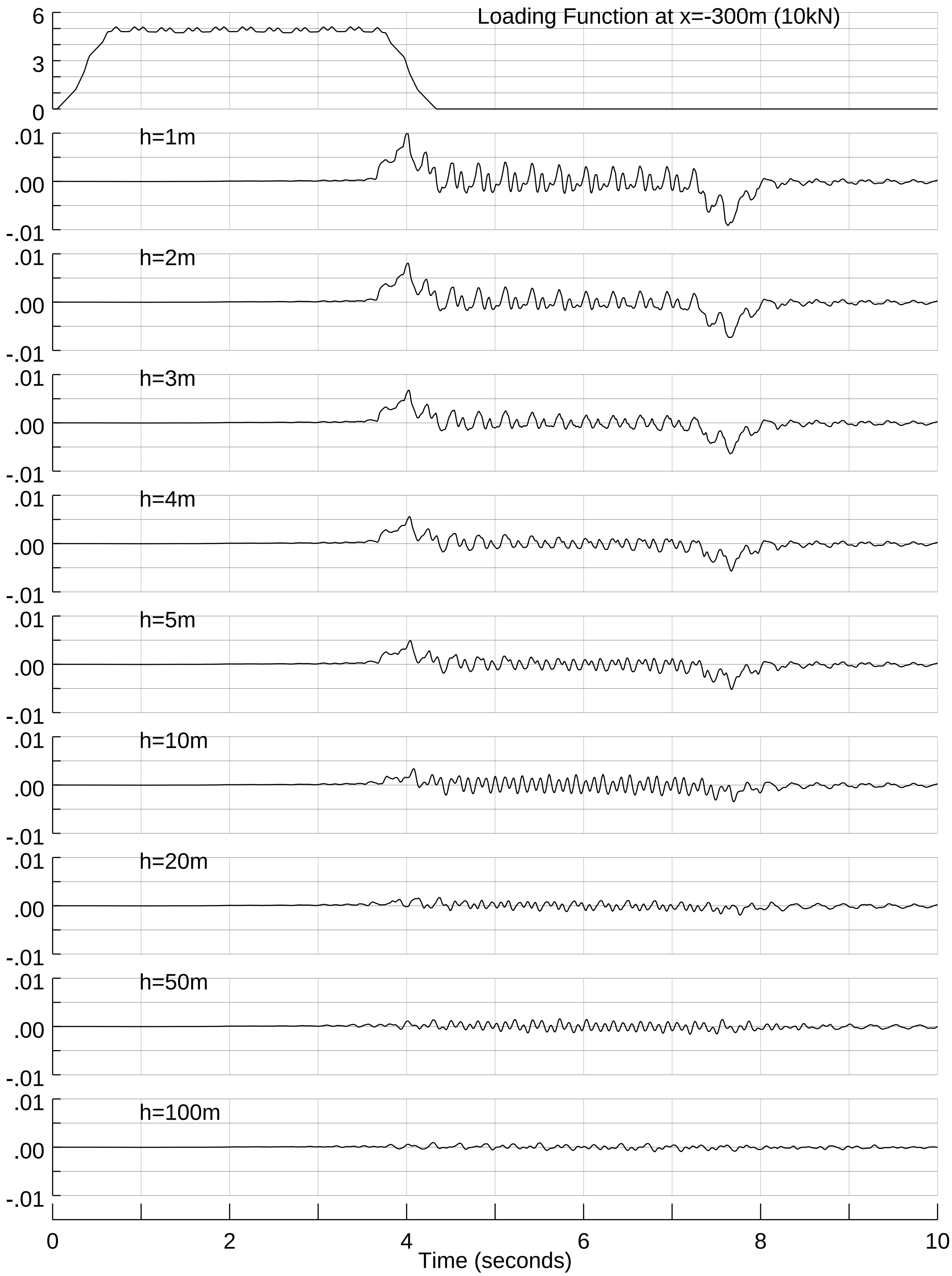

Figure 3.24 – Vertical velocities (cm/sec) induced by a fast train on Soil Profile #4. Pile depth: 40m.

Chapter Four
Dynamic Response of Rail-Support Bridges

There has been reports of possible resonance problem for the rail-support system, a serious safety issue which require special attention. In the THSR project in Taiwan, an unusually high percentage of the high speed track are elevated for several reasons. (1) To reduce the cost when passing through locations with high real estate value. For most of the developed regions of Taiwan that THSR serves, this is the case because those locations of Taiwan are the second most densely populated area in the world, behind only Bangladesh. (2) To avoid having any other activity on the track because accidents would be castastrophic when the high speed with which the trains operate is so high. (3) To control the slope of the bridge over the areas with small but sudden change of elevations. (4) To improve the foundation of the track when the soil condition of the site is not suitable. It is less costly to have piles driven in locations 30 meters apart than to improve the soil condition continuously. It is well known that the elevated bridge, which spans from Changhua to the south of Taiwan, is the longest continuous elevated bridge in the world.

It is proposed here to simulate the interaction between the train, the bridge and the pile supported foundation system. Since the analysis for the pile foundation, constructed withmultiple long piles, typically 5 piles in a group, driven into the soil medium, is difficult and the complete analysis is best performed using a substructures approach.

Shown in Fig. 4.1 is a schematic of a rail-support system, consisting of a hollow concrete horizontal structure placed continuously over columns which are 30 meters apart. The 8-meter tall columns are rectangular with dimensions of 4 meters by 3.5 meters. The columns are supported by pile foundation for locations with soft layers and on large concrete

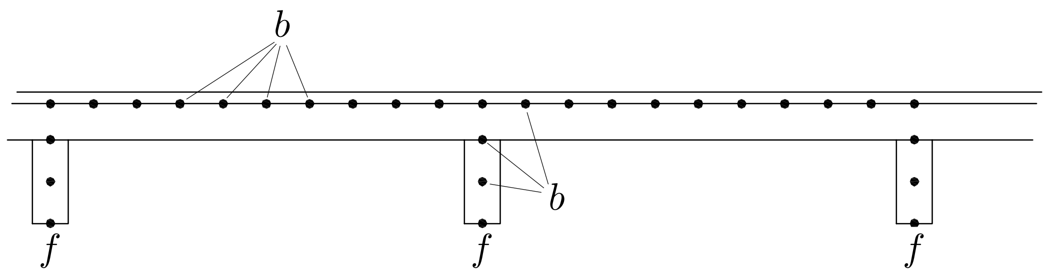

Figure 4.1 – Schematic of a Substructure Model for the Rail-Support System.

base footings at hard rock locations. In many cases, the piles are over 26 meters in length, and in extreme conditions, some piles are longer 50 meters.

4.1 – A Substructuring Formulation

It is proposed to analyze this problem using a substructures approach. It allows the two major components, (a) the rail-system and (b) the pile foundation, to be analyzed independently, and later, combined for an interaction analysis. This method is feasible for all linear problems and for this particular case, the relatively low level of excitation makes this linear superposition problem appropriate.

Rearranging the node numbers of the superstructure model such that the degrees of freedom for the bridge and those at the foundation level are separated so that the equation of motion for the superstructure can be written in a partition matrix equation of the form:

$$\begin{bmatrix} [M_{bb}] & [M_{bf}] \\ [M_{fb}] & [M_{ff}] \end{bmatrix} \begin{Bmatrix} \{\ddot{x}_b\} \\ \{\ddot{x}_f\} \end{Bmatrix} + \begin{bmatrix} [C_{bb}] & [C_{bf}] \\ [C_{fb}] & [C_{ff}] \end{bmatrix} \begin{Bmatrix} \{\dot{x}_b\} \\ \{\dot{x}_f\} \end{Bmatrix} + \begin{bmatrix} [K_{bb}] & [K_{bf}] \\ [K_{fb}] & [K_{ff}] \end{bmatrix} \begin{Bmatrix} \{x_b\} \\ \{x_f\} \end{Bmatrix} = \begin{Bmatrix} \{f_b\} \\ \{f_f\} \end{Bmatrix} \tag{4.1}$$

in which the subscribes b and f refer to degrees of freedom assigned to the bridge and to the foundation, respectively.

Using a Fourier Transformation, the equation of motion can be written in the frequency domain as

$$\begin{bmatrix} \left[Z_{bb}(\omega)\right] & \left[Z_{bf}(\omega)\right] \\ \left[Z_{fb}(\omega)\right] & \left[Z_{ff}(\omega)\right] \end{bmatrix} \begin{Bmatrix} \left\{X_b(\omega)\right\} \\ \left\{X_f(\omega)\right\} \end{Bmatrix} = \begin{Bmatrix} \left\{F_b(\omega)\right\} \\ \left\{F_f(\omega)\right\} \end{Bmatrix} \quad , \tag{4.2}$$

in which $X_b(\omega)$, $X_f(\omega)$ and $F_b(\omega)$ are Fourier Transforms of $x_b(t)$, $x_f(t)$ and $f_b(t)$ in Eq. (4.1), respectively, and the submatrices, Z, are defined as

$$\left[Z_{ii}(\omega)\right] = -\omega^2\left[M_{ii}\right] + i\omega\left[C_{ii}\right] + \left[K_{ii}\right] \quad . \tag{4.3}$$

A separation procedure can now be implemented by dividing Eq. (4.2) into two smaller matrix equations as

$$\left[Z_{bb}\right]\vec{X}_b = \vec{F}_b - \left[Z_{bf}\right]\vec{X}_f \quad , \tag{4.4}$$

and

$$\left[Z_{ff}\right]\vec{X}_f = -\left[Z_{fb}\right]\vec{X}_b + \vec{F}_f \quad . \tag{4.5}$$

in which the vector notation $\vec{X}$ is used interchangeably with an earlier notation of $\left\{X\right\}$.

Proceed now to solve Eq. (4.4) by inverting the matrix, $\left[Z_{bb}\right]$, and the harmonic displacement $\vec{X}_b$ can be expressed in terms of $\vec{X}_f$ as

$$\vec{X}_b = \left[Z_{bb}\right]^{-1}\vec{F}_b - \left[Z_{bb}\right]^{-1}\left[Z_{bf}\right]\vec{X}_f \quad . \tag{4.6}$$

Substitute $\vec{X}_b$ from Eq. (4.6) into Eq. (4.5) to yield a matrix equation with the unknown $\vec{X}_f$ as

$$\left[Z_{ff}\right]\vec{X}_f = -\left[Z_{fb}\right]\left[Z_{bb}\right]^{-1}\vec{F}_b + \left[Z_{fb}\right]\left[Z_{bb}\right]^{-1}\left[Z_{bf}\right]\vec{X}_f + \vec{F}_f \quad . \tag{4.7}$$

Gather now the terms involving $\vec{X}_f$ on the left side as

$$\Big(\left[Z_{ff}\right] - \left[Z_{fb}\right]\left[Z_{bb}\right]^{-1}\left[Z_{bf}\right]\Big)\,\vec{X}_f = -\left[Z_{fb}\right]\left[Z_{bb}\right]^{-1}\vec{F}_b + \vec{F}_f \quad , \tag{4.8}$$

and the solution for unknown $\vec{X}_f$ can be expressed as

$$\vec{X}_f = -\left(\left[Z_{ff}\right] - \left[Z_{fb}\right]\left[Z_{bb}\right]^{-1}\left[Z_{bf}\right]\right)^{-1}\left(\left[Z_{fb}\right]\left[Z_{bb}\right]^{-1}\vec{F}_b + \vec{F}_f\right) \qquad . \tag{4.9}$$

After the motion at the foundation level, $\vec{X}_f$, is determined, the motion on the bridge can be computed using Eq. (4.6).

The solution procedure above has to be performed for each frequency ω and the inversion for the large superstructural matrix $\left[Z_{bb}\right]$ can require a large number of floating point operations. A more efficient method is to use modal superposition. First define a matrix, $\left[\Phi\right]$, which contains as its column vectors the mass normalized eigenvectors of the eigenvalue problem, $-\omega^2\left[M_{bb}\right]\{\phi\} + \left[K_{bb}\right]\{\phi\} = 0$. The matrix $\left[\Phi\right]$ has the properties,

$$\left[\Phi\right]^T\left[M_{bb}\right]\left[\Phi\right] = \left[I\right] \qquad , \tag{4.10}$$

and

$$\left[\Phi\right]^T\left[K_{bb}\right]\left[\Phi\right] = \left[\text{diag}(\omega_i^2)\right] \qquad , \tag{4.11}$$

in which ω_i are the natural frequencies of the bridge structure.

Using the matrix $\left[\Phi\right]$, the dynamic matrix $\left[Z_{bb}(\omega)\right]$ can also be diagonalized as

$$\left[\Phi\right]^T\left[Z_{bb}(\omega)\right]\left[\Phi\right] = \left[D(\omega)\right] \qquad , \tag{4.12}$$

with the diagonal elements of $\left[D(\omega)\right]$ are defined as

$$D_{ii}(\omega) = \left(\omega_i^2 - \omega^2\right) + 2i\omega\omega_i\xi_i \qquad . \tag{4.13}$$

The parameter, ξ_i, in Eq. (4.13) is the modal damping factor assigned to the i-th mode. For concrete structures, $\xi_i = 0.02$ is an often used value.

To implement the modal analysis, express the motion of the superstructure, $\vec{X}_b$, as a linear combination of the modal ordinate $\vec{\eta}$ as

$$\vec{X}_b = \left[\Phi\right]\vec{\eta} \qquad , \tag{4.14}$$

and its substitution into Eq. (4.4) and the subsequent premultiplication of the equation by $\left[\Phi\right]^T$ yields

$$\left[\Phi\right]^T\left[Z_{bb}\right]\left[\Phi\right]\vec{\eta} = \left[\Phi\right]^T\vec{F}_b - \left[\Phi\right]^T\left[Z_{bf}\right]\vec{X}_f \qquad . \tag{4.15}$$

Since the matrix on the left side of of the above equation is now diagonal, the solution of the modal ordinate can then be obtained by inverting the diagonal matrix $\left[D(\omega)\right]$ as

$$\vec{\eta} = \left[D(\omega)\right]^{-1}\left[\Phi\right]^T\vec{F}_b - \left[D(\omega)\right]^{-1}\left[\Phi\right]^T\left[Z_{bf}\right]\vec{X}_f \qquad . \tag{4.16}$$

Using Eq. (4.16), the motion in the superstructure can be expressed in terms of the foundation motion as

$$\vec{X}_b = \left[\Phi\right]\vec{\eta} = \left[\Phi\right]\left[D(\omega)\right]^{-1}\left[\Phi\right]^T\vec{F}_b - \left[\Phi\right]\left[D(\omega)\right]^{-1}\left[\Phi\right]^T\left[Z_{bf}\right]\vec{X}_f \qquad , \tag{4.17}$$

and the subsequent substitution into Eq. (4.5) yields

$$\left[Z_{ff}\right]\vec{X}_f = -\left[Z_{bf}\right]\left[\Phi\right]\left[D\right]^{-1}\left[\Phi\right]^T\vec{F}_b + \left[Z_{bf}\right]\left[\Phi\right]\left[D\right]^{-1}\left[\Phi\right]^T\left[Z_{bf}\right]\vec{X}_f + \vec{F}_f \quad . \tag{4.18}$$

Introduce the modal participation factor $\left[\beta\right]$ as

$$\left[\beta\right] = \left[\Phi\right]^T\left[Z_{bf}\right] \qquad , \tag{4.19}$$

Eq. (4.18) can be simplified as

$$\left(\left[Z_{ff}\right] - \left[\beta\right]^T\left[D(\omega)\right]^{-1}\left[\beta\right]\right)\vec{X}_f = -\left[\beta\right]^T\left[D(\omega)\right]^{-1}\left[\Phi\right]^T\vec{F}_b + \vec{F}_f \qquad , \tag{4.20}$$

and the solution for $\vec{X}_f$ follows easily. The computation efficiency of Eq. (4.20) should be superior to Eq. (4.8) since the modal matrices $\left[\Phi\right]$ and $\left[\beta\right]$ are constant throughout the analysis and the diagonal matrix $\left[D(\omega)\right]$ can be inverted easily. Also, the number of modes used in the analysis can be sognificantly reduced from the total number of degrees of freedom of the superstructure.

The term $\vec{F}_f$ in Eq. (4.20) is where the effects of soil-structure interaction can be implemented. Let the foundation force vector be introduced as the resisting force from the pile foundation,

$$\vec{F}_f = -[K_s(\omega)]\vec{X}_f \qquad , \tag{4.21}$$

and the substitution of the above equation into Eq. (20) yields the soil-structure interaction as

$$\left(\left[Z_{ff}\right] + \left[K_s\right] - \left[\beta\right]^T \left[D(\omega)\right]^{-1} \left[\beta\right]\right) \vec{X}_f = -\left[\beta\right]^T \left[D(\omega)\right]^{-1} \left[\Phi\right]^T \vec{F}_b \qquad . \tag{4.22}$$

The above equation combines all the information from the superstructure and the soil medium using the principle of superposition. The foundation motion, F_f, is obtained in the frequency domain and the time response can be obtained using the Fourier Transform.

4.2 – The Analysis of the Superstructure

Shown in Fig. 4.2 are the undeformed sectional views of the Finite Element Model of the THSR elevated bridge. It is a highly refined model with over 16,000 three-dimensional nodes. The horizontal beams have a span of 30 meters and they are approximately 4.5 meters by 6 meters in cross section and the thickness of the concrete surfaces is about 0.3 to 0.5 meters for the top face and about 0.8 meters on the side walls. The thin-face construction of the beam is to reduce weight for transport during construction. The large cross sectional area is to improve its strength against torsional loads. Since the same bridge supports traffic in two directions, the loading condition in nearly every case is eccentric. The model was built using shell elements, and the actual thicknesses of the box beam is used for the different sides of the beam even though the schematic of the beam discretization does not show thicknesses. The models used in this analysis are geometrical compliance to the actual structure. It is hopeful that the dynamic properties are sufficiently accurate to model the resonance behavior when the load is applied based on the operating speed of the train.

The columns and their support systems are massive, they are spaced every 30 meters apart. The columns are 3.5 meters by 4 meters in cross section and they are supported by pile groups in weak soil conditions. The connections between the simply supported beams are also much thicker, having a concrete thickness of over 1 meter in most locations. As shown in Fig. 4.2, the subtle details of the bridge structure are included into the model, a possibility afford by the modern computers and the newer versions of SAP2000.

Shown in Fig. 4.3 are the first 5 modes of the 5-span bridge model. The frequency of the first mode is approximately 4 cycles/sec, and the subsequent modes have gradually increasing frequencies. Recall, the bridge structure rests on a rigid base, it is expected that the modal frequency will decrease depending on the soil conditions. For a very stiff rock site, the frequency should be approximately the same. But if the soil condition is poor, as is the case for many columns resting on muddy agricultural fields, the natural frequency could decrease significantly. From most observations, the natural frequency of the existing bridges are approximately 3 Hz. It appears that the first few mode shapes are of the torsional type, it is something which the designers wish to avoid. It is possible that for a certain speed of train, these modes might be excited to create a less safe environment.

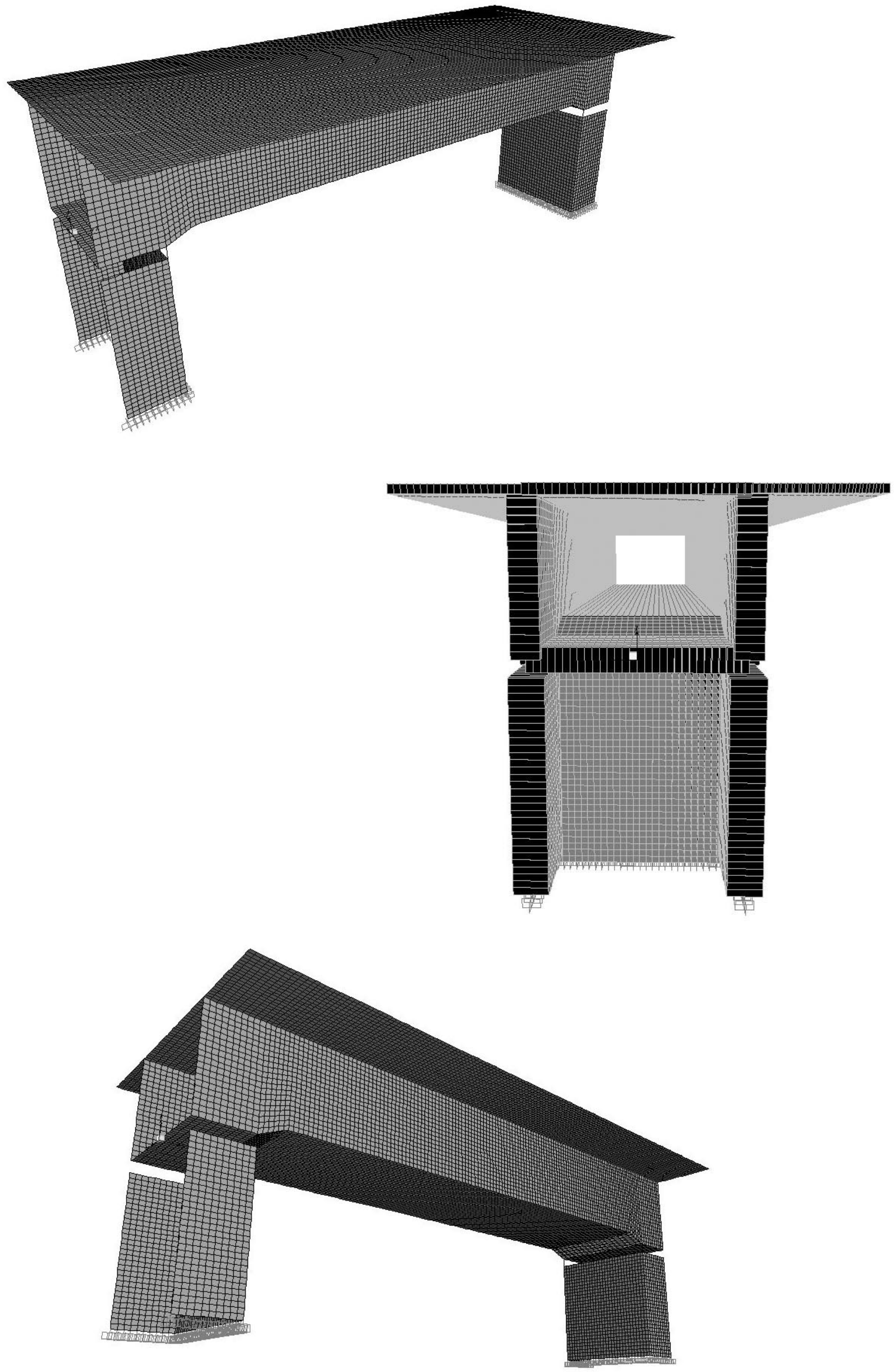

Figure 4.2 – Sectional Views of Railway Bridge Finite Element Model.

Shown in Fig. 4.4 are the second 5 modes of the finite element model. This set has several modes with prominent vertical displacements. Since the load from the train is vertical, it is anticipated that these modes could contribute to the amplification of vibration larger than those obtained from static analysis. Since a typical train which operates on this bridge is of the order of 300 meters long, it is to be supported by more than 10 spans of bridges. To make modelling simpler, mode shapes of one-span, two-span and five-span models were also made. It was found that the modal frequencies are extremely close, showing that the mode shapes are periodic and that no new modes are created by having a longer model because the fixed supports every 30 meters restriction those longer period modes from developing.

In the theoretical development of Section 4.1, the matrix factor $\left[Z_{bf}\right]$ was heavily involved. It is the connection between the pile foundation and the bridge, without it, the support structure would be considered fixed. $\left[Z_{bf}\right]$ allows the effects of soil-structure interaction to be included in the analysis and the softening of the support will effectively lower the resonance frequencies and make the response of the rail support system different from expected in the design stage.

Shown Table 4.1 is the effect of a softer spring under the foundation mats of the bridge structure under consideration. In the case where the stiffness is infinite, the foundation node is fixed, as in the case of most finite element models. In the second case, a value of K_0 is used for a constant spring, the value of K_0 is consistent with that of a firm soil medium, that of a bedrock. From that, it is clear that the natural frequencies for the first 3 modes decreased by approximately 10%. More cases are considered with the stiffness being $K_0/10$, $K_0/25$, $K_0/50$, and $K_0/100$. It is clear that drastic reduction of the natural frequencies can occur depending on the soil conditions.

Figure 4.3 – First Five Modes Shapes of a 5-span Finite Element Model.

Soil Spring	f_{n1}	f_{n2}	f_{n3}
$K_{zz} = \infty$	3.988	8.9547	9.3069
$K_{zz} = K_0$	3.666	8.5768	8.9722
$K_{zz} = K_0/10$	3.1099	7.7124	7.7657
$K_{zz} = K_0/25$	2.8615	6.1712	6.1723
$K_{zz} = K_0/50$	2.6014	4.6456	4.6614
$K_{zz} = K_0/100$	2.2489	3.3715	3.4163

Table 4.1 – Effect of soil stiffness on modal frequencies.

4.3 – Moving Loads on Bridge Structure

The forcing function to the modal analysis of the bridge is contributed through the factor $[\Phi]^T \vec{F}_b$ in Eq. (4.22). Since the $[\Phi]$ matrix contains the mode shapes of the bridge as its column vectors, $[\Phi]^T \vec{F}_b$ are the modal participation factors which determine which mode is excited by the load on the bridge, $\vec{F}_b$.

Since the load is applied at selected nodes on the top surface of the bridge, only the degrees of freedom of those loaded nodes are needed to form the matrix product. In addition to the modal ordinates, the location x is needed to define the load function. Let x_0 be a reference point at which the loading function $L_0(t)$ is defined. The Fourier Transform of $L_0(t)$ is defind as

$$L_0(\omega) = \int_{-\infty}^{\infty} L_0(t)\, e^{-i\omega t}\, dt \qquad . \tag{4.23}$$

Figure 4.4 – Second Five Modes Shapes of a 5-span Finite Element Model.

The loading function at location x_i has a phase delay, therefore, the Fourier Transform of the loading function at x_i is

$$L_i(\omega) = \int_{-\infty}^{\infty} L_0(t-\tau)\, e^{-i\omega t}\, dt \qquad , \tag{4.24}$$

in which τ is the time delay defined as

$$\tau = \frac{x_i - x_0}{c} \qquad . \tag{4.25}$$

Using a variable substitution, $q = t - \tau$ and $t = q + \tau$,

$$\begin{aligned} L_i(\omega) &= \int_{-\infty}^{\infty} L_0(q)\, e^{-i\omega(q+\tau)}\, dq \\ &= e^{-i\omega\tau} \int_{-\infty}^{\infty} L_0(q)\, e^{-i\omega q}\, dq = e^{-i\omega\tau} L_0(\omega) \end{aligned} \tag{4.26}$$

with the above relationship, the modal forcing term in the frequency domain can be determined as

$$[\Phi]^T \vec{F}_b = [\Phi]^T \begin{Bmatrix} L_1(\omega) \\ L_2(\omega) \\ \vdots \\ L_m(\omega) \end{Bmatrix} = L_0(\omega)[\Phi]^T \begin{Bmatrix} \exp(-i\omega(x_1 - x_0)/c) \\ \exp(-i\omega(x_2 - x_0)/c) \\ \vdots \\ \exp(-i\omega(x_m - x_0)/c) \end{Bmatrix} \qquad . \tag{4.27}$$

The interesting contribution in the above equation is that product is influence heavily by the train speed, c. Therefore, it is possible that a certain critical certain train speed can excite mode shapes to cause unsafe vibrations.

Shown in Figures 4.5 through 4.7 are the modal participation factors, $[\Phi]^T \vec{F}_b$, without the contribution from the loading function $L_0(\omega)$. With the inner product of the mode shapes with the unit phase delay factors, the plots in the figures show how the load velocity affects the response of the modes. In each figure, factors for three different speeds of 300, 225 and 150 km/hr are shown. The plots only show the amplitude of complex values as a function of frequency.

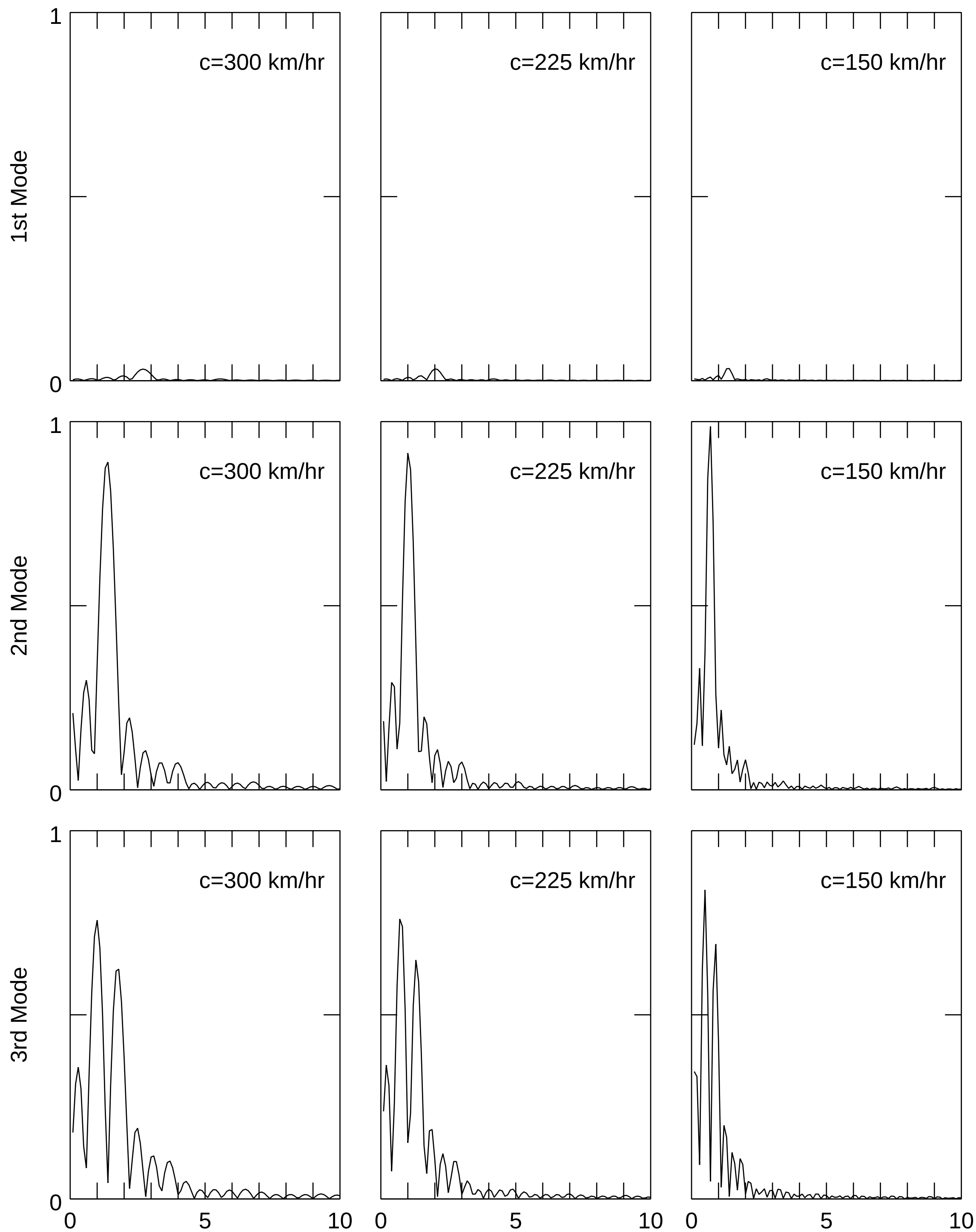

Figure 4.5 – Normalized Modal Participation Factors for Modes 1, 2 and 3.

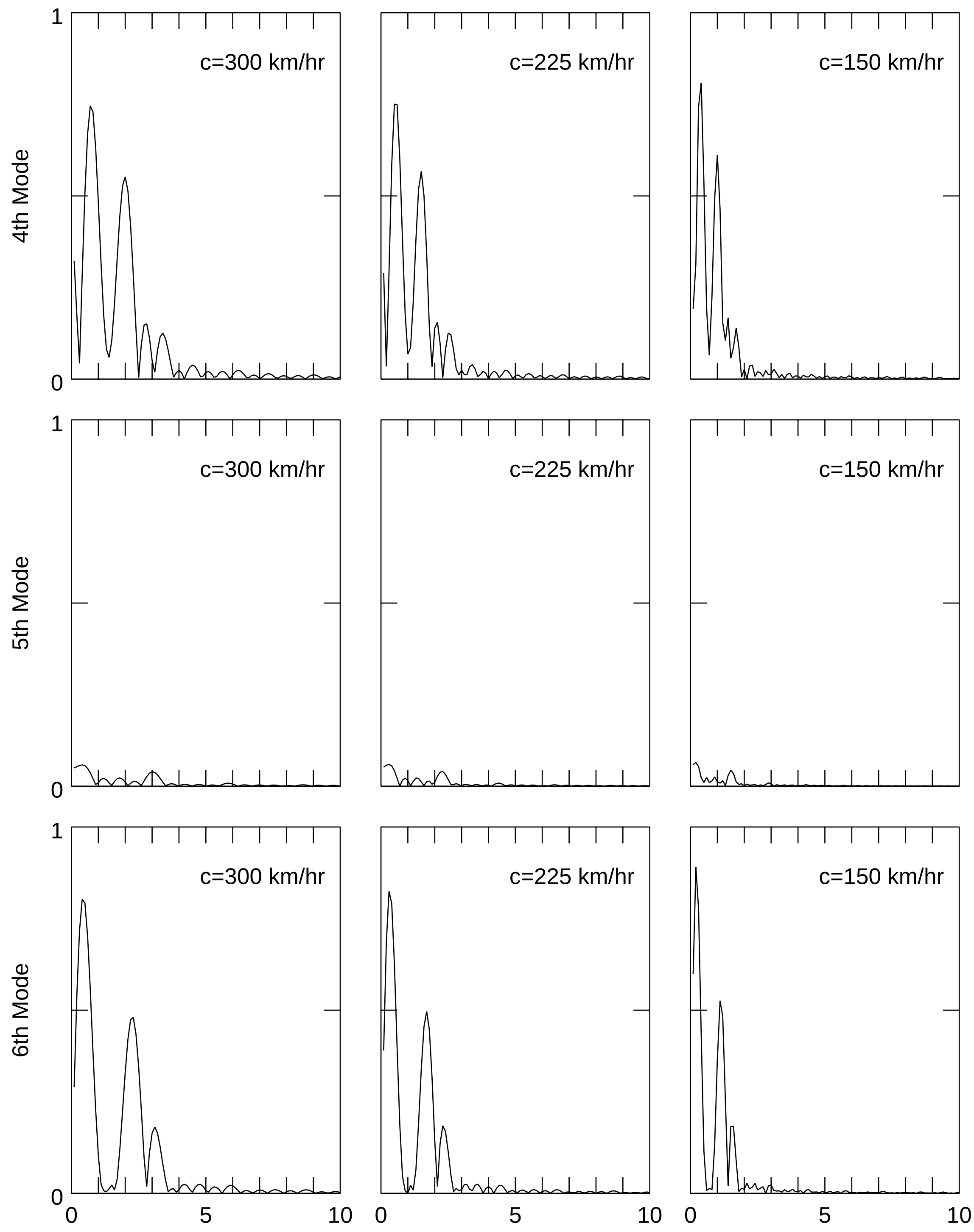

Figure 4.6 – Normalized Modal Participation Factors for Modes 4, 5 and 6.

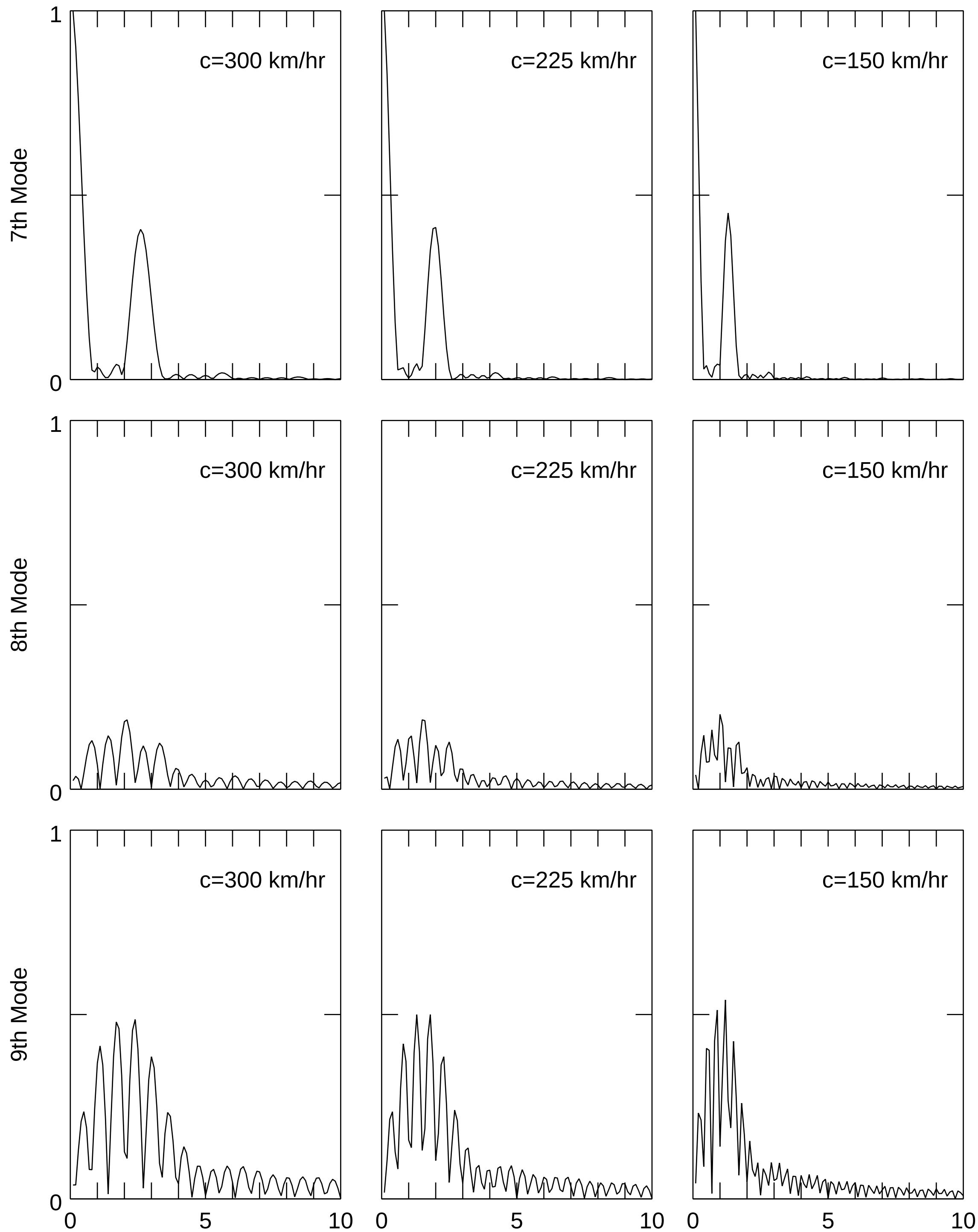

Figure 4.7 – Normalized Modal Participation Factors for Modes 7, 8 and 9.

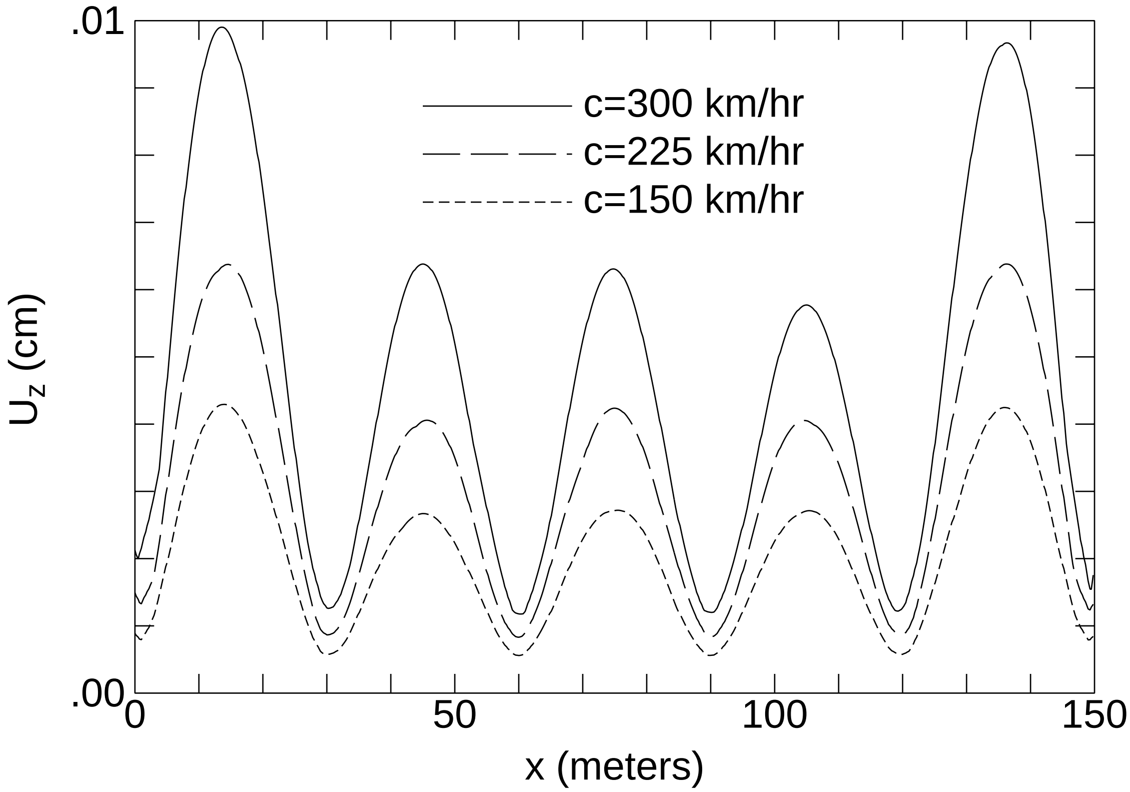

Figure 4.8 – Displacement of 5-span model from train loads.

To better assess how each mode is excited, the amplitude of the modal participation factors were arbitrarily normalized to the largest number for the first nine modes. The largest values was a static value in mode #7. As shown in Fig. 4.5, the first mode has a low value, nearly 20 times smaller than a higher mode. The fifth mode, shown in Fig. 4.6, is also small when driven by the load of the speed under consideration. The other modes has higher contributions.

Shown in Fig. 4.8 is the rigid-base displacement response of the 5-span model to train loads operating at the speed of 300, 225 and 150 km/hr. From the stiffness of the model used, perhaps overestimating the strength of the horizontal members, the maximum displacement is less than one tenth of a millimeter at mid-span. However, it is clear that the faster load

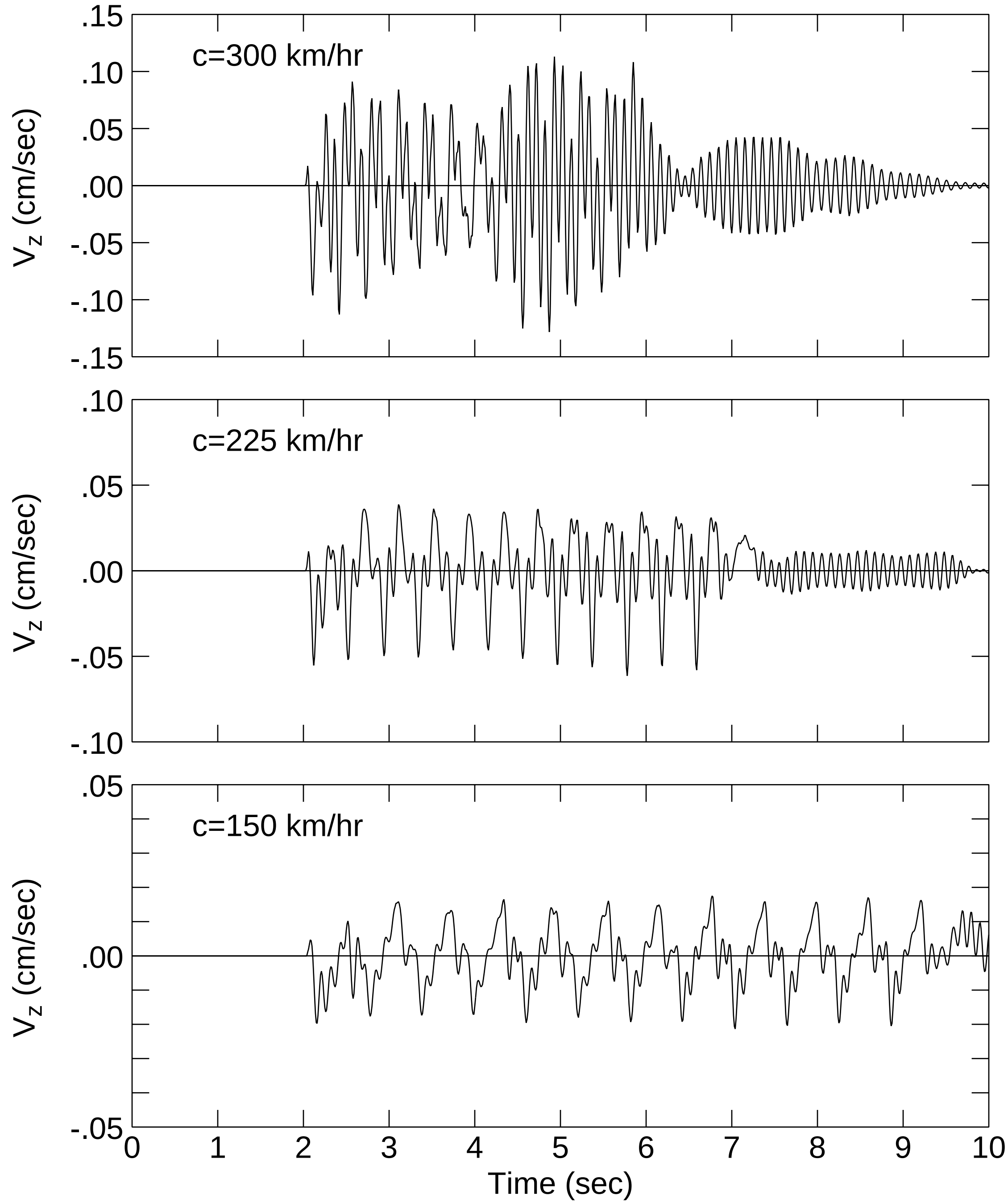

Figure 4.9 – Velocities of 5-span model from train loads.

causes more vibration of the bridge than the lower speeds. Perhaps the low displacement value can be explained by the fact that the columns are on a rigid ground since the model

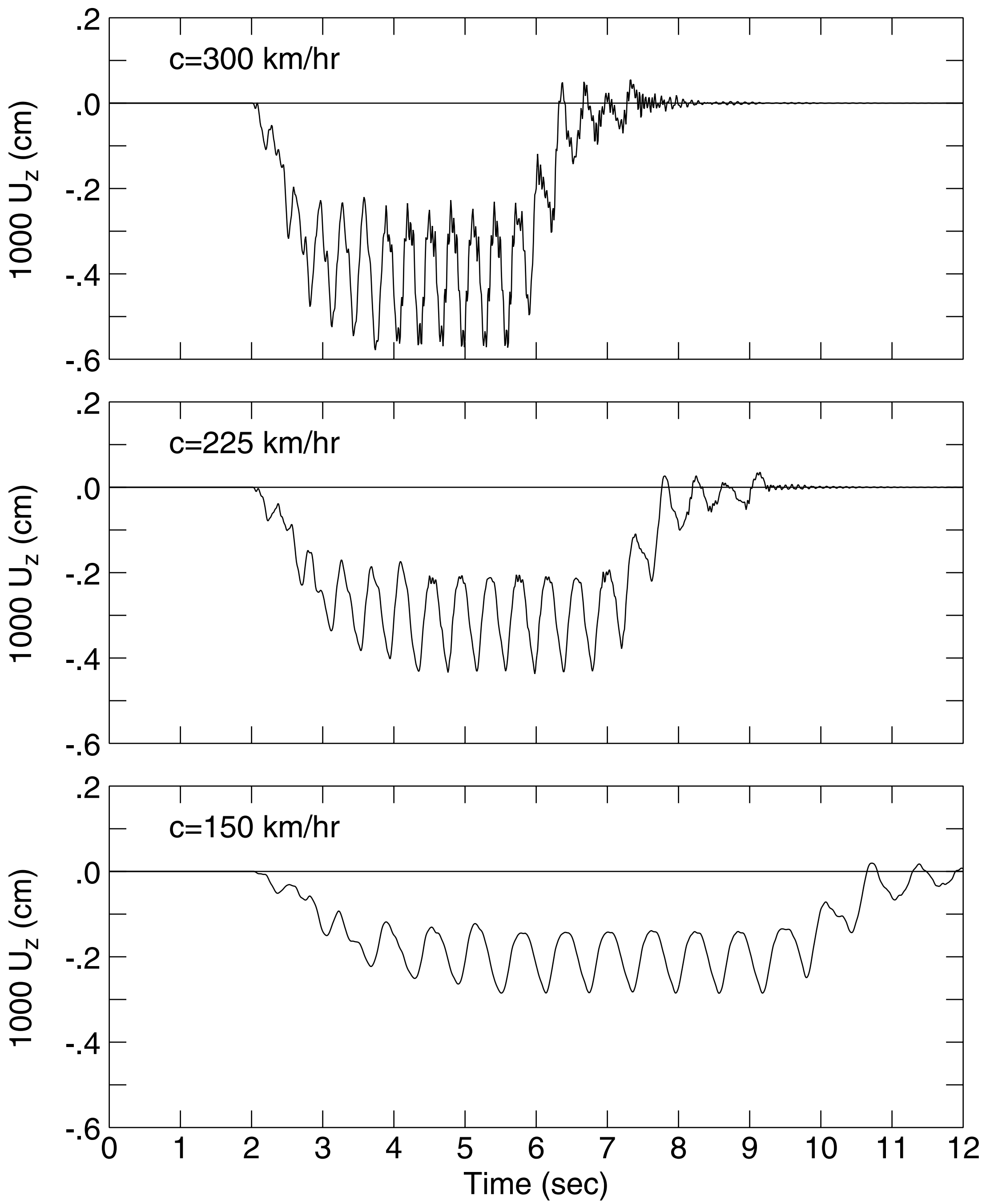

Figure 4.10 – Displacement of nodes above the foundation level.

assumes the base of the columns are fixed. When the effect of soil-structure interaction is considered with softer soil profiles, the displacement may be significantly higher.

Shown in Fig. 4.9 is the velocity response of the bridge subjected to the same train loads of speeds 300, 225 and 150 km/hr. The highest response is a fraction of one cm/sec. Again, a fixed base model is used. The results indicated that the higher modes are excited, with about 15 cycles/sec for the 300 km/hr load case and about 11 cycles/sec for the 150 km/hr load case. Although the velocity amplitudes of the slower loads are much lower, the duration of the vibration is longer.

To estimate the dynamic forces that a resonant bridge can exert on its foundations, the displacements at the locations right above the foundation are needed. Designate the displacements of these nodes by $\vec{X}_q$ and they can be calculated using the mode shapes at the same location, Φ_q as

$$\vec{X}_q = \left[\Phi_q\right]^T \left[D(\omega)\right]^{-1} \left[\Phi\right]^T \vec{F}_b \qquad , \tag{4.28}$$

and the force applied by the bridge structure on the foundation can be calculated as

$$\vec{F}_f = \left[K_{fb}\right] \vec{X}_q \qquad . \tag{4.29}$$

Shown in Fig. 4.10 is the displacement $\vec{X}_q$ in column 2 of the 5-span bridge model. The response is higher for the faster train speeds and the peak displacement is of the order of 0.5×10^{-3} cm. For this particular bridge model and the size of its columns, the value of the spring K_{fb} is approximately 73.7×10^6 tonnes/m. Using the RMS value of X_q of about $0.2 \times 10{-}3$ cm, the applied force at the foundation can be about 147 tonnes, 20 to 30 times higher the load used in Chapter Three based on a rigid bridge assumption. The difference can be attributed to the dynamic effects of the bridge. The large values will decrease significantly when soil-structure interaction is considered. The soil damping as well as radiation damping from the spreading of wave energy will alter the rigid-base response. But the load on the foundation, nevertheless, could be higher than those used for wave propagation analyses in Chapter Three.

Chapter Five
Vertical Impedance of Pile Groups

To analyze the dynamic behavior of a pile group, the methods are difficult because the flexibility of the piles must be considered along with the soil properties deep into the soil medium. There are approximate methods suggested to simplify the problem by making various assumptions, sometimes using unproven concepts by assuming the soil medium behaves as stack of independent layers. But clearly some assumptions must be made to make this problem solvable. Fortunately, the dynamic response of a bridge induced by external loading from a train is significantly simpler than the dynamic response caused by an earthquake. The Most important simplification comes from the fact that the loads are all vertical and that allows the smaller horizontal components to be de-emphasized. Generally, the horizontal components are the most difficult to analyze for pile groups because the long piles are quite flexible in the lateral dimension. For the analysis in this thesis, the following assumptions will be made:

- Use a relaxed boundary condition for the vertical impedance calculation by neglecting the coupling of horizontal stresses between piles within the pile group. This assumption was proven to be effective for many rigid foundation problems and it is a reasonable assumption for the present analysis because the aspect ratio of the pile group's vertical dimension is more than 5 times the lateral dimensions.

- Assume the piles are rigid in the vertical (longitudinal) direction. This is a reasonable assumption from the point of view for calculating impedance functions becasue the fine details of the stress distribution does not affect the accuracy of the end product, the impedance function, to be obtained by integration. This assumption would not be acceptable if a detail analysis of the piles is required.

Using the above assumptions, an integral equation formulation using the Green's Functions for a layered medium developed by Luco and Apsel (1983a, 1983b) will be implemented. Their developed method and computer program can calculate, for a point force in any given direction, the displacement vector and stress tensor at any observation point. The only requirement is that the layers are horizontal and the material properties are viscoelastic. The application in this chapter would use just a small fraction of what is available in that program because only the vertical displacement from a vertical point load is required using the "Body Force Method" to be introduced in the next section. Although this method is applicable only for rigid foundations, it is useful for the present analysis because the pile group is assumed to be rigid in the vertical direction.

5.1 – An Integral Equation Formulation

Using the Green's Functions and the Principle of Superposition, the vertical displacement u_z at the observation point $\vec{r}_o = (x_o, y_o, z_o)$ caused by a vertical point load P_z at the source point $\vec{r}_p = (x_p, y_p, z_p)$ can be expressed as

$$\int_V G_{zz}(\vec{r}_o|\vec{r}_p)\, f_z(\vec{r}_p)\, dV = u_z(\vec{r}_o) \quad , \tag{5.1}$$

in which G_{zz} is vertical displacement Green's Function caused by a vertical point load, and V is the volume containing the sources with a force distribution prescribed by the function f_z.

A numerical solution of Eq. (5.1) can be accomplished by first subdividing the volume, V, into many smaller subregions as shown in Fig. 5.1. The total number of subregion is $N = nM$, with V subdivided into $V_i, i = 1, 2, \ldots, N$. M is the number of piles in the pile

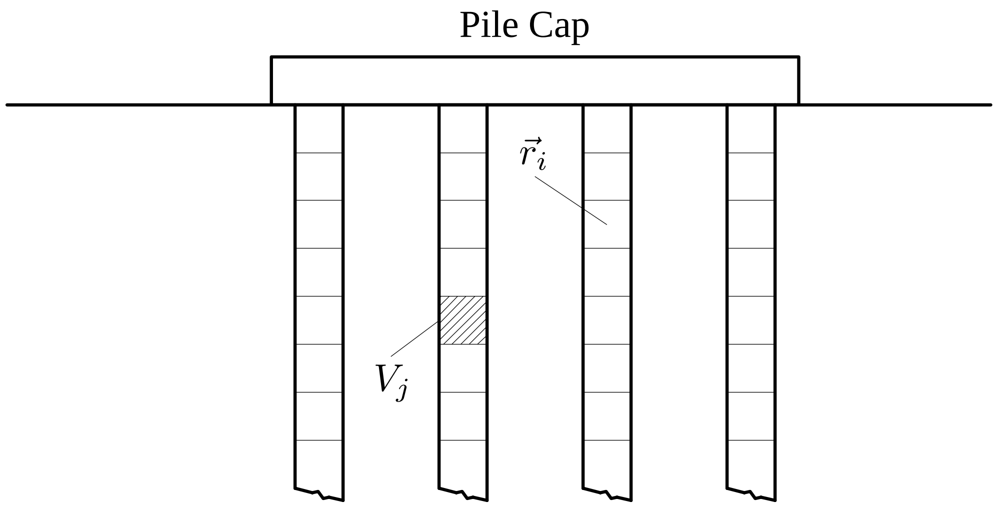

Figure 5.1 – Numerical Discretization of Pile Group Model.

group and n is the number of subregions per pile. With that subdivision, Eq. (5.1) can be rewritten as

$$\sum_{j=1}^{N} \int_{V_j} G_{zz}(\vec{r}_o|\vec{r}_p) f_z(\vec{r}_p)\, dV = u_z(\vec{r}_o) \quad . \tag{5.2}$$

The next step is to approximate $f_z(\vec{r}_p)$ as a uniform force distribution, f_j, inside V_j. Eq. (5.2) can be simplified as

$$\sum_{j=1}^{N} \left(\int_{V_j} G_{zz}(\vec{r}_o|\vec{r}_p)\, dV \right) f_j = u_z(\vec{r}_o) \quad . \tag{5.3}$$

Assign now the observation point $\vec{r}_o$, to be $\vec{r}_i$, the centroid of the subregion V_i, Eq. (5.3) can be expressed as

$$\sum_{j=1}^{N} \psi_{ij}\, f_j = u_i \quad , i = 1, 2, \ldots, N, \tag{5.4}$$

in which the complex influence function, ψ_{ij}, is defined as

$$\psi_{ij} = \int_{V_j} G_{zz}(\vec{r}_i|\vec{r}_p)\, dV \qquad . \tag{5.5}$$

ψ_{ij} relates the displacement at $\vec{r}_i$, the centroid of subregion V_i, to the uniform force distribution $\vec{f}_j$ in subregion V_j. The summation in Eq. (5.4) can be written in the form of an $N \times N$ matrix equation as

$$\left[\Psi\right]\vec{f} = \vec{u} \qquad , \tag{5.6}$$

in which $\vec{f}$ and $\vec{u}$ contains the distributed forces and displacements at the centroids of the N subregions, respectively.

To adapt Eq. (5.6) to the calculation of a vertical impedance function for a pile group, let the displacement vector, $\vec{u}$, be defined as

$$\vec{u} = \begin{bmatrix} 1 \\ 1 \\ \vdots \\ 1 \end{bmatrix} \Delta e^{i\omega t} = \left[1\right]\Delta e^{i\omega t} \qquad , \tag{5.7}$$

in which $\left[1\right]$ is an $N \times 1$ column vector with each element assigned a value of 1, and Δ is the harmonic vertical rigid body displacement of the pile group, assumed to be a constant from the pile cap all the way to the end of the pile. It is assumed that the piles carry the vertical load through their lengths. The solution of the matrix equation, Eq. (5.6), can be obtained numerically as

$$\vec{f} = \left[\Psi\right]^{-1}\left[1\right]\Delta \qquad , \tag{5.8}$$

in which $\vec{f}$ is a $N \times 1$ column vector containing the force distribution which satisfy the displacement compatibility conditions specified by Eq. (5.7).

The final step of the formulation is to accumulate the forces into a total foundation force F_f as

$$F_f = \left[1\right]^T\left[f_z\right] = \left[1\right]^T\left[\Psi\right]^{-1}\left[1\right]\Delta \qquad . \tag{5.9}$$

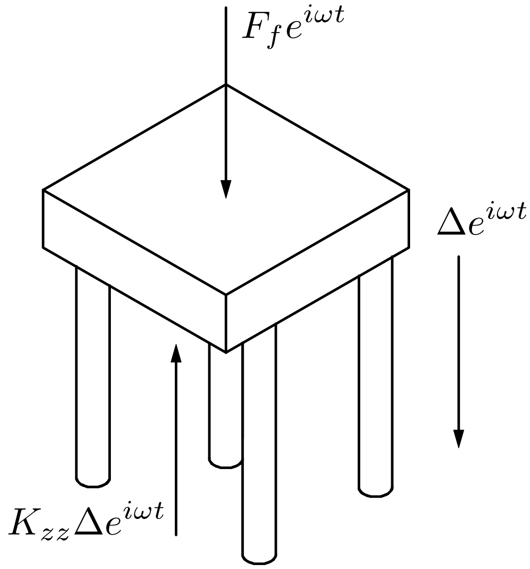

Figure 5.2 – The Definition of Impedance Function, K_{zz}.

To obtain the vertical impedance function, K_{zz}, consider the force diagram in the z-direction as shown in Fig. 5.2. The impedance function is equivalent to a frequency dependent spring and dashpot in the diagram. The applicaiton of Newton's Second Law yields

$$F_f\, e^{i\omega t} - K_{zz}(\omega)\Delta\, e^{i\omega t} = m_t\left(-\omega^2\Delta\right)\, e^{i\omega t} \qquad , \tag{5.10}$$

in which m_t is the total mass of the soil to be excavated from the volume V. Removing the time factor $e^{i\omega t}$ as an implied entity, Eq. (5.10) can be rewritten as

$$K_{zz}\Delta = F_f + \omega^2 m_t \Delta \qquad . \tag{5.11}$$

By substituting Eq. (5.9) into Eq. (5.11),

$$K_{zz}\Delta = \left[1\right]^T \left[\Psi\right]^{-1} \left[1\right]\Delta + \omega^2 m_t \Delta \qquad . \tag{5.12}$$

Remove now the common factor Δ and the vertical impedance function can be written as

$$K_{zz} = \left[1\right]^T \left[\Psi\right]^{-1} \left[1\right] + \omega^2 m_t \qquad . \tag{5.13}$$

In many analyzes, K_{zz} is referred to as the soil spring, but it is called an impedance because the effects of the soil mass surrounding the piles, the resistance to motion, the soil damping, and the radiation damping caused by geometrical spread of outgoing waves, are all included in that function. It is frequency dependent, that is why it cannot be represented by a simple soil spring.

5.2 – Numerical Calculation of Influence Functions

From Eq. (5.5), the influence function, ψ_{ij}, was defined as

$$\psi_{ij} = \int_{V_j} G_{zz}(\vec{r}_i|\vec{r}_p)\, dV \qquad .$$

The Green's Function, $G_{zz}(\vec{r}_i|\vec{r}_p)$, can be computed using the computer program created by Luco and Apsel (1983a, 1983b) and the result can be expressed in the form:

$$G_{zz}(\vec{r}_i|\vec{r}_p) = f_{zz}(R)/R \qquad , \tag{5.14}$$

in which R is the radial distance between $\vec{r}_i$ and $\vec{r}_p$ and it is computed as

$$R = |\vec{r}_i - \vec{r}_p| = \sqrt{(x_i - x_p)^2 + (y_i - y_p)^2} \qquad . \tag{5.15}$$

The depth effects of the source and the observer are embeded in the function $f_{zz}(R)$.

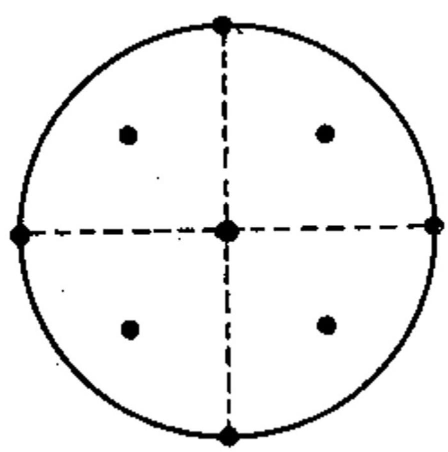

Figure 5.3 – Sample Points for 6th Order Circular Integration.

When the source point i is not within the volume V_j, the integrand for ψ_{ij} contains no singularity and it can be integrated by assuming the integrand is uniform in the z -direction and the circular area can be integrated to the $O(a^6)$ accuracy by using sample points strategically placed as shown in Fig. 5.3. The numerical integral can be represented as

$$\psi_{ij} = \int_{V_j} G_{zz}(\vec{r}_i|\vec{r}_p)\, dV \approx \pi a^2 h \sum_{k=1}^{9} w_k \frac{f_{zz}(R_{ij})}{R_{ij}} \qquad , \tag{5.16}$$

in which h is the height of the volume V_j, a is the radius of the pile, and

$$R_{ij} = \sqrt{(x_i - (x_k + x_j))^2 + (y_i - (y_k + y_j))^2} \qquad . \tag{5.17}$$

For this particular algorithm, the weight w_k and its corresponding sample point locations are shown in Table 5.1.

(x_k, y_k)	w_k
$(0, 0)$	1/6
$(\pm a, 0)$	1/24
$(0, \pm h)$	1/24
$(\pm h/2, \pm h/2)$	1/6

Table 5.1 – Sample Point Locations and Weights for Integration Over a Circular Area.

To calculate ψ_{ij} when $i = j$, the singularity of the Green's Function of the form $1/R$ is within the volume V_j. Normally, that is a difficult task which calls for the static singularity to be integrated in close-form coupled with the dynamic nonsingular part to be integrated numerically. It is fortunate, in the present case, that the piles have a circular geometry and that the integral can be performed in polar coordinates. The Green's Function, as defined in Eq. (5.14) can be written as

$$G_{zz}(\vec{r}_i|\vec{r}_p) = f_{zz}(r)/r \qquad , \tag{5.18}$$

in which r is simply the radial coordinate measured from the center of the pile. The influence function for the diagonal term of the matrix can therefore be simplified as

$$\psi_{ii} = \int_{V_i} G_{zz}(\vec{r}_i|\vec{r}_p)\, dV \approx 2\pi h \int_0^a \frac{f_{zz}(r)}{r}\, r\, dr \qquad , \tag{5.19}$$

in which $2\pi h$ is the result of the integration of a constant in the azimuthal and in the vertical direction. The integral of the form,

$$\int_0^a f_{zz}(r)\, dr \qquad , \tag{5.20}$$

without any singularity, can be integrated routinely by Gaussian Quadrature or other numerical integration schemes. Accurate results can be obtained without difficulties.

5.3 – Numerical Results

The pile foundation design for most columns in the THSR bridge support is composed of 5 piles in a pile group. Each pile has a diameter of 1.8 meters and 4 piles are arranged at the 4 corners of a sqaure of dimension 7.5 meters. There is also one center pile in the middle of that square. The pile cap is a thick concrete block with a dimension of 10 meters by 10 meters. The length of the piles is dependent of the soil condition; but the worst case of soil condition calls for piles as deep as 55 meters.

The objective of the foundation analysis is to obtain a frequency dependent function known as the impedance function. To explain the frequency dependency of this function, it is suggested that a single degree of freedom oscillator could be used as an example. In the frequency domain, the mass-damper-spring system has the impedance of $(-\omega^2 m+k)+i\omega c$, in which the real part of the impedance includes the inertia force and the spring force and the imaginary part, divided by frequency, is the dashpot, or damper. Although the soil spring is a constant, the real part is frequency dependent because of the mass. Similarly, if the entire soil medium is to be represented by a function, it must account for the inertia effects of the soil mass, the stiffness of soil provided by the elastic property of the soil and the damping provided by the energy dissipation properties of soil. In addition to material damping, the energy lost due to the spreading of outgoing waves adds another factor known as radiation damping. All these effects combine to make the impedance function frequency dependent.

For the analysis of the THSR bridge response to a moving train, only the vertical impedance is required. For most earthquake problems, all six components, three translations and three rotations, are sometimes necessary. In addition to this simplification, the pile group is also assumed to be rigid in the vertical direction. Although the elastic effect of a long slender pile is neglected, this formulation provides adequate results for the relatively low-level excitation generated by a train.

Consider the results obtained for a pile group in soil profile #1 and shown in Fig. 5.5. The pile depths analyzed are 24, 32 and 40 meters. Most likely, shorter piles would be used for a firm site as described by this soil profile. Similar to the results in Chapter Three, the impedance functions for this soil profile have smooth results. The real part of the impedance function is labeled as “soil spring” in the graph. It is normalized by the shear modulus of the soil medium, $\mu = \rho\beta^2$. In this particular case, $\rho = 2650$ kg/m^3 and $\beta = 500$ m/sec. The imaginary part is divided by the frequency and it appears to be a constant for most of the frequency range.

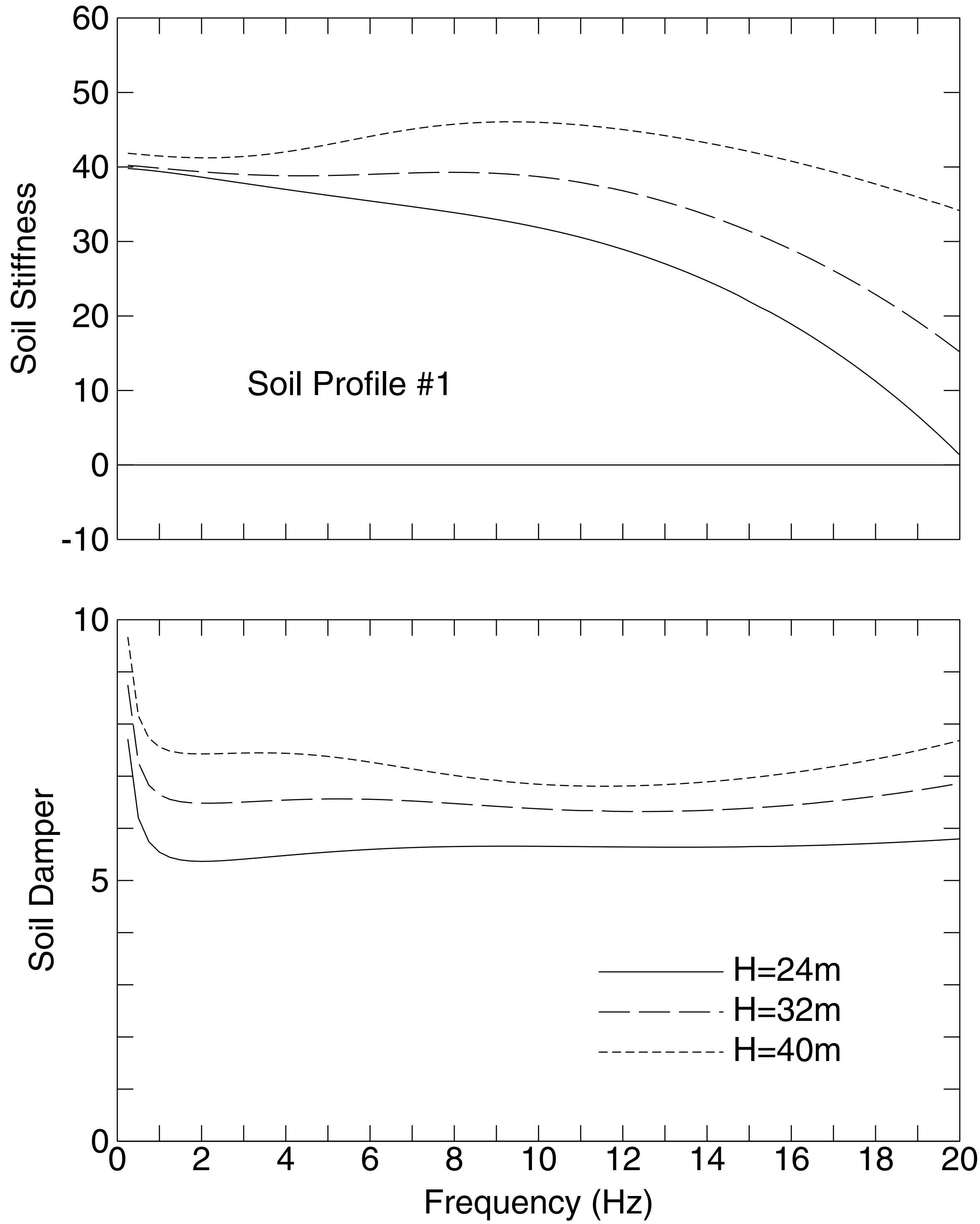

Figure 5.4 – Impedance function for pile group in soil profile #1.

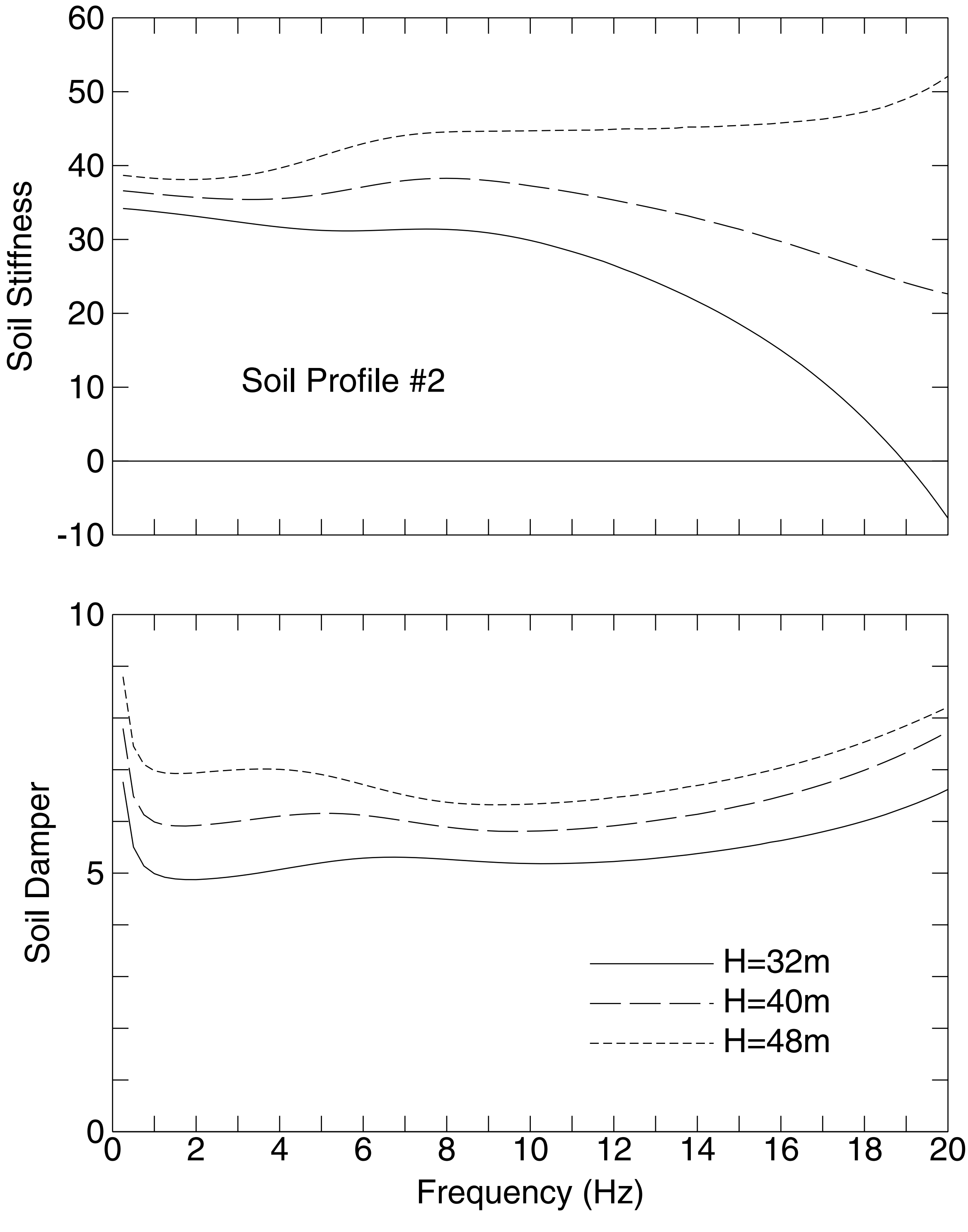

Figure 5.5 – Impedance function for pile group in soil profile #2.

Not too different from soil profile #1 is soil profile #2. Slightly deeper pile are used for this analysis as the depths were chosen to be 32, 40 and 48 meters. The results in Fig. 5.6 are normalized by the same shear modulus as that in soil profile #1.

Unlike the other two soil profiles, the results for soil profile #3 is high osillatory because of the resonance of the top layers. The near static stiffness is about two and one half smaller, therefore, deeper piles are needed to provide a stiffer spring constant. For this particular soil profile, the numerical results do not appear to be stable, especially at higher frequencies.

The results for soil profile #4 in Fig. 5.7 is more smooth than those of the previous figure. The near static stiffness value is about six times smaller than that of soil profile #1. The oscillatory behavior for the impedance function is caused by the soft layers on top of a firm half space.

Figures 9 to 11 show how higher material damping values can reduce the oscillatory behavior of the soft-soil impedance functions. It is quite likely that higher material damping values should be used for the top soil layers with small stiffness.

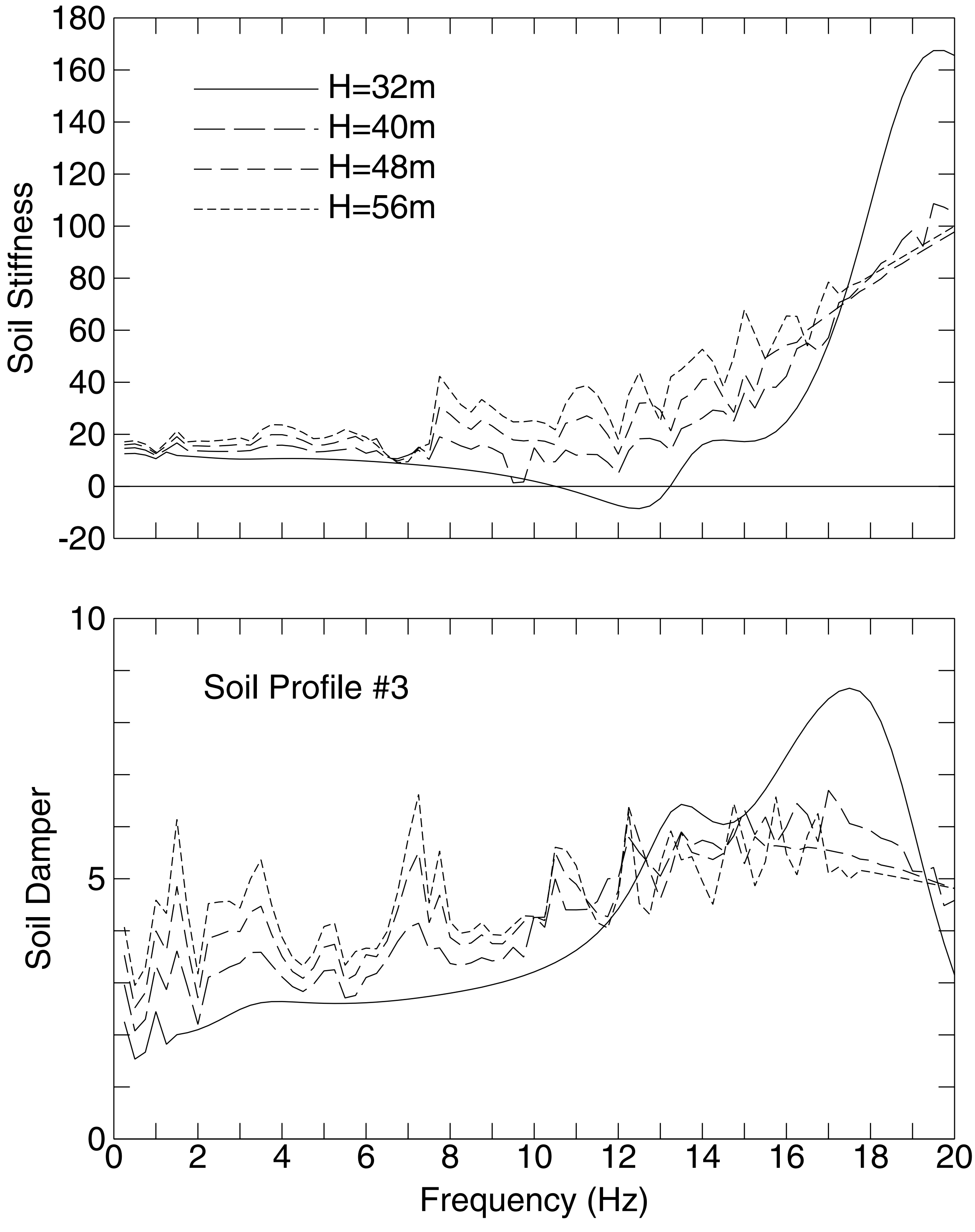

Figure 5.6 – Impedance function for pile group in soil profile #3.

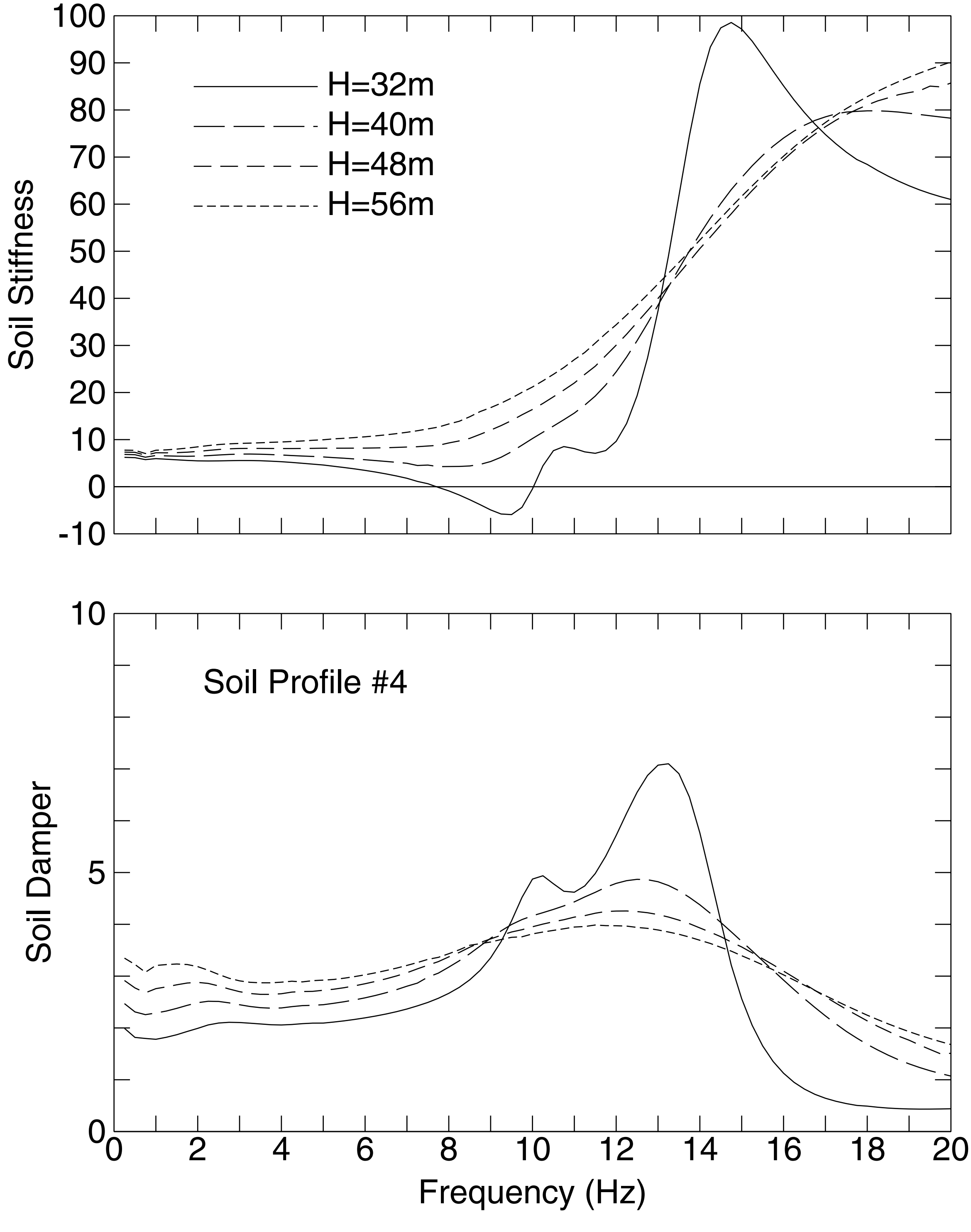

Figure 5.7 – Impedance function for pile group in soil profile #4.

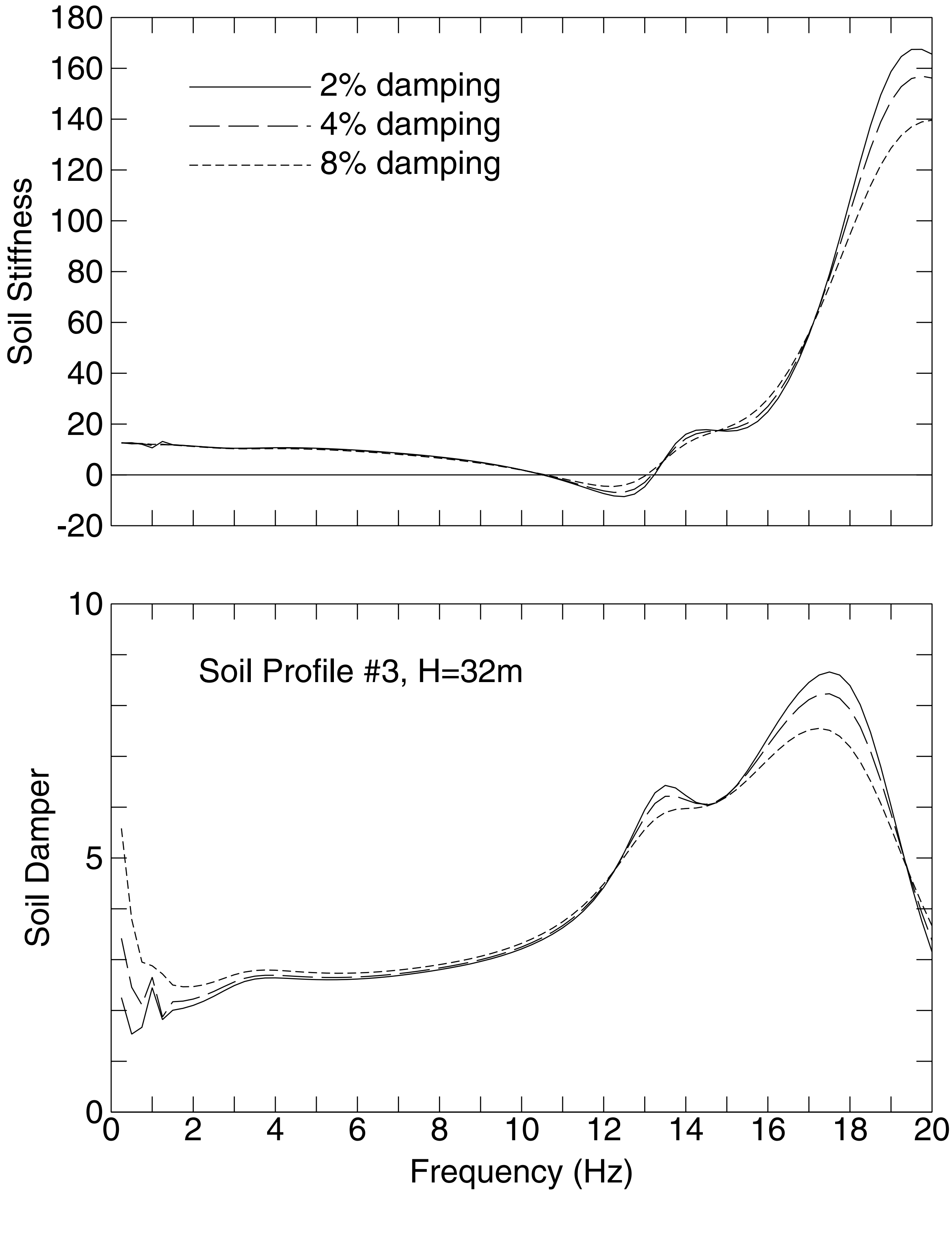

Figure 5.8 – Impedance function for pile group in soil profile #3.
Pile depth 32 meters, various soil damping values.

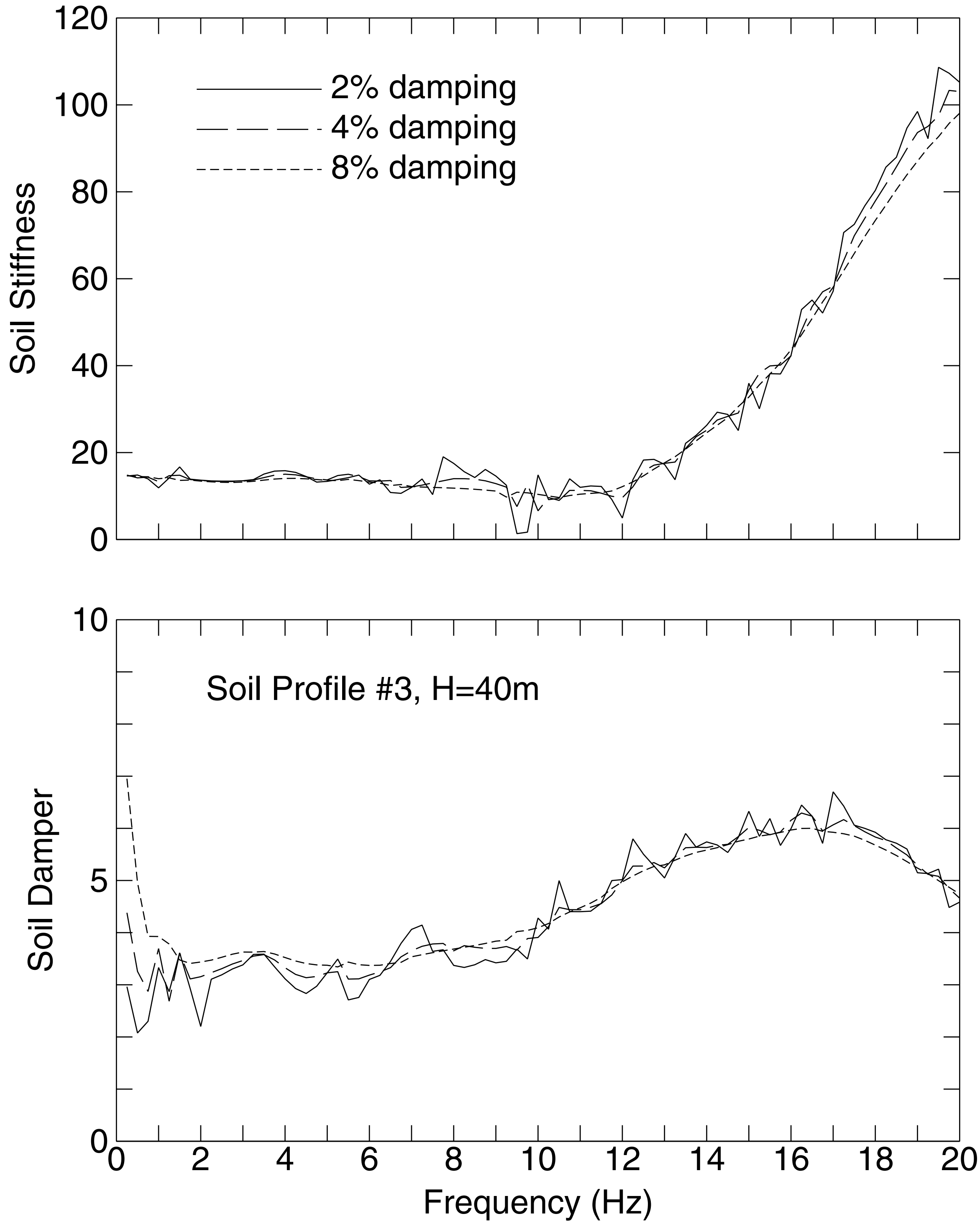

Figure 5.9 – Impedance function for pile group in soil profile #3.
Pile depth 40 meters, various soil damping values.

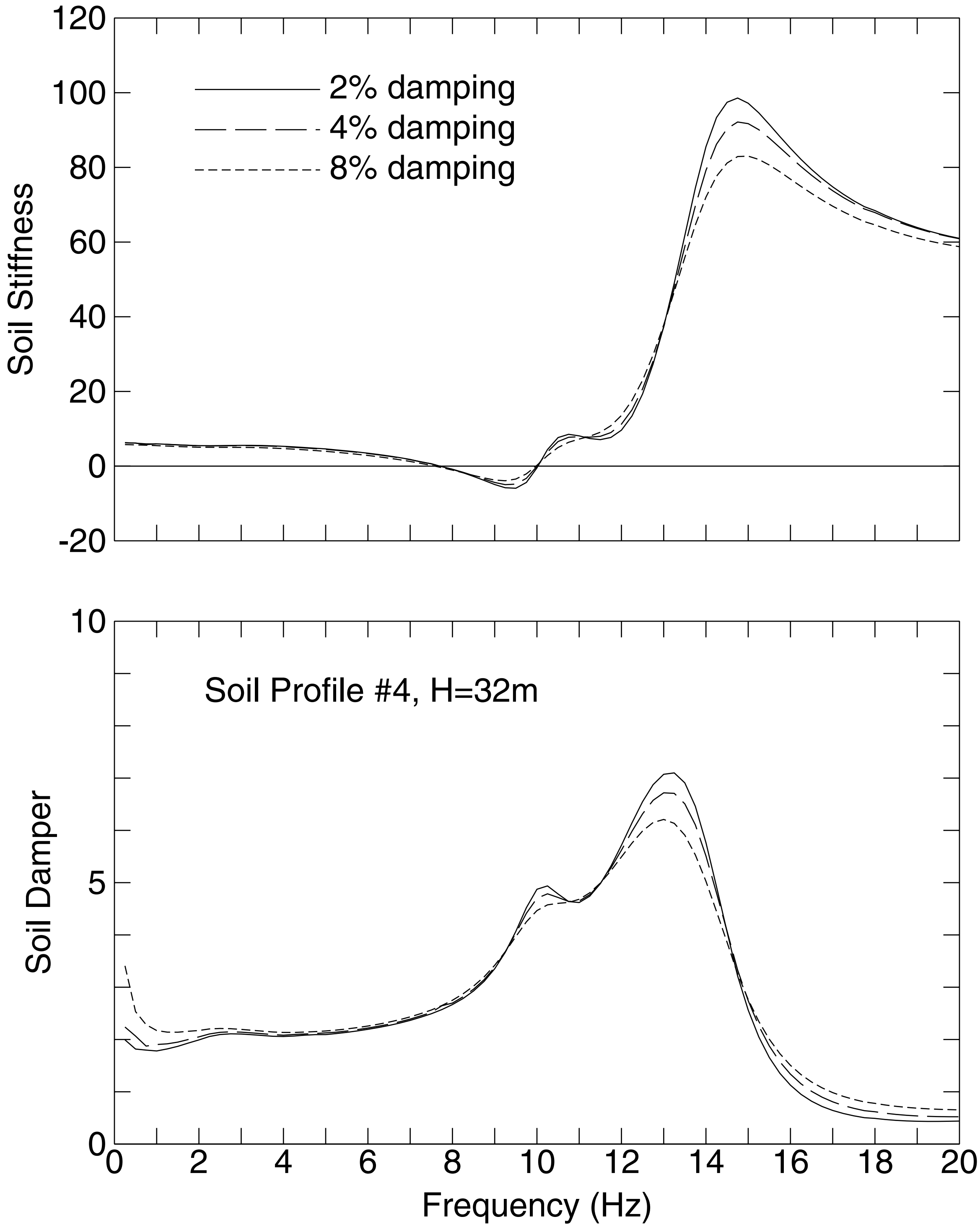

Figure 5.10 – Impedance function for pile group in soil profile #4.
Pile depth 32 meters, various soil damping values.

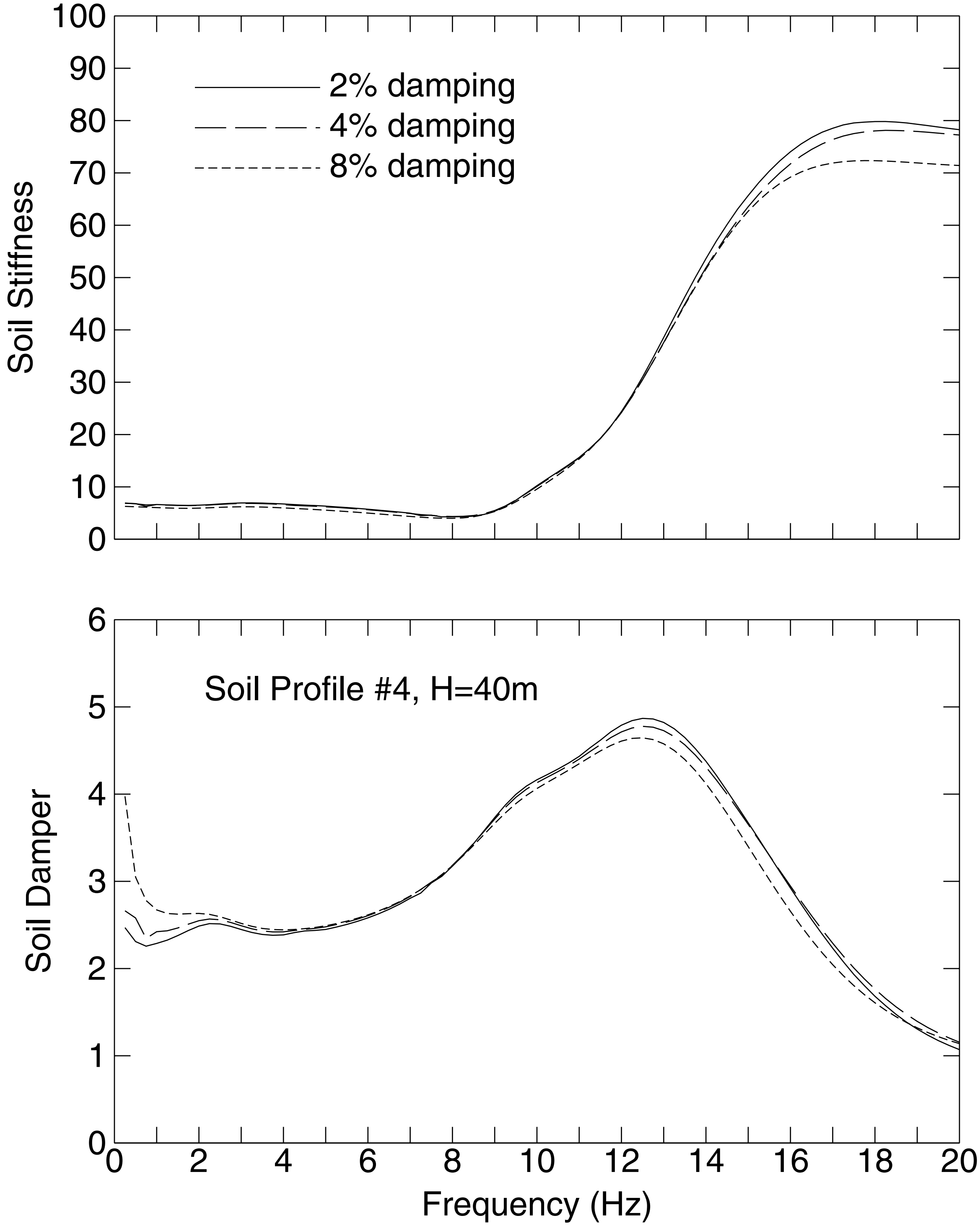

Figure 5.11 – Impedance function for pile group in soil profile #4.
Pile depth 40 meters, various soil damping values.

Chapter Six
Conclusions

A case study of the THSRC high speed train system was performed in this dissertation. Extensive data were gathered of vehicle characteristics, support structure information as well as soil conditions of sites along the route. Pertinent information about the operation of the THSR system was reviewed as of August 2008 in the introduction.

In Chapter Two, borehole ground data were studied. From the wealth of geological information made available through Taiwan's earthquake studies, the pertinent sites of THSRC were singled out. Four vastly different soil profiles were developed for later analyses, as most of the soil condition in that country can be roughly be classified into one of those idealized soil profiles.

In Chapter Three, a preliminary analysis of ground waves generated by a high speed train on four representative soil conditions was performed. For train tracks on the surface of the soil medium, it is concluded that the vibration level diminishes very rapid away from the track even for the soft soil condition. For elevated bridges with columns founded on pile groups, the attenuation pattern is much slower as the distant waves can be attributed to surface waves generated by the buried sources. It is concluded that elevated tracks generate a smaller vibration near the track but the wave amplitudes diminsh slower over distance. Therefore, vibration can be felt at a greater distance away.

In Chapter Four, a methodogy for analyzing a train moving on a flexible bridge supported by columns on pile foundations was developed. It has been shown that resonance behavior of the bridge contributes to an increased foundation load and that would the increased vibration of the area. Safety for the train is also an issue if vibration from resonance exceed a recommended level. The stiffness of the soil condition can also play an important role as it can alter the resonance frequency of the bridge. The soil damping and the radiation damping from the spreading of wave energy through the soil medium decreases the response of the structure and therefore, reduces the vibration level of the area. It is clear from the analysis in Chapter Four that the dynamic effects of the bridge structure is a factor in the transmission of vibration to the soil through the pile foundations.

In Chapter Five, a Green's function formulation was given by assuming the pile group is rigid in the vertical direction. Vertical impedance functions were calculated for 4 different soil profiles and compared. The impedance function represents the soil stiffness, soil inertial effects, soil damping and damping due to radiation of waves. With these impedance functions, the effect of soil-structure interaction can be implemented to the response of the bridge structure.

The case study of the THSRC provided useful information for designs of future transit system. Vibration levels can be computed for the purpose of analyzing environemental impact. Numerical computation of wave levels can be significantly less costly than the conduction of experiments.

References

Abramowitz, M.A., and I.A. Stegun (1970). "Handbook of Mathematical Functions," Fover 0-486-61272-4, New York.

Al-Hussaini, T.M., Ahmad, S. and Baker, J.M. (2000) "Numerical and experimental studies on vibration screening by open and in-filled trench barriers," Wave 2000, pp.241-250.

Auersch L. (2005) "The excitation of ground vibration by rail traffic: theory of vehicle-track-soil interaction and measurements on high-speed lines," Journal of sound and vibration, pp.103-132.

Bode, C. , Hirschauer, R. and Savidis, S.A. (2000) "Three-dimensional time domain analysis of moving loads on railway tracks on layered soils," Wave 2000, pp.3-12.

Chouw, Nawawi and Pflanz, Gero (2000) "Reduction of structural vibrations due to moving load," Wave 2000, pp. 251-268.

Ciesielski, R. and Kwiecieh (2000) "Underground propagation of vibration excited on soil surface," Wave 2000, pp.161-170.

Clouteau, D., Degrande, G. and Lombaert, G. (2000) "Some theoretical and numerical tools to model traffic induced vibrations," Wave 2000, pp.13-28.

De Barros F.C.P., Luco J.E., (1992). "Moving Green functions for a layered visco-elastic half-space," Report, University of California at San Diego, La Jolla, California.

Degrande, G. and Lombaert, G. (2000) "High-speed train induced free field vibrations: In situ measurements and numerical modelling," Wave 2000, pp. 29-41.

Dominguez, J. (2000) "Boundary element method for simulation of wave propagation," Wave 2000, pp.337-356.

Dowding, Charles H. (2000). "Effects of ground motions from high-speed trains on structures, instruments, and humans," Wave 2000, pp. 269-288.

Ekevid, T. and Wiberg N.-E. (2000) "Wave propagatio related to moving loads close to critical speed," Wave 2000, pp. 43-52.

Ewing, W.M., W.S. Jardetsky, and F. Press (1957). "Elastic Waves in Layered Media," McGraw-Hill Book Company, Inc., New York.

Guo, C.M., Huang, C.S. and Tzeng, C.W. (2001) "Vibration analysis of rail structure," Tainan science park vibration prevention seminar, pp.90-108.

Hao, H. and Wu, C. (2000) "Numerical modeling of underground explosion-induced stress wave propagation in rock mass," Wave 2000, pp.369-378.

High-Speed Ground Transportation Noise and Vibration Impact Assessment. Manual from proposed high-speed ground transportation (HSGT) projects. http://project1.parsons.com/ptgnechsr/noise_manual.htm

Hirose, S. (2000) "Boundary element modelling and analysis of moving loads in time and frequency domains," Wave 2000, pp.71-82.

Ishida, Yoshio (2005) "The future of high-speed train," East Japan Railway Company.

Jiang, P.W., Liu, S.W. and Song, J.C. (2001) "Simulation of surface ground vibration induced by high speed rail," Tainan science park vibration prevention seminar, pp.121-150.

Jones, C.J.C., Sheng, X. and Thompson, D.J. (2000) "Ground vibration from dynamic and quasi-static loads moving along a railway track on layered ground," Wave 2000, pp.83-98.

Ju, S.H. (2001) "3D finite element analyses of wave barriers for reduction of train-induced vibrations," Tainan science park vibration prevention seminar, pp.32-49.

Kim, M.K., Lee, P.K., Kim, D.H. and Kwon, H.O. (2000) "Vibration isolation using flexible rubber chip barriers," wave 2000, pp. 289-298.

Lai, C.G., Callerio, A., Faccioli, E. and Martino, A. (2000). "Mathematical modelling of railway-induced ground vibrations," Wave 2000, pp. 99-110.

Laue, J. and Studer, J.A. (2000) "Harassment and damage caused by vibrations: Prediction and evaluation in theory and practice," Wave 2000, pp.317- 324.

Lee, Jong-Sub and Santamarina, J. Carlos (2005) "Bender elements: Performance and Signal interpretation," Journal of geotechnical and geoenvironmental engineering, pp.1063-1070.

Lin, H.D. and Ju, S.H. (2001) "Research of resonance problems caused by high speed rail," Tainan science park vibration prevention seminar, pp. 50-60.

Lombaert, G., Degrande, G. and Clouteau, D. (2000) "Road traffic induced free field vibrations: Numerical modelling and in situ measurements," Wave 2000, pp.195-208.

Love, A.E.H. (1926). "A Treatise on the Mathematical Theory of Elasticity," ISBN 0-486-60174-9, Dover Publications, New York.

Luco, J.E. and R.J. Apsel (1983). "On the Green's Functions for a Layered Half-Space, Part I," Bulletin of Seismological Society of America, Vol. 73, No. 4, pp. 907-929.

Luco, J.E. and R.J. Apsel (1983). "On the Green's Functions for a Layered Half-Space, Part II," Bulletin of Seismological Society of America, Vol. 73, No. 4, pp. 931-951.

Luco, J.E., H.L.Wong and F.C.P. de Barros (1990). Three-dimensional Response of a Cylindrical Canyon in a Layered Half-space, International Journal of Earthquake Engineering and Structural Dynamics, 19(6), 799-817.

Man, A.P.de and Kok, A.W.M. (2000) "Recording, estimating and managing the dynamic behavior of railway tracks," Wave 2000, pp.209-218.

Massarsch, K.R. (2000) "Settlemens and damage caused by construction-induced vibrations," Wave 2000, pp.299-316.

Metrikine, A.V. and Vrouwenvelder, A.C.W.M. (2000) “Ground vibration induced by a high-speed train in a tunnel: Two-dimensional model,” Wave 2000, pp.111-120.

Mindlin, R. (1936). “Force at a Point in the Interior of a Semi-Infinite Solid,” Phys.7, 195–202.

Naprstek, J. (2000) “Dynamic response of an overhead contact wire and pantograph collector to high speed moving load,” Wave 2000, pp.121-130.

Pflanz, Gero, Garcia, Julio and Schmid, Gunther (2000) “Vibrations due to loads moving with sub-critical and super-critical velocities on rigid track,” wave 2000, pp. 131-148.

Popp, K. and Kruse, H. (2000) “The influence of wave propagation in the subsoil on the train-track dynamics,” Wave 2000, pp.171-184.

Saeki, M. and Higashihara, H. (2000) “Analysis of harmonic seismic wave fields as a basis of new tomography method,” Wave 2000, pp.399-408.

Shu, D.S., Tseng, G.C. and Yeh, H.H. (2001) “Strategy of vibration reduction by trench in Tainan science park,” Tainan science park vibration prevention seminar, pp.61-89.

Tamaskovics, N. and Klapperich, H. (2000) “Initial condition formulation for a wave-field in nearly saturated soil generated by a deep underground explosion,” Wave 2000, pp.409-420.

Wang, J.F., Lin, C.C. and Chen, B.L. (2000) “Supperssion of bridge vibrations due to train loading using multiple tuned mass dampers,” Wave 2000, pp.325-336.

Wolf, J.P. (2000) “Far-field displacements of 3-D soil in scaled boundary finite-element method,” Wave 2000, pp.421-432.

Yau, J.D., Lin, C.L. and Yang, Y.B. (2000) “Dynamic response of bridges with elastic bearings due to high speed trains,” Wave 2000, pp.149-160.

Yokoyama, Hidehumi, Ashiya, Kimitoshi, and Iwata, Naoyasu (2006) “Ground vibration characteristics induced at high-speed by Shinkansen and evaluation method for speed dependency,” Tetsudo Gijutsu Kenkyu Jo, pp.156-161.

Yoshioka, Osamu (2000). “Basic characteristics of Shinkansen-induced ground vibration and its reduction measures,” Wave 2000, pp. 219-237.

Zhang, Nan and Xia, He (2005) “Dynamic analysis of railway bridge under high speed train,” Engineering machanics, pp.144-151.